8-2022

Efficient Control Approaches for Guaranteed Frequency Performance in Power Systems

Samaneh Morovati
University of Tennessee, Knoxville, smorovat@utk.edu

To the Graduate Council:

I am submitting herewith a dissertation written by Samaneh Morovati entitled "Efficient Control Approaches for Guaranteed Frequency Performance in Power Systems." I have examined the final electronic copy of this dissertation for form and content and recommend that it be accepted in partial fulfillment of the requirements for the degree of Doctor of Philosophy, with a major in Electrical Engineering.

Seddik M. Djouadi, Major Professor

We have read this dissertation and recommend its acceptance:

Kevin Tomsovic, Joe Chow, Xiaopeng Zhao, Dan Wilson

Accepted for the Council:

Dixie L. Thompson

Vice Provost and Dean of the Graduate School

(Original signatures are on file with official student records.)

Efficient Control Approaches for Guaranteed Frequency Performance in Power Systems

A Dissertation Presented for the

Doctor of Philosophy

Degree

The University of Tennessee, Knoxville

Samaneh Morovati

August 2022

To my wonderful family

Acknowledgments

I would like to express my deepest gratitude and appreciation to my academic co-advisors, Dr. Seddik M. Djouadi and Dr. Kevin Tomsovic, for their time, dedication, guidance, and support during my study. Their noble scientific research spirits could sky the limit for me and have profoundly reshaped my point of view on the academic world. Their support and persistence to solve problems from new perspectives and to bring novel insights initiated a life goal for me in the world of research and inspired me to dream beyond all limitations. Moreover, they always supported me in my academic experience and personal life with their admirable personality.

My acknowledgments also go to my committee, Dr. Joe Chow, Dr. Xiaopeng Zhao and Dr. Dan Wilson for their support, guidance, helpful comments and suggestions. I also would like to thank Dr. Yichen Zhang and Dr. Fatima Taousseer for their invaluable discussions and support. I am also thankful to Dr. Mohammed Olama from Oak Ridge National Laboratory for providing me ideas, help and support. I am very thankful to the University of Tennessee and CURENT for providing me an amazing atmosphere and facilities to conduct my research. In addition, I would like to thank my colleagues and friends for the camaraderie and their assistance in research and personal life.

And last but not least, I would like to express my appreciation and love to all my family for their unconditional love, encouragement, and support, which made it possible for me to finish this work.

It is not the brains that matter most, but that which guides them — the character, the heart, generous qualities, progressive ideas.

- by Fyodor Dostoevsky

Abstract

Due to high penetration of renewable energy, converter-interfaced sources are increasing in power systems and degrading the grid frequency response. Synthetic inertia emulation and guaranteed primary frequency response is a challenging task. Still, there is high potential for application of highly controllable converter-interfaced devices to help performance. Renewable energy sources and demand side smart devices also need to be equipped with innovative frequency control approaches that contribute to frequency regulation operations.

First, the wind turbine generator is chosen to represent an example of a converter-interfaced source. An augmented system frequency response model is derived, including the system frequency response model and a reduced-order model of the wind turbine generator representing the supportive active power due to supplementary inputs. An output feedback observer-based control is designed to provide guaranteed frequency performance. System performance is analyzed for different short circuit ratio scenarios where a lower bound to guarantee the performance is obtained.

Second, the load side control for frequency regulation with its challenges is introduced. 5G technology and its potential application in smart grids are analyzed. The effect of communication delays and packet losses on inertia emulation are investigated to show the need of using improved communication infrastructure.

Third, a robust delay compensation for primary frequency control using fast demand response is proposed. Possible system structured uncertainties and communication delays are considered to limit frequency variations using the proposed control approach. An uncertain governor dead-band model is introduced to capture frequency response characteristics.

Guaranteed inertial response is achieved and compared with a PI-based Smith predictor controller to show the effectiveness of the proposed method.

Fourth, set theoretic methods for safety verification to provide guaranteed frequency response are introduced. The Barrier certificate approach using a linear programming relaxation by Handelman's representation is proposed with its application to power systems.

Finally, the Handelman's based barrier certificate approach for adequate frequency performance is studied. The computational algorithm is provided for the proposed method and validated using power system benchmark case studies with a discussion on a safety supervisory control (SSC).

Table of Contents

List of Tables

List of Figures

List of Abbreviations and Symbols

List of Abbreviations

ACE Area Control Error

AGC Automatic Generation Control

BESS Battery Energy Storage System

CIPR Converter Interfaced Power Resources

COI Center of Inertia

CURENT Center for Ultra-Wide-Area Resilient Electric Energy Transmission Networks

DER Distributed Energy Resource

DFIG Double Fed Induction Generator

DR Demand Response

DSG Diesel Synchronous Generator

FOC Field-Oriented Control

GSC Grid-Side Converter

HJ PDE Hamilton-Jacobi Partial Differential Equation

HVDC High-Voltage Direct Current

IAC Inverter-Interfaced Air Conditioners

IE Inertia Emulation

IoT Internet of Things

LFT Linear Fractional Transformation

LP Linearing Programming (Program)

LQR Linear Quadratic Regulator

MDA Minimum Degree Approximation

MIMO Multiple-Input Multiple-Output

MPPT Maximum Power Point Tracking

NCS Networked control systems

NERC North American Electric Reliability Council

ODE Ordinary Differential Equations

PFC Primary Frequency Control

PI Proportional–Integral

PSS Power System Stabilizer

PV Photovoltaics

ROA Region of Attraction

ROCOF Rate of Change of Frequency

ROS Region of Safety

RSC Rotor-Side Converter

SCR Short Circuit Ratio

SDP Semi-Definite Programming (Program)

SFR System Frequency Response

SI International System of Units

SMA Selective Modal Analysis

SMIB Single Machine Infinite Bus

SOSP Sum of Squares Programming (Program)

SOS Sum of Squares

SSC Safety Supervisory Control

VSG Virtual Synchronous Generator

WECC Western Electricity Coordinating Council

WTG Wind Turbine Generator

Chapter 1

Introduction

The work in this dissertation is inspired by the high penetration of distributed energy resources (DERs) connected by inverter-based devices resulting in new power system dynamics, particularly in terms of the frequency response. DERs are small and modular energy generation and storage technologies, including wind turbines, micro-turbines, photovoltaics (PV), and energy storage systems. Power system DERs, including renewable resources such as wind turbine generator (WTG), PV, and battery energy storage system (BESS), have received a lot of attention to address problems such as environmental impact, high energy cost and low electric power reliability. Increased penetration of these devices into the power networks with complex behaviors impacts frequency regulation services. DER control along with demand side contributions can provide a stronger and more resilient grid.

Control synthesis towards guaranteed frequency performance is challenging, requiring supplementary control loops for synthetic inertial and primary frequency response in power systems. Moreover, building energy equipment is moving rapidly towards the Internet of Things (IoT)-driven devices, which allows consumer connectivity and device management. These device-level interfaces, along with improved communication infrastructure such as 5G networks, can be leveraged to develop power system architectures with a large number of monitoring and control devices to provide real-time reliable energy services [81]. Estimation of the safety region is another challenging task impacting guaranteed frequency response. Here, the term safety means a well-defined and allowable operating region, and a safe response means the trajectories of all concerned states stay within defined safety limits. This dissertation aims at establishing systematic frameworks for controller synthesis towards guaranteed performance and focuses on the frequency control problem.

1.1 Background

Renewable generation resources, such as, wind and solar are gradually replacing conventional synchronous generators. Among these renewable resources, wind energy has received lots of investment and has become one of the fastest-growing energy sources globally. The modern electric power grid should include adequate resources to meet customers' energy requirements [14]. The generation and load within a power grid should be maintained at a balanced level at all times to provide reliable performance [120]. Significant power imbalances may lead to severe frequency deviations, stability problems, or even widespread system blackouts [76]. System frequency performance is an indicator of balance and imbalance in operating conditions that must be well controlled during disturbances.

Diesel synchronous generators (DSGs) are a common choice for powering microgrids in remote locations. A renewable source can reduce the operating cost by partially replacing the usage rate of expensive diesel generators [132], [83]. Renewable energy resources, such as, wind and solar, are mainly connected to the grid using power electronic interfaces that ensure power injection at the rated grid frequency [62]. The variable nature of renewable power poses challenges for frequency control in mixed diesel-renewable microgrids [61]. This variability may result in large frequency fluctuations without proper controls [119]. Furthermore, unacceptable frequency excursions caused by deterioration of inertial response in the presence of large disturbances can adversely impact system reliability [121]. To address the frequency stability challenges, renewable energy sources need to be equipped with frequency control approaches that contribute to frequency regulation operations [27], [82], [83]. Utilizing stored energy as a synthetic inertial response, commonly referred to as inertia emulation, is one of the widely proposed approaches [112]. These controls can be employed either in grid-connected mode or in island mode [135], [83].

The U.S. electric grid is evolving from a large, centralized power generation and control architecture to a hybrid system that incorporates various DERs near the load. Utilizing the response from the demand side as a synthetic inertial response can also help reduce the rate of change of frequency (ROCOF) and provide a supplementary primary frequency control loop. Utilizing demand control to provide grid services requires synchronized wide-area control of a significant number of loads to deliver sufficient response. At the grid edge where consumers connect to the grid, sensor arrays, high-speed networks, and advanced communications create a dynamic space where energy is not only passively consumed but generated, stored, managed, and traded [65]. The communication delays and packet losses in sensors and actuators are an important challenge for inertia emulation control in power systems with demand response (DR) [25], [137].

1.1.1 Traditional Frequency Regulation

Balancing generation and load continuously is difficult due to minute to minute load and generation changes. This balancing can also be affected by longer-term variability resulting from predictable load and weather patterns. Generation also may have fluctuation because of unexpected trips or generation schedule failures [53]. In traditional frequency regulation, synchronous generators are mainly accomplished for frequency control in the presence of disturbances by adjusting their output based on the frequency measurements. Frequency regulation basics represent frequency response on time scales that can be categorized into three periods, namely, inertial response, primary control response, and secondary control response as is illustrated in Fig. 1.1 [83]. The inertial and primary control responses have a similar time scale of seconds, while the secondary control response has a slower time scale, which is tens of seconds to minutes [128]. Secondary control response is out of the scope of this dissertation and will not be discussed.

Inertial Response

In the presence of disturbances that cause an imbalance power in the grid, synchronous generators and motors start to release kinetic energy of their rotating mass, which prevents

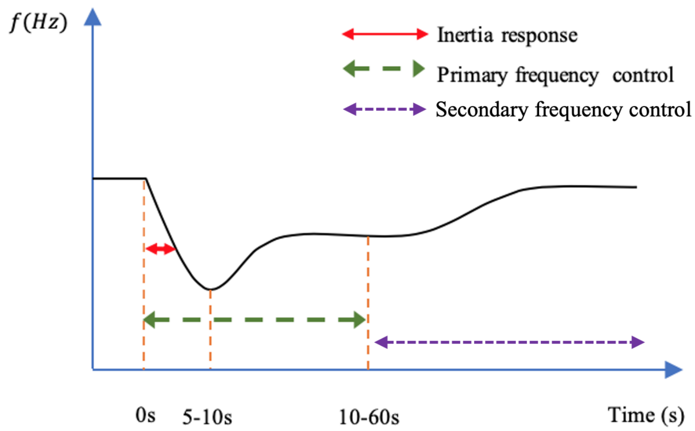

Figure 1.1: Typical frequency response after a generator trip.

severe frequency drop; this characteristic is called inertial response. The inertial response provided by synchronous generators or motors can reduce the ROCOF but can lasts for only a few seconds [120]. In power system analysis, the inertia characteristics are represented by the inertia constant, defined as the kinetic energy in watt-seconds at rated speed divided by the VA base, which mathematically serves as the time constant of the swing equation [128].

Primary Frequency Response

The primary frequency response is the first part of frequency control that stabilizes the frequency in response to frequency deviations. As rotor speed slows down, the turbine-governor senses the speed reduction and adjusts the prime movers output to stabilize the rotor speed [120]. The primary frequency response can be provided by generator governor, load, and other devices that can provide an immediate response based on their local control. Primary response is mainly determined by the proportional gain and the dynamics of the governors and turbines.

1.1.2 Frequency Performance with High Penetration of Renewable Energy

The electric grid underlies our economy and daily lives. Large and centralized power systems are changing fast to a hybrid system with high penetrations of DERs. Increased penetration of DERs results in unacceptable frequency excursions due to the deterioration of inertial response in the presence of disturbances. The primary frequency response deviation refers to the transient events since it denotes the part of the response before the steady-state condition. Most renewable resources such as WTGs are connected to the grid through inverters, reducing the natural inertial response to grid frequency changes. The doubly-fed induction generator (DFIG) can be controlled to compensate for this reduction and provide a faster response than traditional synchronous machines [83]. There are many worldwide occasions as an example for degradation in frequency response in the presence of renewable resources. For instance, a decline in the primary control response has been recorded in the Eastern Interconnection of the United States. Since 1994, the Eastern Interconnection primary control response has declined roughly 20% even though it should have been increasing in proportion to a 20% increase in customer demand [86].

Inadequate frequency response is defined as noncompliance with minimum ROCOF constraints that result by generators' ROCOF relays. Instantaneous minimum frequency requirements may also result due to under-frequency load shedding relays known as the nadir inadequacy [21]. The latter is the primary concern as larger excursions of frequency and tie-line power may trigger unnecessary relay actions, in which case enough capacity is available to achieve a safe and efficient steady-state operation in grids with high renewable penetration [128].

Time and space-variant system inertia will make the availability of frequency control services more uncertain and challenging in terms of the risk of significant frequency deviations [128]. High penetration of renewable causes larger inertia variations that take place in shorter time windows. Even at the same time, different locations could have different penetration levels, and thus frequency dynamics vary in separate areas. Therefore, situational awareness and adaptivity can be named a primary part of the frequency control that should be considered when adding supplementary frequency control loops in power systems.

1.1.3 Frequency Control with Inverter-Interfaced Resources

Recently, inverter-interfaced sources have received lots of attention as a grid-feeding part of grid-supporting functions. Primary frequency control can be equipped for most inverter-interfaced DERs, where WTGs are the most suitable candidate since the stored kinetic energy in the rotating mass can be readily utilized without additional storage [83]. Existing inertia emulation methods generally couple the stored kinetic energy of WTGs to the ROCOF [84, 51]. However, other applicable sources must operate at de-load conditions or integrate with energy storage units to contribute to frequency regulations. The main two categories for frequency control are known as synchronization signal-based [36, 125, 126] and supplementary signal-based primary frequency control methods [22, 51, 71, 84]. Supplementary signal-based primary frequency control is well known as a common method in power systems frequency regulation services.

Supplementary signal-based methods are the most common and representative methods to provide an additional signal to contribute to primary frequency control. This method provides a signal associated with the measured grid frequency deviation or its differential to the output power or defined speed reference value to be tracked [41, 128]. The ROCOF can be generated by filtering the frequency through a washout filter [51], while the synthetic primary control response consistent with the frequency deviation. For off-shore wind farms connected with high-voltage direct current (HVDC) transmission networks, the energy stored in the DC-link can contribute with the kinetic energy for a longer support duration [128, 48, 71]. However, the effective inertial response using such methods can be challenging to quantify as the emulated inertia constant is time-varying [117, 134, 83].

1.1.4 Frequency Control with Demand Response

The electric grid that underlies our economy is changing rapidly, and it is evolving from an architecture of centralized power generation to a hybrid system that incorporates DERs near the load. High penetration of DERs can result in severe frequency deviations in the presence of disturbances. Utilizing response from the demand side as a synthetic inertial response can help reduce ROCOF [81].

Utilizing demand control to provide grid services requires synchronized wide-area control of a significant number of loads to deliver the needed response. At the grid edge, consumers are connected to the grid with sensor arrays, high-speed networks, and advanced communications that create a dynamic space to generate, store, manage, and trade energy. The communication delays and packet losses in sensors and actuators are an essential challenge for inertia emulation control in power systems with DR [25], [137]. The illustration of frequency control with DR response and communication delay is shown in Fig. 1.2. As shown in this loop, for utilizing DR in frequency excursions, the communication infrastructure features, latency, and probability of packet losses play a crucial role by affecting the obtained supplementary frequency control signal.

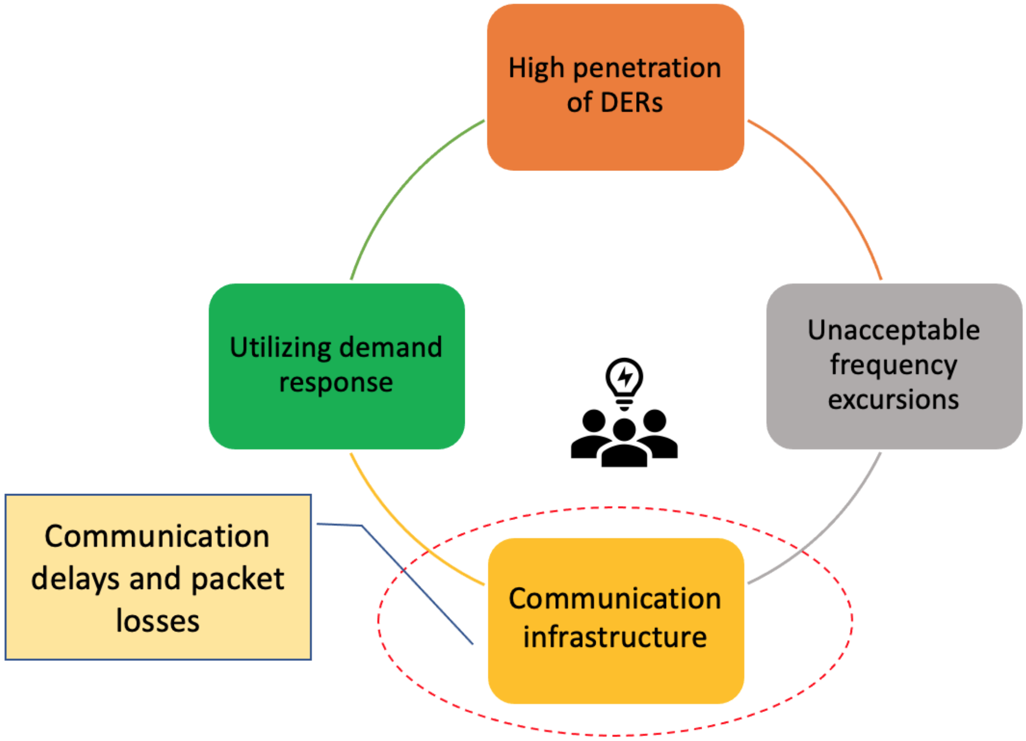

Figure 1.2: DR loop for frequency regulation.

1.2 Motivation and Objective

Despite the numerous suggested approaches for frequency control, utilizing these functions towards adequate frequency response, i.e., bounded within the defined safety, is challenging. Here, the term safety means a well-defined and allowable operating region, and a safe response means the trajectories of all concerned states stay within defined safety limits, see Fig. 1.3 [5]. Many studies have proposed different techniques for synthetic inertia emulation, and primary frequency control [16, 98, 114, 134, 132, 83, 81]. This dissertation proposes some robust frequency response considering different control approaches with performance guarantees.

One of the most challenging aspects lies in designing controllers for the large-scale power system models, including some nonlinearities. Providing a robust frequency regulation service is a critical point in control design. Model reduction is vital for the control design of large-scale systems such as the power grid, as they are governed by differential equations where the number of states can be extremely large [102]. The goal is to provide a low-dimensional model that has similar response characteristics as the original system and allows a level of storage and computational requirements manageable for practical design and implementation [9], [83]. Model reduction is also beneficial for implementation and deployment of dynamic feedback controllers which are dynamic systems and have the same order as the plant, in general. The full-order plant contains faster electromagnetic dynamics and slower electromechanical dynamics. The former are less relevant to the frequency response, while the latter dominate the frequency behavior. Without model reduction, the controller dynamics will also include the fast electromagnetic modes that are less relevant to the frequency response but require small steps to simulate, and consume computation resources of the embedded system once deployed [83].

Investigation of the effects of communication delays and packet losses on inertia emulation control in a power system is another challenge in frequency regulation service. Networked control systems (NCS) such as smart grids are spatially distributed systems in which the communication between sensors, actuators, and controllers occurs through a shared band-

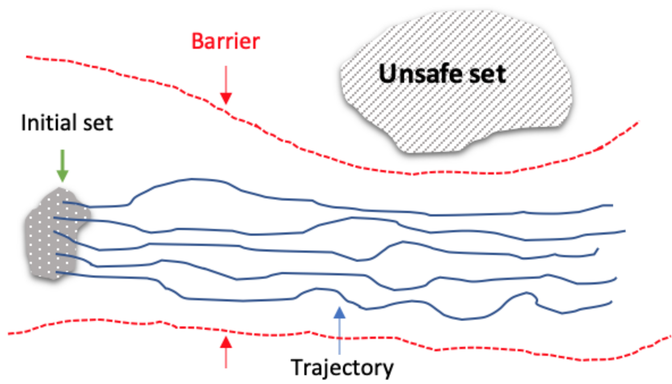

Figure 1.3: Safety verification by barrier function.

limited digital communication network [127]. This system structure requires ensuring data packets are successfully transmitted between the control components to ensure the reliability of such NCS. Addressing the network-induced delays and packet dropouts in NCS, a scalable and pervasive communication infrastructure is crucial in both the construction and operation of a smart grid [42]. As improved communication infrastructure are available with high reliability, security, and massive input-output capability, frequency regulation using DR can help in frequency regulation services in smart grids.

The aforementioned issues open a new door to the following research problem to provide accurate frequency control in the presence of disturbances. The accuracy of the frequency response can be indexed by a safe performance, where the safe performance means that all trajectories should be maintained in a defined safe region. As pointed out in [116], the available response time (equivalent to the deadband setting) for converter interfaced sources to maintain bounded frequency response is usually uncertain [128]. There are a few proposed methods for safety verification in frequency control of power system [134, 131]. In this dissertation, reachability using barrier function technique is introduced. A linear programming (LP) relaxation is suggested to analyze and synthesize the safety region based on the desired range of frequency deviations in the power system. The Handelman's based barrier certificate approach for guaranteed frequency performance is proposed, and validated using power system benchmark case studies with a discussion on further control guidelines.

1.3 Dissertation Outline

This dissertation is organized as follows:

In Chapter 2, a robust output feedback control design for inertia emulation by wind turbine generators is proposed. Necessary models for frequency control are developed, and system frequency response (SFR) model and the concept of inertia emulation is discussed. This work represents the WTG as a selected renewable converter-interfaced resource to help frequency regulation in an islanded microgrid. Balanced truncation model reduction technique is applied to the WTG and compared with selective modal analysis (SMA)-based model reduction technique. By combining the SFR model and the reduced-order model of the WTG, an augmented SFR is obtained. The emulated inertial and primary control responses are approximately evaluated by employing both linear quadratic regulator (LQR) and H_∞ methods in an output feedback control structure.

In Chapter 3, load-side control for frequency regulation is analyzed and investigated. This work examines inertial response and ROCOF in a power system with inverter-interfaced air conditioners (IACs). The control loop considers time delays and packet losses to show the need to switch to 5G networks as an improved communication infrastructure in future smart grids to have a guaranteed frequency regulation service.

In Chapter 4, a delay compensator for the DR controller using robust H_∞ and μ-synthesis control methods is proposed to guarantee inertial response and reduce the ROCOF in the presence of disturbances. The robust control method considers model uncertainties, including uncertain communication delays, governor dead-bands, and governor time constants. The approach is validated using an illustrative example of a power system with IACs, where the control loop includes defined parametric uncertainties.

In Chapter 5, the approaches on safety verification and its application in power systems for guaranteed frequency response are discussed. The proposed techniques are classified by set operation-based methods and passivity-based methods. The barrier certificate approach as a vital class of passivity-based methods is widely employed to obtain a region of safety (ROS). LP relaxation by Handelman's representation as an alternative to the sum of squares (SOS) for safety verification is proposed to encode the polynomial positivity problem and reduce this problem to linear programming.

In chapter 6, guaranteed frequency performance using the Handelman's based barrier certificate approach is proposed. The proposed method is successfully implemented and verified using power system benchmark examples. Further control guidelines on the barrier certificate approach are discussed and verified on a diesel/wind fed microgrid to provide guaranteed frequency response.

In chapter 7, the works in this dissertation are summarized, and future works are proposed.

1.4 Summary of Contributions

The contributions of this dissertation are summarized as follows:

- First, compared with the common inertia emulation methods for current-mode DERs that lead to time-varying synthetic inertia responses, this dissertation studies the model reference control (MRC) framework, which allows us to emulate the inertia precisely and provide guaranteed performance for the frequency response. The proposed method on the modified 33-node microgrid using a detailed full-order three-phase simulation model is verified in MATLAB Simulink.

- Since MRC is more of a control task than a design method, the output feedback LQR and H_∞ controls are proposed with the Luenberger observer to realize the MRC-based inertia emulation (IE). Compared with other proposed methods which use state-feedback control design, the technical benefits are freedom to use a variety of model reduction techniques, and more practical implementation since state measurements are not available all the time.

- The investigation of the effects of communication delays and packet losses on inertia emulation control in a power system with DR setting, where IACs represent the demand load, is presented. The need to use improved communication structures such as the 5G network is discussed and validated by comprehensive simulation results.

- The state-space representation of a power system with DR, including communication delays and governor dead-band is provided. The model uncertainties affecting the primary frequency response include the governor dead-band, governor time constant and uncertain communication delays. The governor dead-band as a critical operating component is included in the system dynamic model using an uncertain droop curve. The actual communication delay and dead-band are implemented in simulations to provide realistic results.

- The robust H_∞ and μ-synthesis output feedback delay compensation for primary frequency with DR is designed using both frequency deviation and ROCOF to provide accurate frequency regulation. The performance robustness is guaranteed in the presence of model uncertainties affecting the primary frequency response and disturbances. A comparative study of the proposed method and the conventional PI-based Smith predictor control method is presented.

- A set theory-based method for safety verification is presented. The Handelman's representation is introduced as a linear relaxation approach to show the barrier function's positivity. The proposed technique is verified on an illustrative example, and the application in power systems is discussed.

- The computational algorithm for Handelman's based barrier certificate approach to verify safety region for guaranteed frequency performance is presented. The proposed method is successfully implemented using power system benchmark examples, including SMIB, two-area power system, and diesel/ wind fed microgrid. The safety supervisory control (SSC) based on the barrier certificate approach is investigated on a diesel/wind fed microgrid to provide guaranteed frequency response.

Chapter 2

Robust Output Feedback Control for Inertia Emulation

This chapter proposes a robust output feedback control for inertia emulation using wind turbine generators and it is organized as follows. A mathematical model for frequency control is presented beside discussion on traditional SFR and the objective of inertia emulation control in Section 2.1. The diesel wind system modeling and the balanced truncation model reduction technique are presented in Section 2.2. The proposed model reduction technique is compared with the SMA-based model reduction. A LQR is designed and compared with an H_∞ control approach in Section 2.3. The proposed approach is validated by comprehensive simulation results in Section 2.4. The results in this chapter appeared in [83].

2.1 Inertial Response

Traditional frequency response in the presence of a disturbance is led by synchronous generators that limit the ROCOF by converting kinetic energy into electric power, known as the inertial response. As the rotor speed slows down, the turbine-governor system adjusts the prime mover output to arrest the speed deviation. The regulated primary frequency is related to the governor response [99], [60]. Due to the frequency dead-band and response time of the turbine-governor, the inertial response is dominant at the beginning of disturbance occurrence. The swing equation models this process:

$$2Hs\Delta\omega = \Delta P_m - \Delta P_d \tag{2.1}$$

where s is the Laplace operator, $2Hs\Delta\omega$ denotes the inertial response, $\Delta\omega$ denotes the primary frequency response and ΔP_d denotes the disturbance. With more renewable energy penetration, fewer synchronous generators will be committed leading to smaller inertia H in the system, and potentially inadequate inertial response. Wind turbines, for example, are effectively decoupled from grid frequency and will not naturally respond to frequency changes. Thus, controls must be designed to limit the ROCOF if grid support is needed. Controlling the power output proportional and opposing the ROCOF is known as inertia emulation. The traditional approach of an inertia emulation strategy for a WTG is illustrated in Fig. 2.1. In a such strategy, the stored kinetic energy in a WTG will be released in proportion to ROCOF. The speed of the induction motion will decline due to the energy conversion [118]. Considering the conceptual representation of the inertia emulation in Fig. 2.1 (b), the swing equation is compensated by the power from the WTG:

$$2Hs\Delta\omega = \Delta P_m - \Delta P_d + \underbrace{G_w(s)K_{\text{ie}}s\Delta\omega}_{\Delta P_g} \tag{2.2}$$

where $G_w(s)$ represents the dynamic response of WTG to generate the inertia emulation power ΔP_g according to the ROCOF $K_{\text{ie}}s\Delta\omega$. As described in [132] and [84], the configuration in Fig. 2.1 can only produce synthetic inertial response where the equivalent parameters are time varying and may be difficult to tune. This is easy to see if we rearrange (2.2) as follows:

$$(2H - G_w(s)K_{\text{ie}})s\Delta\omega = \Delta P_m - \Delta P_d \tag{2.3}$$

This poses challenges for dynamic security assessment, stability analysis and system performance guarantees. See [132] and [118] for details on the derivation of equivalent parameters of frequency response model under emulated inertia.

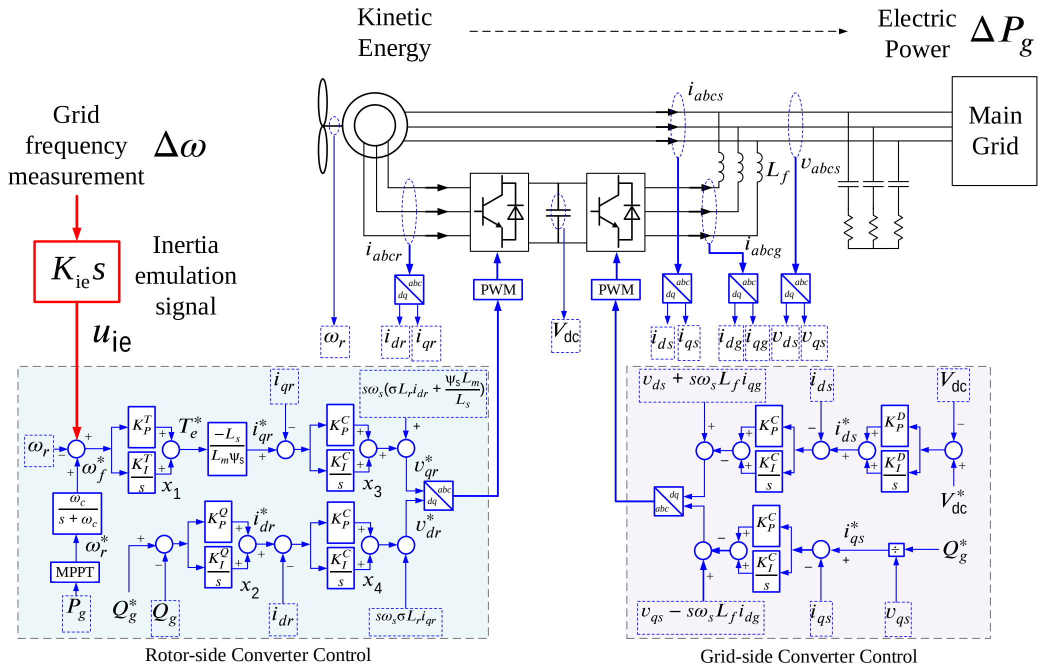

(a)

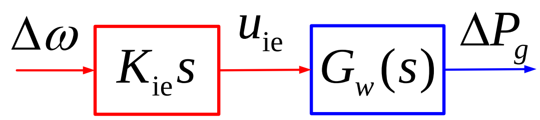

(b)

Figure 2.1: Traditional inertia emulation function within a wind turbine. (a) Detailed view. (b) Conceptual view.

To overcome the aforementioned difficulties, the objective of the proposed controller is to provide a specific amount of inertia emulation to achieve near-ideal response in the time scale of inertial response in the sense that the equivalent parameters are nearly constant [83]. In other words, we need to compensate the negative effect induced by $G_w(s)$ in (2.3), which mainly includes the primary mover dynamics and the internal controller response time which is inherent and cannot be compensated by external controllers. So the synthetic inertial response can only be "near-ideal" compared with the conventional inertial response. Fortunately, inner control loops of the converter are too fast (in the time scale of milliseconds) to have sizable impacts on the frequency control [107]. On the other hand, the negative impact induced by the primary mover dynamics, that is, the motion dynamics of the WTG, can be compensated.

The idea to achieve near-ideal synthetic inertial response of WTG can be recast as a tracking problem with respect to a dynamic reference model, known as the MRC. In the MRC, we define a frequency response model with desired parameters as the reference. The objective is to make the DSG speed precisely track the reference frequency using the support from the WTG as shown in Fig. 2.2. Intuitively, the frequency response of the augmented physical plant consisting of the diesel generator and the WTG will be the same as the response of the reference model. Therefore, the emulated inertia constant is close to the one of the reference model. To see this, let $2H_{rf}s\Delta\omega_{rf}$ and $2H_D s\Delta\omega_d$ be the inertial response of the reference model and DSG in Fig. 2.2, respectively, where H_{rf} is the desired inertia constant and $H_{rf} - H_D = H_{\mathrm{ie}} > 0$. The power balance condition holds as:

$$\Delta P_d = 2H_{rf}s\Delta\omega_{rf} = 2H_D s\Delta\omega_d + \Delta P_g \tag{2.4}$$

If the speed of DSG can track the speed of the reference model with the support of WTG, that is, $\Delta\omega_{rf} \approx \Delta\omega_d$, then the following relation holds:

$$\Delta P_g \approx 2H_{rf}s\Delta\omega_d - 2H_D s\Delta\omega_d = 2H_{\mathrm{ie}}s\Delta\omega \tag{2.5}$$

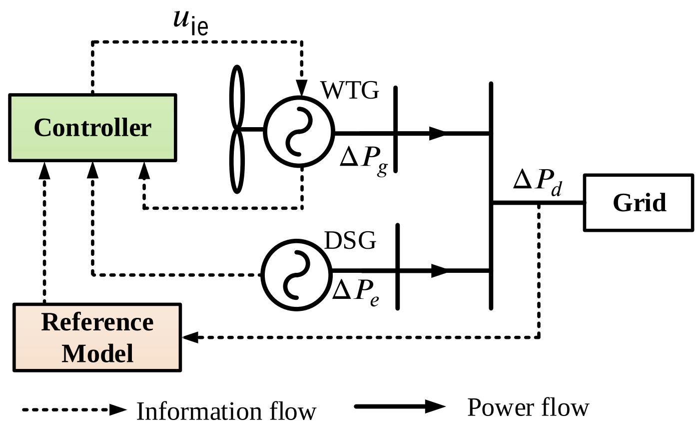

Figure 2.2: Model reference control-based inertial emulation control diagram.

Therefore, the synthetic inertial response $2H_{\mathrm{ie}}s\Delta\omega_d$ is emulated by the WTG. Traditional strategy in Fig. 2.1 can be considered as an open-loop control with respect to the WTG since no status information of the WTG is fed back to the inertia emulation module. Since the MRC-based inertia emulation generates the control signal using both grid frequency and WTG states as shown in Fig. 2.2, it can compensate the negative effect induced by the motion dynamics of WTG. Nevertheless, the MRC is more of a control task than a design methodology. In the following, a mathematical model incorporating both the diesel and WTG will be derived, where an output feedback LQR and H_∞ controllers will be designed to realize the MRC-based inertia emulation.

2.2 Diesel-Wind System Modeling

In this section, the dynamic model of the WTG is presented. The wind turbine model is assumed to be a type-3 WTG, which is one of the most common wind turbines used in practice. Type-3 wind turbines are also called DFIG-based wind turbines. Note that the proposed paradigm can be applied to any type of converter-interfaced DERs. But WTGs are more readily suitable due to their inherit kinetic energy.

2.2.1 Wind Power and Wind Turbine

The power output of wind turbine in the form of kinetic energy in the wind crossing at a speed v_{wind} [m/s] and surface A_{wt} [m^2] is expressed by [1]

$$P_{\mathrm{wind}} = \frac{1}{2}\rho \underbrace{\pi R_t^2}_{A_{wt}} v_{\mathrm{wind}}^3 \quad \text{[W]} \tag{2.6}$$

where ρ denotes the air density, R_t is the radius of the wind turbine in meter and A_{wt} represents the wind turbine swept area. The output power of the wind turbine from P_{wind} can be obtained by [128]

$$P_M = \frac{1}{2}\rho \underbrace{\pi R_t^2}_{A_{wt}} v_{\text{wind}}^3 C_P(\lambda, \theta_t) \quad \text{[W]} \tag{2.7}$$

The term $C_P(\lambda, \theta_t)$ denotes the power coefficient, as a dimensionless parameter that describes the energy extraction efficiency of a wind turbine, and is usually as a function of the tip speed ratio λ and the pitch angle θ_t [degree] [128].

The relation between the turbine speed and the rotor mechanical and electric speed of the electric machine can be expressed by

$$\omega_R = p \times \omega_M = p \times k \times \omega_T \quad \text{[rad/s]} \tag{2.8}$$

$$\omega_r = \omega_m = \omega_t \quad \text{[p.u.]} \tag{2.9}$$

where ω_T is the turbine speed, ω_M and ω_R are the rotor mechanical and electric speed of the electric machine, respectively. k represents the gear ratio between the turbine and the machine, and p is the pole pair number of the electric machine [128]. Here, the tip speed ratio is

$$\lambda = \frac{v_{tip}}{v_{\text{wind}}} = \frac{R\omega_T}{v_{\text{wind}}} = \frac{R\omega_R}{pkv_{\text{wind}}} = \frac{R\omega_r \overline{\omega}_R}{pkv_{\text{wind}}} \tag{2.10}$$

where (2.11) is the common expression used for the power coefficient [99].

$$C_p = 0.22 \left(\frac{116}{\lambda_i} - 0.4\theta_t - 5 \right) e^{-\frac{12.5}{\lambda_i}} \tag{2.11}$$

and,

$$\lambda_i = \left(\frac{1}{\lambda + 0.08\theta_t} - \frac{0.035}{\theta_t^3 + 1} \right)^{-1} \tag{2.12}$$

The theoretical maximum value of the power coefficient is 0.593, i.e., $C_{P,\max} = 0.593$, which is the so-called Betz's limit [1]. The mechanical torque input to the electric machine can be defined as

$$T_M = \frac{P_M}{\omega_M} \quad \text{[Nm]} \tag{2.13}$$

In this dissertation instead of aggregating hundreds of WTGs in a wind farm, we will use one electric machine with the desired rating and scale the wind turbine up closely to this rating.

2.2.2 Doubly-Fed Induction Generator and Converter Model

The converter of the wind turbine generator includes the rotor-side and grid-side converters, which control the speed of the generator and inject power into the grid, respectively [49]. Since, the rotor-side converter controls the generator speed by regulating the electromagnetic torque, the frequency support function should be included within this subsystem. The grid-side converter has less impact on the frequency support since the time scale of the DC regulation is much faster than the rotor-side control current loop for stability reasons [132].

The differential equations of the fluxes in the dq axes and algebraic equations of the DFIG are given by:

$$\frac{d\lambda_{qs}}{dt} = \omega_b[V_{qs} - R_s i_{qs} - \omega_s \lambda_{ds}] \tag{2.14}$$

$$\frac{d\lambda_{ds}}{dt} = \omega_b[V_{ds} - R_s i_{ds} + \omega_s \lambda_{qs}] \tag{2.15}$$

$$\frac{d\lambda_{qr}}{dt} = \omega_b[V_{qr} - R_r i_{qr} - (\omega_s - \omega_r)\lambda_{dr}] \tag{2.16}$$

$$\frac{d\lambda_{dr}}{dt} = \omega_b[V_{dr} - R_r i_{dr} + (\omega_s - \omega_r)\lambda_{qr}] \tag{2.17}$$

$$\lambda_{qs} = L_s i_{qs} + L_m i_{qr} \tag{2.18}$$

$$\lambda_{ds} = L_s i_{ds} + L_m i_{dr} \tag{2.19}$$

$$\lambda_{qr} = L_r i_{qr} + L_m i_{qs} \tag{2.20}$$

$$\lambda_{dr} = L_r i_{dr} + L_m i_{ds} \tag{2.21}$$

The dynamics of the induction machine are presented in (2.22)-(2.27), where, τ_m and τ_e are the mechanical and electromagnetic torques ($\tau_e = (L_m/L_s)(\lambda_{qs}i_{dr} - \lambda_{ds}i_{qr})$). $\omega_{f_{ref}}$ is the filtered reference speed for the wind turbine generator and $\omega_{r_{ref}}$ is the reference rotor speed which is computed as an optimal speed based on the maximum power point tracking (MPPT) curve in a relation with the measured electric power as shown in Fig. 2.3 (Eq. (2.28)) [115], [83]. The state variables related to the speed controller of the WTG are represented as x_1 and x_2. Also, x_3 and x_4 are defined as state variables related to the reactive power controller. Q_g and P_g are the reactive and active power of the wind turbine generator [99].

$$\frac{d\omega_r}{dt} = \frac{(\tau_m - \tau_e)}{2H_w} \tag{2.22}$$

$$\frac{d\omega_{f_{ref}}}{dt} = \omega_c(\omega_{r_{ref}} - \omega_{f_{ref}}) \tag{2.23}$$

$$\frac{dx_1}{dt} = K_{I_\tau}(\omega_{f_{ref}} - \omega_r + u_c) \tag{2.24}$$

$$\frac{dx_2}{dt} = K_{I_Q}(Q_{ref} - Q_g) \tag{2.25}$$

$$\frac{dx_3}{dt} = K_{I_c}(i_{qr_{ref}} - i_{qr}) \tag{2.26}$$

$$\frac{dx_4}{dt} = K_{I_c}(i_{dr_{ref}} - i_{dr}) \tag{2.27}$$

$$\omega_{r_{ref}} = -0.67(P_g)^2 + 1.42(P_g) + 0.51 \tag{2.28}$$

The algebraic relations of the electric power are expressed in (2.29) and (2.30). The loop of algebraic equations is closed by the algebraic relations in (2.31) and (2.32) [132], where $\sigma = (L_rL_s - L_m^2)/(L_rL_s)$ is the leakage coefficient of the induction machine.

$$P_g = V_{qs}i_{qs} + V_{ds}i_{ds} + V_{qr}i_{qr} + V_{dr}i_{dr} \tag{2.29}$$

$$Q_g = V_{qs}i_{ds} - V_{ds}i_{qs} + V_{qr}i_{dr} - V_{dr}i_{qr} \tag{2.30}$$

$$\begin{aligned} V_{qr} &= x_3 + K_{P_c}(i_{qr_{ref}} - i_{qr}) \\ &+ (\omega_s - \omega_r)(\sigma L_r i_{dr} + (\frac{\Psi_s L_m}{L_s})) \end{aligned} \tag{2.31}$$

$$V_{dr} = x_4 + K_{P_c}(i_{dr_{ref}} - i_{dr}) - (\omega_s - \omega_r)(\sigma L_r i_{qr}) \tag{2.32}$$

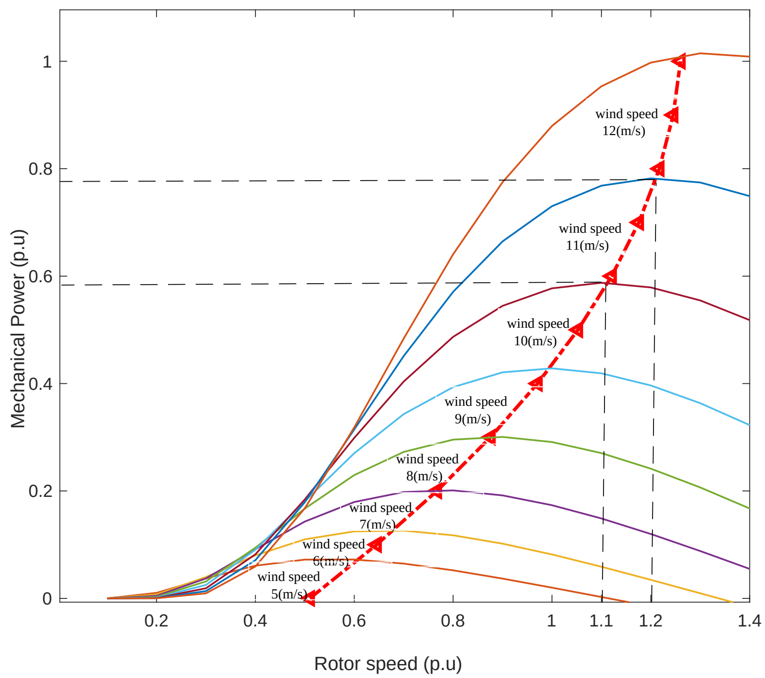

Figure 2.3: Mechanical power extracted from wind turbine based on rotor speed.

where $i_{qr_{ref}}$ and $i_{dr_{ref}}$ are expressed by (2.33) and (2.34).

$$i_{qr_{ref}} = \frac{-L_s \tau_{e_{ref}}}{L_m \Psi_s} \tag{2.33}$$

$$i_{dr_{ref}} = x_2 + K_{P_Q}(Q_{g_{ref}} - Q_g) \tag{2.34}$$

The model used for the DSG is the complete model as described in (2.35)-(2.37). This model shows speed changes of the diesel generator based on power, mechanical power and valve position variations [134], [60].

$$\frac{d\Delta\omega_d}{dt} = \frac{f_b}{2H_D}(\Delta P_m - (\Delta P_d - \Delta P_g)) \tag{2.35}$$

$$\frac{d\Delta P_m}{dt} = \frac{1}{\tau_d}(-\Delta P_m + \Delta P_v) \tag{2.36}$$

$$\frac{d\Delta P_v}{dt} = \frac{1}{\tau_{sm}}(-\Delta P_v - (\frac{\Delta\omega_d}{f_b R_D})) \tag{2.37}$$

Here, ΔP_d is the disturbance which is the measured power flow variation at a specified location [132] as shown in Fig. 2.2.

2.2.3 Model Reduction Technique

To reinforce the analysis in the following chapters, a reduced-order model of the WTG is derived. Model reduction is critical for control design of large-scale systems, such as the power grid, as they are governed by differential equations where the number of states can be extremely large [102]. The goal is to provide a low-dimensional model that has a similar response characteristics as the original system and allows a level of storage and computational requirements manageable for practical design and implementation [9].

The model reduction is also beneficial for implementation and deployment of dynamic feedback controllers which are dynamic systems and have the same order as the plant. The full-order plant contains faster electromagnetic dynamics and slower electromechanical dynamics. The former is less relevant to the frequency response, while the latter dominates the frequency behavior. Without model reduction, the controller dynamics will also contain the fast electromagnetic modes that are less relevant to the frequency response but require small steps to simulate, and consume considerable computation resources of the embedded system once deployed [83].

One popular model reduction technique is the balanced truncation, which is a simple efficient model reduction technique broadly used in reducing model orders of high order linear systems. Balanced reduction was first introduced by Moore [80]. It has been shown to provide accurate reduced order model representations of state-space systems. Since the reduction procedure is based only on system inputs and outputs, model reduction may be heavily dependent on the scaling of the states. However, balanced truncation is independent of the particular system scaling since it uses balanced state space realizations [122].

This dissertation presents the balanced reduction method for large scale power systems instead of the traditional reduction method defined as SMA [132]. Although the SMA method has a nice physical interpretation in many cases, it is not the ideal method from a control point of view, since it only relies on certain modes to reduce the order of a large model. This dissertation is suggesting a more accurate method that can maintain the main dynamical features of the whole system in the reduced model. The characteristic of this method can help us provide a reliable reduced order model and design a proper, optimized and robust controller to guarantee desired performance.

Assume a stable linear time-invariant system as illustrated by the n dimensional state-space model in (2.38).

$$\dot{x}(t) = Ax(t) + Bu(t);\;\; y(t) = Cx(t) \tag{2.38}$$

In balanced truncation, a balanced realization is first obtained to make the controllability and observability Gramians Q_c and Q_o equal to the diagonal matrix of the Hankel singular values, i.e., $\Sigma = diag(\sigma_1, \ldots, \sigma_N)$. These two Gramians should satisfy the Lyapunov equations:

$$\begin{aligned} AQ_c + Q_cA^T + BB^T &= 0 \\ A^TQ_o + Q_oA + C^TC &= 0 \end{aligned} \tag{2.39}$$

In addition, Q_c and Q_o form the bases for the controllable and observable subspaces [19]. Hence, the system is balanced when the controllability and observability Gramians are equal [136].

The controllability and observability Gramians are described as follows [136]:

$$Q_o = \int_0^\infty e^{A^T t} C^T C e^{At} dt;\ Q_c = \int_0^\infty e^{At} B B^T e^{A^T t} dt \tag{2.40}$$

In order to transform a realization into a balanced form, a coordinate transformation matrix T is needed to transform the balanced state vector x_b to the original state vector x, where, $x = Tx_b$, such that the transformed observability and controllability Gramians are diagonal and equal [122] as computed by the following equations:

$$\tilde{Q}_o = T^{-T} Q_o T^{-1};\ \tilde{Q}_c = T Q_c T^T \tag{2.41}$$

The transformation T can be computed by first calculating the matrix $Q_{co} = Q_c Q_o$ [19] and determining its eigenmodes $Q_{co} = T\Sigma^2 T^{-1}$. Note that the transformation T is chosen such that the following identities are satisfied [136]:

$$\tilde{Q}_c = \tilde{Q}_o = T^{-1} Q_c T^{-T} = T^T Q_o T := \Sigma \tag{2.42}$$

So, the balanced state-space model (2.38) is obtained by taking $TA_bT^{-1} = A$, $C_bT^{-1} = C$ and $TB_b = B$ [136]:

$$\dot{x}_b(t) = A_b x_b(t) + B_b u(t); \quad y_b(t) = C_b x_b(t) \tag{2.43}$$

The balanced realization gives us the new order of states based on observability and controllability, where the first states are the most controllable and observable states [19]. Hence, (2.44) expresses the reduced order model by keeping n_r states $(x_1, \ldots, x_{n_r})$ that are the most controllable and observable states and most relevant from the control viewpoint

[122].

$$\dot{x}_r(t) = A_r x_r(t) + B_r u(t);\;\; y_r(t) = C_r x_r(t) \tag{2.44}$$

Therefore, we can compute the reduced state space matrices using $T_r = \begin{bmatrix} I_r & 0 \end{bmatrix} T$ as:

$$A_r := \begin{bmatrix} I_r & 0 \end{bmatrix} T^{-1} A T \begin{bmatrix} I_r \\ 0 \end{bmatrix};\;\; B_r := \begin{bmatrix} I_r & 0 \end{bmatrix} T^{-1} B;\;\; C_r := CT \begin{bmatrix} I_r \\ 0 \end{bmatrix} \tag{2.45}$$

The error bound of balanced truncation is given by [136]:

$$\Big\| y(t) - y_r(t) \Big\|_2 \leq 2 \sum_{n_r+1}^{n} \sigma_i \Big\| u(t) \Big\|_2;\;\; \forall u \in L^2 \tag{2.46}$$

where L^2 denotes the space of finite energy signals (i.e., the measurable square integrable functions). In order to make the controller design procedure simple, a reduced linearized model about the equilibrium point for the type-3 WTG based on balanced reduction technique is used. A comparison with the SMA technique proposed in [132] is presented. It provides us with a benchmark on how close the reduced model is to the full order linearized model and its performance for all frequency ranges. The linearized full order model of the WTG around the equilibrium point is given as:

$$\Delta \dot{x}_f = A_f \Delta x_f + B_f u_c;\;\; \Delta y_f = C_f \Delta x_f + D_f u_c \tag{2.47}$$

where

$$x_f = \Big[\lambda_{qs}, \lambda_{ds}, \lambda_{qr}, \lambda_{dr}, \omega_r, \omega_{f_{ref}}, x_1, x_2, x_3, x_4 \Big]^T \tag{2.48}$$

The full order model is a 10^{th} order model and Δ gives the variation of each variable around the equilibrium. Δy_f is considered as the WTG power output variation, (P_g), due to the inertia emulation input. Then, the reduced order model of the WTG is expressed in (2.49), where we keep only the most controllable and observable states with the highest

Hankel singular value magnitudes and truncate the rest of the state variables from the reduced realization. In other words, we are eliminating the states that are at the same time difficult to control and difficult to observe [9].

$$\Delta \dot{x}_{red}(t) = A_{red}\Delta x_{red} + B_{red}u_c$$
$$\Delta y_{red} = C_{red}\Delta x_{red} + D_{red}u_c \tag{2.49}$$

where, A_{red}, B_{red}, C_{red} and D_{red} are the state, control input, output and control feed-forward matrices of the reduced order model, respectively.

2.3 Robust Observer-Based Control Design

In this section, two different control methods, a LQR and a static state feedback H_∞ control for reference tracking are proposed. Since not all the state variables are available for measurements and only the reduced model is used in the control design stage, a Luenberger observer to estimate the state variables based on the measurements is employed. This results in dynamic output feedback LQR and H_∞ controllers.

2.3.1 Linear Quadratic Regulator

A tracking problem is considered for a defined physical plant as an aggregated model of the DSG and WTG. This physical plant is the combination of (2.35)-(2.37) and (2.49) which is given by:

$$\dot{x}_p = A_p x_p + B_p u_c + E_p u_d; \; y_p = C_p x_p \tag{2.50}$$

where, $x_p = \left[\Delta\omega_d, \Delta P_m, \Delta P_v, \Delta x_{r1}, \Delta x_{r2}, \Delta x_{r3}, \Delta x_{r4}\right]^T$, $y_p = \Delta\omega_d$ and u_d is the disturbance that is considered as the measured power flow variation [132] shown in Fig. 2.2 and the state-space model is

$$A_p = \begin{bmatrix} 0 & \frac{f_b}{2H_D} & 0 & \frac{f_b[C_{red}]}{2H_D} \\ 0 & \frac{-1}{\tau_d} & \frac{1}{\tau_d} & 0_{1\times 4} \\ \frac{-1}{f_b \tau_{sm} R_D} & 0 & \frac{-1}{\tau_{sm}} & 0_{1\times 4} \\ 0_{4\times 1} & 0_{4\times 1} & 0_{4\times 1} & [A_{red}] \end{bmatrix}; B_p = \begin{bmatrix} \frac{f_b[D_{red}]}{2H_D} \\ 0 \\ 0 \\ [B_{red}] \end{bmatrix}$$

$$E_p = \begin{bmatrix} \frac{-f_b}{2H_D} \\ 0 \\ 0 \\ 0_{4\times 1} \end{bmatrix}; C_p = \begin{bmatrix} 1 & 0 & 0 & 0 & 0 & 0 & 0 \end{bmatrix}$$

The reference signal ($\Delta\omega_{drf}$) for tracking is specified from the reference model similar to the DSG model as:

$$\dot{x}_{rf} = A_{rf} x_{rf} + E_{rf} u_{d_{rf}};\ y_{rf} = C_{rf} x_{rf} \tag{2.51}$$

where $x_{rf} = \begin{bmatrix} \Delta\omega_{drf}, \Delta P_{mrf}, \Delta P_{vrf} \end{bmatrix}^T$, $y_{rf} = \Delta\omega_{drf}$ and

$$A_{rf} = \begin{bmatrix} \frac{-f_b D_{rf}}{2H_{rf}} & \frac{f_b}{2H_{rf}} & 0 \\ 0 & \frac{-1}{\tau_{drf}} & \frac{1}{\tau_{drf}} \\ \frac{-1}{f_b \tau_{smrf} R_{rf}} & 0 & \frac{-1}{\tau_{smrf}} \end{bmatrix}; E_{rf} = \begin{bmatrix} \frac{-f_b}{2H_{rf}} \\ 0 \\ 0 \end{bmatrix}; C_{rf} = \begin{bmatrix} 1 & 0 & 0 \end{bmatrix}$$

To formulate the control problem, we consider the LQR cost function:

$$J = \int_0^\infty [x^T Q x + u^T R u] dt \tag{2.52}$$

where $Q = C^T Q' C$ is a diagonal, symmetric, positive semi-definite matrix of $\Delta\omega_d - \Delta\omega_{drf}$ weights and R is a diagonal, symmetric, positive definite matrix of control weights. The optimal control problem minimizes (2.52) over all controls $u \in L^2(0, \infty)$ with the tracking constraint. The LQR problem has a unique solution for a controllable system and the optimal input u^* is given by [136]:

$$u^* = -Kx = -\begin{bmatrix} K_p, K_{rf} \end{bmatrix} x \tag{2.53}$$

Finally, the augmented closed loop system $x_{aug} = \begin{bmatrix} x_p, x_{rf} \end{bmatrix}^T$ is defined below:

$$\begin{aligned} \dot{x}_{aug}(t) &= \hat{A} x_{aug}(t) + \hat{B} x_{aug}(t) + \hat{E} d(t) \\ y(t) = y_p - y_{rf} &= \hat{C} x_{aug}(t) + \hat{D} x_{aug}(t) \end{aligned} \tag{2.54}$$

where, $d = \begin{bmatrix} u_d, u_{d_{rf}} \end{bmatrix}$, $\hat{C} = \begin{bmatrix} C_p, -C_{rf} \end{bmatrix}$, $\hat{D} = \begin{bmatrix} D_p K_p, D_p K_{rf} \end{bmatrix}$, $\hat{A} = \begin{bmatrix} A_p & 0 \\ 0 & A_{rf} \end{bmatrix}$, $\hat{B} = \begin{bmatrix} B_p K_p & B_p K_{rf} \\ 0 & 0 \end{bmatrix}$ and $\hat{E} = \begin{bmatrix} E_p & 0 \\ 0 & E_{rf} \end{bmatrix}$.

To compute the feedback law, the observer in (2.55) is used to estimate the states and we use the physical plant output measurements to get an output feedback controller as an inertia emulation controller. Therefore, the LQR based-observer controller is expressed as follows:

$$\begin{aligned} \dot{\hat{x}}(t) &= \hat{A}\hat{x}(t) + \hat{B} u^* + L(y(t) - \hat{y}(t)) + \hat{E} d(t) \\ \hat{y}(t) &= \hat{C}\hat{x}(t) \end{aligned} \tag{2.55}$$

which can be written as:

$$\dot{\hat{x}}(t) = (\hat{A} + \hat{B}K - L\hat{C})\hat{x}(t) + Ly(t) + \hat{E}d(t)$$
$$u_{ie} = K\hat{x}(t) \tag{2.56}$$

where L is any matrix such that $\hat{A} - L\hat{C}$ is stable [136].

2.3.2 H_∞ Control

The theoretical formulation of the H_∞ control problem has been addressed in many books and papers, see [136] for example. In this section, a static state feedback control for reference tracking based on the H_∞ control structure is used that is fully described in [132]. In this case, the objective is the sub-optimal problem:

$$\min \left\| G_{y/d} \right\|_\infty < \gamma\,; \quad \gamma > 0 \tag{2.57}$$

where $G_{y/d}$ is the transfer function from the disturbance to the tracking error where $\left\| G_{y/d} \right\|_\infty$ is defined as $\sup_{ess} \bar{\sigma}(G_{y/d}(j\omega))$ [136]. $\bar{\sigma}(.)$ is the largest singular value of $G_{y/d}(j\omega)$. Equivalently, we can solve the multi-objective optimization problem defined in (2.58). Necessary and sufficient conditions for solving this problem are presented in [132]:

$$\min \gamma + \alpha + \beta$$
$$\begin{bmatrix} -\alpha I & \bar{K} \\ \bar{K} & -I \end{bmatrix} < 0\,, \quad \begin{bmatrix} \beta I & I \\ I & -\bar{P} \end{bmatrix} > 0\,, \quad \bar{F} < 0 \tag{2.58}$$

where there exists scalar variables $\gamma, \alpha, \beta > 0$ and matrix variables $\bar{P}, \bar{Q}, \bar{L}_i > 0$, $\bar{M}_i, \bar{V}_i$ for $i = 1, 2$ and $\bar{K}$. $\bar{F}$ is a symmetric linear matrix inequality (LMI), which can be computed based on [132]. Therefore, the controller given in (2.53) can guarantee the system performance, where the static gain $K = \bar{K}\bar{P}^{-1}$. Hence, similar to the LQR case, the use of the Luenberger observer gives a dynamic controller based on the computed static H_∞ control, and results in a dynamic output feedback controller.

The control structure for the LQR and H_∞ as output feedback control for reference tracking based on inertia emulation control is illustrated in Fig. 2.4. The controller $\hat{K}$ is a dynamic output feedback controller based on the observer expressed in (2.56). The signal d represents disturbances and Z represents measurements while y denotes the observed outputs ($\Delta\omega_d$ and $\Delta\omega_{drf}$) from the physical plant. The dynamic of the controller $\hat{K}$ can be represented by

$$\begin{aligned} \dot{\hat{x}}(t) &= (\hat{A} + \hat{B}K - L\hat{C})\hat{x}(t) + Ly(t) \\ u_{ie}(t) &= K\hat{x}(t) \end{aligned} \tag{2.59}$$

where the controller K is designed based on the LQR or H_∞ control techniques.

2.4 Modified 33-Bus Microgrid Simulation Results

The proposed controllers are applied to a modified 33-bus microgrid simulated using MATLAB Simulink platform [13], [104], [83]. The closed-loop system performance is tested using the single diesel-wind system described in [132]. The WTG model is modified based on the DFIG in the Simulink demo library by changing the aerodynamic model to the one detailed in [99], where a two-mass model is reduced to the swing equations with combined inertia of the turbine and generator [132].

For simulation purposes, time constants of turbine-governor system in the reference model are considered equal to that in the diesel synchronous generator. Moreover, we only consider tuning the inertia constants of the reference model and do not emulate load damping effects [87]. The system parameters are given in Appendix A.1.

2.4.1 Model Reduction Results

The reduced 4^{th} order model of the WTG is expressed in (2.61). Since there are only 4 states with the highest Hankel singular value magnitudes, only the 4 most controllable and observable states are kept and the rest of the state variables are truncated from the reduced

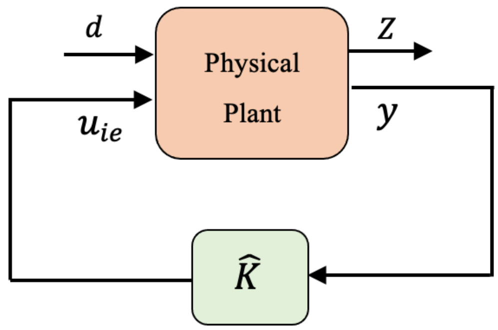

Figure 2.4: Output feedback observer-based control.

realization [83]. In other words, the states that are at the same time difficult to control and difficult to observe are eliminating [9]. The Hankel singular values are:

$$H_s = [1.6 \quad 1.2 \quad 1.1 \quad 1.1 \quad 0.02 \quad 0.01 \quad 0.003 \quad 0.0005 \quad 0 \quad 0]^T \tag{2.60}$$

Observe the sharp decrease in the magnitudes of the singular values after the 4^{th} one justifying keeping only 4 state variables and eliminating the rest in the following reduced model:

$$\begin{aligned} \Delta\dot{x}_{red}(t) &= A_{red}\Delta x_{red} + B_{red}u_c \\ \Delta y_{red} &= C_{red}\Delta x_{red} + D_{red}u_c \end{aligned} \tag{2.61}$$

where,

$$A_{red} = \begin{bmatrix} -638.5 & -35.1 & 72.05 & -288.3 \\ 35.1 & -0.06 & 0.13 & -101.1 \\ -72.05 & 0.13 & -0.28 & 353.7 \\ -288.3 & 101.1 & -353.7 & -135.6 \end{bmatrix};\ B_{red} = \begin{bmatrix} -45.87 \\ 0.37 \\ -0.8 \\ -17.25 \end{bmatrix}$$
$$C_{red} = \begin{bmatrix} 45.87 & 0.37 & -0.8 & 17.25 \end{bmatrix};\ D_{red} = 0.94$$

A comparison of the accuracy using balanced truncation and SMA methods are presented in Fig. 2.5. As shown, we can capture the full order model precisely. In addition, H_∞ norms for the difference between the reduced model transfer function and the full order transfer function $\left(\left\|G_{full} - G_{red}\right\|_\infty\right)$, where $\left\|.\right\|_\infty$ is the H_∞-norm, are given in Table 2.1. Balanced truncation can reduce the order of the model with a much lower H_∞ norm, validating the accuracy.

The responses of the nonlinear system and the reduced order linear model are compared in Fig. 2.6 in order to validate the latter under a step signal input. As shown in Fig. 2.6, the modeling error using the balanced truncation is not significant. The mean squared error between the reduced order model and nonlinear model for the speed of the DSG (ω_d),

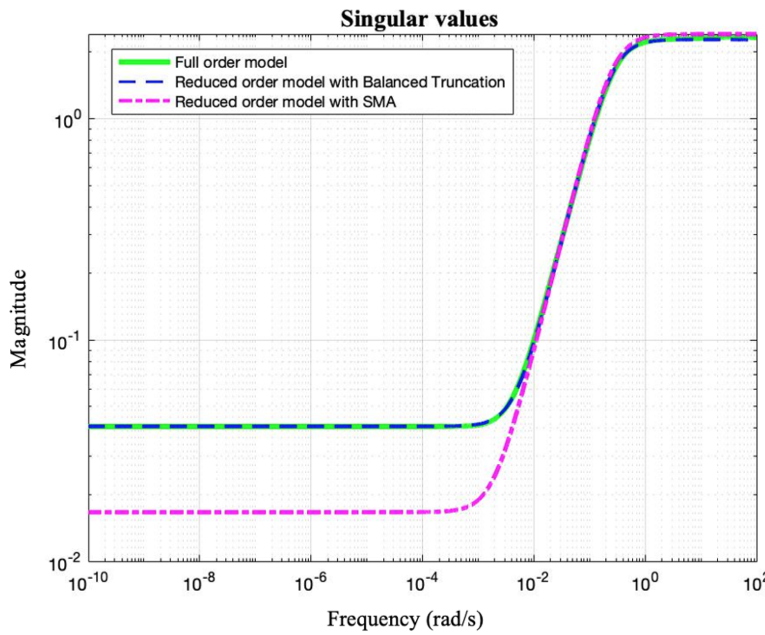

Figure 2.5: Singular values of full order model and reduced models.

Table 2.1: H_∞ norms comparison of reduced ordered models

Reduction Method	H_∞ Norm
Balanced Truncation	0.065
SMA	3.707

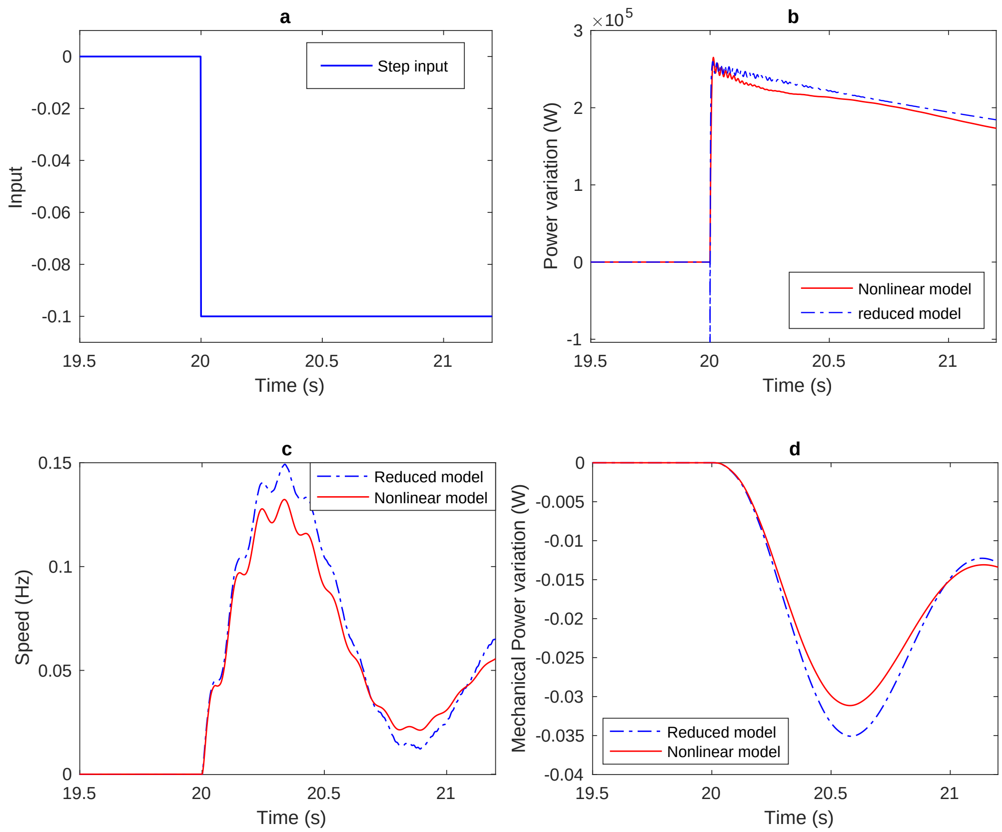

Figure 2.6: Response comparison of nonlinear and reduced order model physical plant. (a) Step input. (b) WTG active power variation. (c) Speed of DSG. (d) Mechanical power variation of diesel generator.

WTG active power variation (P_g) and mechanical power variation of diesel generator (P_m), captured as 0.034Hz, 1.4×10^{-6}W and 0.0013MW, respectively. The closed-loop system performance subject to a step load change at bus 18 as a disturbance is considered for two different cases.

2.4.2 Closed-Loop Performance Under MRC Based IE - Case I

For the first case, the desired inertia in the reference model is two seconds, that is, $H_{rf} = 2$, and the inertia constant of the DSG is set to one second, that is, $H_D = 1$. In other words, we will emulate one second inertia constant from the WTG, that is, $H_{\mathrm{ie}} = 1$. Under the MRC paradigm, we compare three design approaches, that is, LQR, H_∞, and a simple proportional–integral (PI) controller. We also compare the MRC paradigm with the conventional inertia emulation method. The ROCOF is obtained by a washout filter $k_i s/1 + 0.01s$. We index the aforementioned controllers as follows:

- Controller 1: MRC-based IE with LRQ realization
- Controller 2: MRC-based IE with H_∞ realization
- Controller 3: MRC-based IE with PI realization
- Controller 4: Conventional IE using a washout filter

The feedback gains obtained for Controllers 1 and 2 are given in (2.62) and (2.63):

$$K_{lqr} = [-9.98 \quad -2.27 \quad 0.01 \; -4.25 \; 0.04 \; -0.41 \quad -0.47 \quad 9.94 \quad 1.06 \; -0.04] \tag{2.62}$$

$$K_{H_\infty} = [83.01 \quad 2.98 \quad 0.17 \quad 18.74 \quad 0.42 \quad 2.33 \quad 2.24 \quad -83.38 \quad -2.39 \quad 0.12] \tag{2.63}$$

The PI gain for Controller 3 is obtained via the pidtune function in MATLAB and given as $K_p = 0.0113$, $K_I = 0.6471$. The IE gain for Controller 4 can be determined based on Eq. (2.3), that is, $k_i = -H_{\mathrm{ie}}/(2f_b)$. To emulate one second inertia constant, we set $k_i = -0.03$.

The closed-loop performance is illustrated in Fig. 2.7. As shown, the synthetic inertia constant is accurately emulated using Controllers 1 and 2. However, both Controllers 3 and 4 have tracking errors. Fig. 2.7 (a) and (b) present the control inputs and the power outputs of the WTG, respectively. Note that there exists a weak inertial response for the field-oriented controlled DFIG-based WTG even without a supportive controller, and this response is sensitive to the rotor current-controller bandwidth and cannot provide the exact synthetic inertia. To have a precise comparison, the tracking error for each realization is shown in Fig. 2.7 (d). It can be readily observed that Controller 2 outperforms all controllers followed by Controller 1 with the objective to remove tracking error to get precise emulated inertia.

2.4.3 Closed-Loop Performance Under MRC Based IE - Case II

In the second case, setting the desired inertia to five seconds ($H_{rf} = 5$), the closed-loop performance using MRC based IE with different realizations is illustrated in Fig. 2.8. The same indices as in the previous subsection reused to denote the controllers. In this case the computed feedback laws (2.64) and (2.65) for Controller 1 and 2 are

$$K_{lqr} = [-9.98 \quad -2.27 \quad 0.01 - 4.25 \quad 0.04 \quad -0.41 - 0.47 \quad 9.87 \quad 0.33 - 0.05] \tag{2.64}$$

$$K_{H_\infty} = [288.9 \quad 5.86 \quad 0.20\; 44.43 \quad 1.35 \quad -3.51 \quad 13.30 - 289.16 - 1.21 \quad 0.019] \tag{2.65}$$

The re-tuned PI gains for Controller 3 are $K_p = 1.29$ $K_I = 4.56$. For conventional IE (Controller 4), based on $k_i = -H_{\mathrm{ie}}/(2f_b)$, to emulate four seconds inertia constant, k_i is set to -0.12. The performance of all controllers is shown in Fig. 2.8. As seen in the figure, small tracking errors are obtained by Controllers 1 and 2, that is, the closed-loop system can emulate the desired inertia under the presence of disturbance. It is clear that if the desired inertia defined by the reference model increases, Controllers 3 and 4 are unable to track the reference frequency well and their tracking errors are higher relative to the LQR and H_∞ controllers. It can also be observed that Controller 2 outperforms all controllers followed by Controller 1.

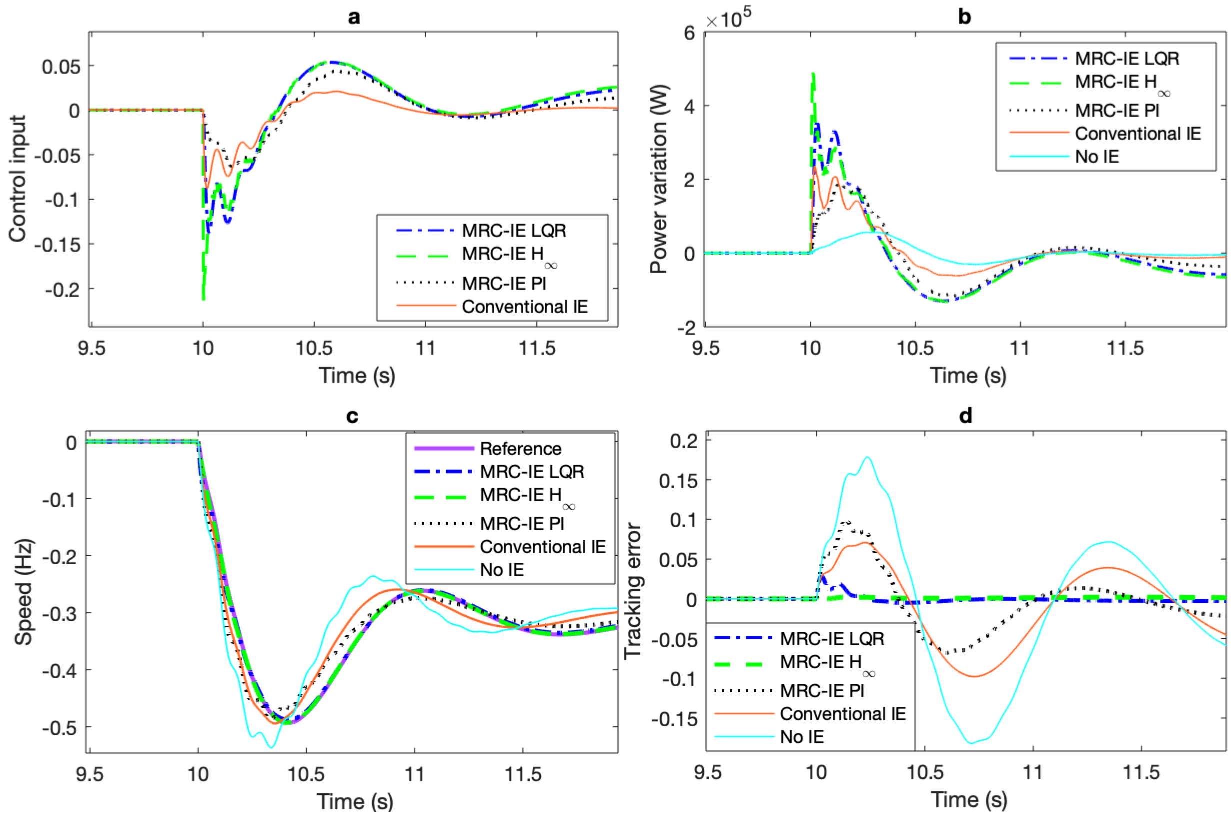

Figure 2.7: Closed-loop performance under MRC based IE with LQR, H_∞, PI controllers realization and conventional IE with desired inertia set to two second. (a) Control input. (b) Active power variation of WTG. (c) Speed of DSG. (d) Tracking error.

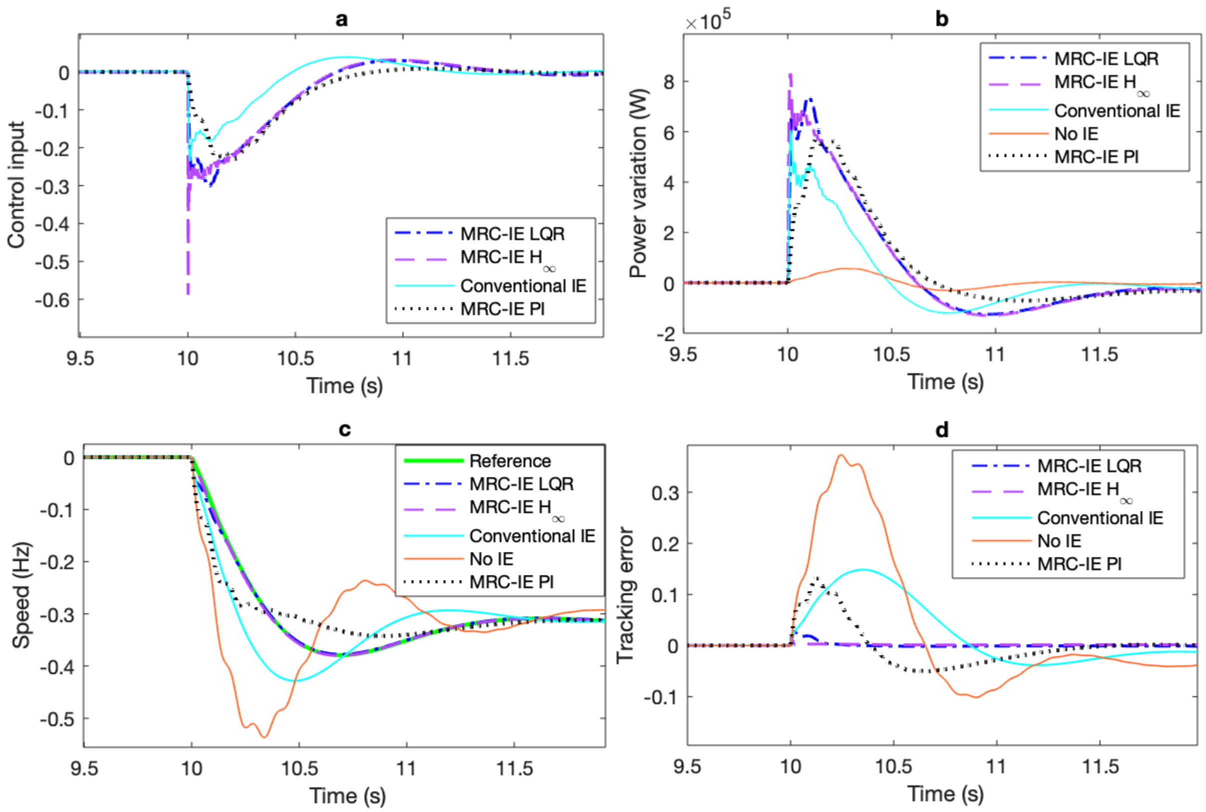

Figure 2.8: Closed-loop performance under MRC based IE with LQR, H_∞, PI controllers realization and conventional IE with desired inertia set to five second. (a) Control input. (b) Active power variation of WTG. (c) Speed of DSG. (d) Tracking error.

For Cases I and II, the H_∞ controller performs better than the LQR and PI controllers since it has improved robustness properties in the presence of plant uncertainties, that is the discrepancy between the reduced order linear model and the full order nonlinear model.

2.4.4 Control Performance for Different Short Circuit Ratios

As known, the SCR is often used as an index for the connection strength. The SCR of a strong grid is discussed in [32], [111], [3]. The SCR is defined as the ratio between short circuit apparent power from a 3-line to ground fault at a given location in the power system to the rating of the inverter-based resource connected to that location [129]. As the numerator of SCR relies on the specific measurement location, this location is usually stated along with the SCR number that is defined as:

$$\mathrm{SCR} = \frac{\mathrm{MVA_{SC}}}{\mathrm{MW_n}} \tag{2.66}$$

where $\mathrm{MVA_{SC}}$ is the short circuit MVA level at the point of interconnection (POI) without the current contribution of the WTG, and $\mathrm{MW_n}$ is the nominal power rating of the WTG being connected at the POI. Here to analyze the sensitivity of the proposed technique, the closed-loop system performance for different SCR values is provided by implementing the MRC based inertia emulation with LQR and H_∞ controllers [83]. The SCR values for three different scenarios in a range of (1.95,5) are provided in Table 2.2 where the $\mathrm{MW_n} = 1.1\mathrm{MVA}$.

The performance for the MRC based inertia emulation with LQR and H_∞ controllers, by setting all parameters and controllers similar to Case II, are provided in Fig. 2.9 and Fig. 2.10, respectively. As it is clear, both proposed controllers can emulate the desired inertia with a small tracking error. The tracking error varies in a negligible range for all scenarios. The captured SCR lower bound by simulations is 0.26, that is the system performance with the proposed techniques is guaranteed for $\mathrm{SCR} \geq 0.26$.

Table 2.2: SCR value for different scenarios

MVA_{SC}	SCR
2.1	1.95
3.4	3.1
5.6	5.1

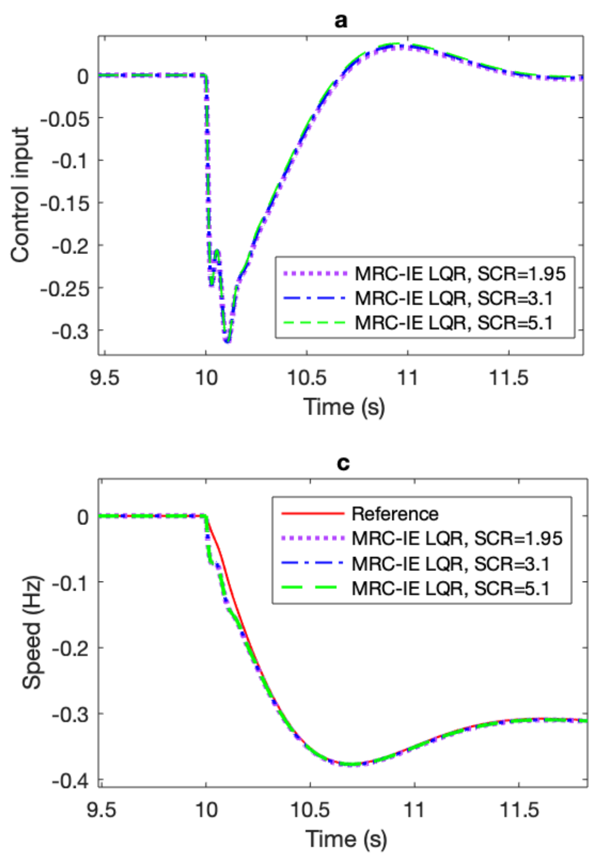

Figure 2.9: Closed-loop performance under MRC based IE with LQR realization for different SCRs. (a) Control input. (b) Active power variation of WTG. (c) Speed of DSG. (d) Tracking error.

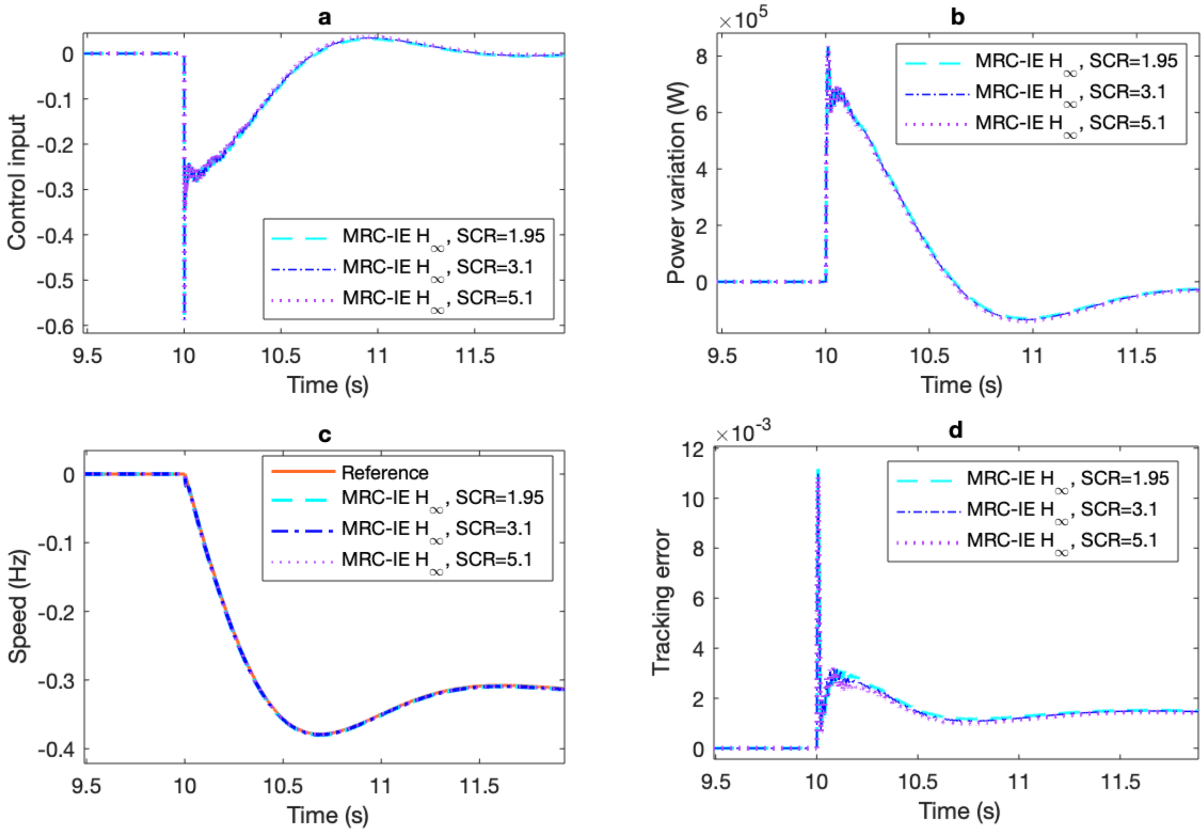

Figure 2.10: Closed-loop performance under MRC based IE with H_∞ realization for different SCRs. (a) Control input. (b) Active power variation of WTG. (c) Speed of DSG. (d) Tracking error.

2.5 Summary

In this chapter, new output feedback LQR and H_∞ control laws for inertia emulation using balanced truncation and the Luenberger observer are proposed. The controllers are applied to the full order nonlinear model and compared favorably to a PI controller and a conventional inertia emulation using a washout filter. The diesel generator speed follows the reference model in the time scale of inertial response, and accurate emulated inertia is guaranteed by generating additional active power from the WTG. The performance of the closed loop system shows improved accuracy with the H_∞ controller relative to the LQR controller, although they both achieve the desired frequency response. The proposed technique is analyzed for different SCR scenarios where a lower bound to guarantee the performance is obtained.

Chapter 3

Primary Frequency Control with Demand Response

Investigating the effects of communication delays and packet losses on inertia emulation and primary frequency control in a power system with DR setting is highly demanded. This chapter reviews communication limits on frequency regulation using demand response and shows the need for improved communication for accurate frequency regulation in smart grids.

This chapter is organized as follows. Section 3.1 reviews communication network in frequency control, including 5G technology. Section 3.2 introduces a power system model with demand response for primary frequency control, including the problem formulation and simulation results. The results in this chapter appeared in [81].

3.1 Communication Network in Demand Response

NCS such as smart grids are spatially distributed systems in which the communication between sensors, actuators, and controllers occurs through a shared band-limited digital communication network [127]. This system structure requires ensuring data packets to be successfully transmitted between the control components to ensure the reliability of such NCS. Addressing the network-induced delays and packet dropouts in NCS, a scalable and pervasive communication infrastructure is crucial in both the construction and operation of a smart grid [42].

3.1.1 5G Technology Potential Application in Demand Response

In the past few years, the 5G network is being promoted widely across the world due to its advantages in transfer speed, reliability, security, power consumption, and large number of connections [2]. Hence, utilizing the 5G network can help achieve fast transfer speed, low communication latency, high security, and a massive number of connections in future smart grids [44]. The critical improvement in this network communication is in transfer capacity, energy efficiency, and interference management. These features can be achieved using 5G network as an ultra-dense cellular network, where 5G base stations are anticipated to be 40–50 (BS/km^2) as compared to 4G network base stations that are close to 8–10 (BS/km^2) [44], [81]. The 5G massive multiple-input multiple-output (MIMO) antennas are similar to existing 3G and 4G base station antennas, but with a significantly higher frequency and beam-steering and beam-forming technologies that help the 5G base station antennas to direct the radio signal to the users and devices rather than in all directions [101], see Fig. 3.1. Moreover, robust security and high reliability are other achievements of using 5G networks. The 5G network architecture can enhance data transfer security and support diversified services via end-to-end service level agreement assurance [44]. The 5G network slices are separated from each other and can be regarded as individual structures managed in the core network [130]. For the 5G network, the core network is being redesigned to better integrate with the Internet and cloud-based services, and it also includes distributed servers across the network that improve response times and reduce latencies [101], [81].

In general, the DR aggregator may receive the area control error (ACE) or other defined control error for the system and send control signals to users to adjust their power consumption and provide regulation power [44]. However, due to the network bandwidth limits and network traffic congestion, usually, network-induced delays and packet dropouts are unavoidable [127].

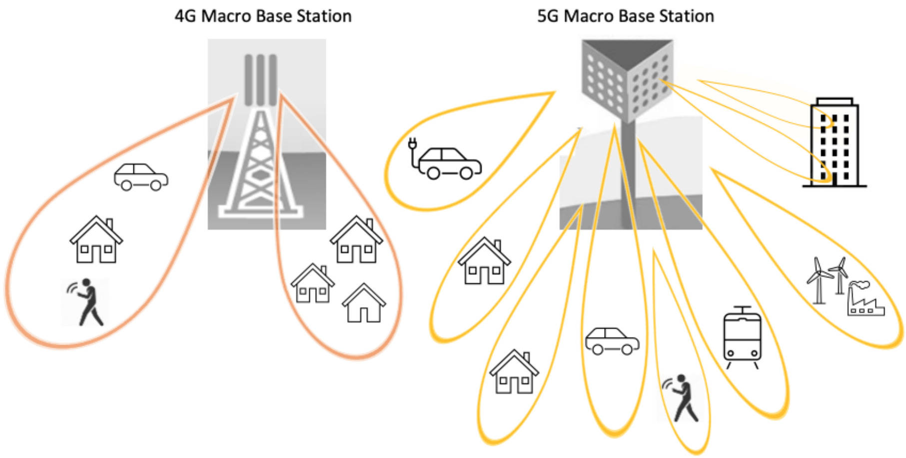

Figure 3.1: The 4G base station with sector antennas and the 5G base station with multi-element massive MIMO antenna array.

In this case, the system frequency regulation as one of the critical regulatory processes will become unstable when the communication delay time is over 0.4–0.5 s [94], [93]. The significant advantages of 5G network make it an application potential for DR in smart grids. In this framework, the massive machine-type communications' feature of 5G network allows to achieve large numbers of communication links among different loads that provide more accurate and applicable demand response control [44], [88]. Moreover, the fast transfer speeds and low communication latencies in 5G networks for remote control allow DR aggregators to send and receive information signal with an acceptable delay and packet loss where the delay time can decrease to 1 ms [81].

This dissertation shows the effects of time delays and packet losses in inertia emulation and ROCOF control using demand response as a part of frequency regulation. The primary aim is to show the need for 5G networks in future smart grids, where low communication delays and low probability of packet losses lead to accurate frequency regulation.

3.2 Communication Effects on Demand Response

This section shows the effects of time delays and packet losses in inertia emulation and ROCOF control using demand response as a part of frequency regulation. The primary aim is to show the need for 5G networks in future smart grids, where low communication delays and low probability of packet losses lead to accurate frequency regulation [81].

3.2.1 Power System Model with IACs

Inertia emulation control in a power system model with inverter-interfaced air conditioners (IACs) is considered to analyze the effects of communication delays and packet losses [43]. The general structure of the power system with IACs is illustrated in Fig. 3.2, where the DR controller is connected to the IACs to provide the required amount of support to the grid. When a disturbance ΔP_L occurs, the system frequency changes. In systems with high levels of renewables, the frequency nadir and the ROCOF can exceed the nominal operational constraints.

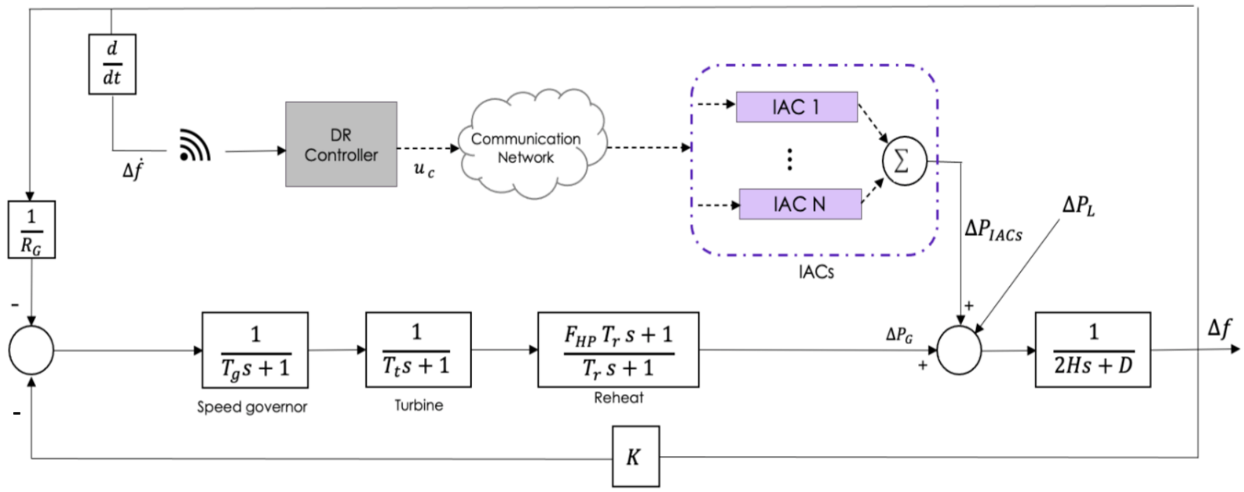

Figure 3.2: Transfer function model of power system with IACs.

Thus, controlling the ROCOF and frequency nadir has a significant role in mitigating the impact of disturbances. ROCOF can be used as a key index for the control of frequency excursion [82, 83]. Generating units will regulate the power generation ΔP_G to recover the system frequency. However, when DR is considered in the power system, the DR controller can also receive the ROCOF ($\Delta \dot{f}$) and send control signals to the IACs to adjust their power consumption and provide regulation power ΔP_{IAC}. However, the measurement and data transfer of ROCOF and control signal (u_c) are subject to communication delays [124].

Considering IACs as the load demand that can be controlled by the DR controller, the frequency regulation capacity can be evaluated as:

$$\Delta f_{IACs}(s) = \frac{(1 + T_c s)(1 + C_i R_i s) DR(s)}{(1 + T_c s)(1 + C_i R_i s) + k_Q R_i C(s)} \Delta f(s) \tag{3.1}$$

where Δf represents the the power system's frequency deviation and Δf_{IACs} is the compressor's operating frequency deviation. Here, by considering the inertia emulation as the short time period of frequency regulation process, the outdoor temperature is assumed to be fixed, and there is no change to the setpoint temperature [45], [43]. C_i and R_i are the thermal capacity, and thermal resistance of room-i, T_c represents the inertia time constant of the compressor, and k_Q is the coefficient of the cooling capacity [43], [45]. The proportional-integral controller $C(s)$ has been verified to achieve the adjustment of the compressor's operating frequency [45]. The controller of the IACs providing regulation capacity for the power system is represented by $DR(s) = -K_{P_{DR}} + -K_{I_{DR}}/s$ that is considered as a DR controller. The power consumption of the IACs can be described as:

$$P_{IACs} = \frac{K_p}{1 + T_c s} f_{IACs}(s) + \mu_p \tag{3.2}$$

where K_p and μ_p are the coefficients of the power consumption. The IACs regulation capacity is expressed in (3.3), where in this framework it is connected to the primary model by $\Delta \dot{f}$ (ROCOF) to provide inertia emulation control [43].

$$\Delta P_{IACs} = \frac{K_p(1 + C_i R_i s)}{(1 + T_c s)(1 + C_i R_i s) + k_Q R_i C(s)} DR(s) \Delta f(s) \tag{3.3}$$

Note that the regulation capacity provided by one IAC is small, so the aggregated regulation capacity of a large-scale IACs is generally considered in modeling and simulation [45], [43].

Based on the presented power system model with IACs in Fig. 3.2, the frequency deviation can be obtained by

$$(2Hs + D)\Delta f(s) = \Delta P_G - \Delta P_L + \Delta P_{IACs} \tag{3.4}$$

where D and H express the load damping and the inertia constant of the system, respectively [43]. The load deviation is represented by ΔP_L, and ΔP_G is the regulation power provided by the generator that can be described as:

$$\Delta P_G = \frac{(F_{HP}T_r s + 1)}{(T_g s + 1)(T_t s + 1)(T_r s + 1)}(-K - \frac{1}{R_G})\Delta f(s) \tag{3.5}$$

where T_g, T_t, and T_r are the time constants of the speed governor, turbine, and reheating process, respectively. F_{HP} represents the high-pressure turbine constant, and R_G denotes the speed droop. Then, the ROCOF can be easily obtained by computing $\Delta\dot{f}$ and will be sent to the DR controller to provide the required regulation power for inertial response in the presence of disturbances.

In the provided model, the system frequency deviation is initially detected by the DR control center, and then a control signal will be sent to each IAC's controller to adjust the required regulation capacity. In this send and receive process, the communication delay ($e^{-\tau s}$) and packet loss can happen due to the network bandwidth limits and network traffic congestion. Here, it has been assumed that an actual delay and packet loss on the ROCOF signal exist, and our comprehensive results are shown to validate the need for 5G networks in future smart grids.

3.2.2 Illustrations and Discussions

In the given model, the generator inertia H is set to 6 s and the load damping factor D to 1. The control parameters for the generator R_G and K_G are 0.1 and 0.5, respectively.

For the DR controller ($DR(s)$), the parameters $K_{P_{DR}}$ and $K_{I_{DR}}$ are set to 200 and 0.02, respectively. Also, the time constants for the speed governor are selected as $T_g = 0.2$ s, $T_t = 0.3$ s, and $T_r = 7$ s. The simulation results for the power system model with IACs control loop and parameters given in [43] are presented in this section with a disturbance of 20 MW step increase in load and a system capacity of 800 MW. Fig. 3.3 shows the frequency regulation for different communication delays in sending ROCOF signal, i.e., the derivative of frequency $\Delta\dot{f}$, to the DR controller. Clearly, increasing the delay lowers the frequency nadir and decreases the emulated inertia, and it could lead to instability of the system. The fluctuations of ROCOF using DR with IACs decrease as time progresses, and they are affected by the communication delays as seen in Fig. 3.4. Furthermore, Fig. 3.5 shows the regulation power in the inertial response time scale.

Fig. 3.6 shows the results for different packet loss durations in the ROCOF signal transmission. The packet loss starts at $t = 0.5$ s and is applied for different time durations. As the results show, losing data impacts the ROCOF and inertial emulation control as it it is clear in Fig. 3.6 and Fig. 3.7. Increasing the duration time of packet loss will lower the frequency nadir and decrease the emulated inertia provided by DR with IACs. Fig. 3.8 shows the impact of data losses on the regulation power. The presented results provide an insight to the impact of different communication technologies on the frequency regulation in power systems, particularly future smart grids with many loads to deliver a deterministic and necessary response to the grid. Note that using a 5G network can reduce the delay to 1-10 ms and help guarantee inertial response. The packet loss as an infinite delay can also be reduced using 5G network, and it can help provide a more reliable and secure grid.

3.3 Summary

This chapter investigates the effect of communication delays and packet losses on inertia emulation using a power system model considering services provided by IACs. The results show that time delays and packet losses in the transmission of the ROCOF signal to the DR aggregator through the communication network can cause instability and/or severe frequency

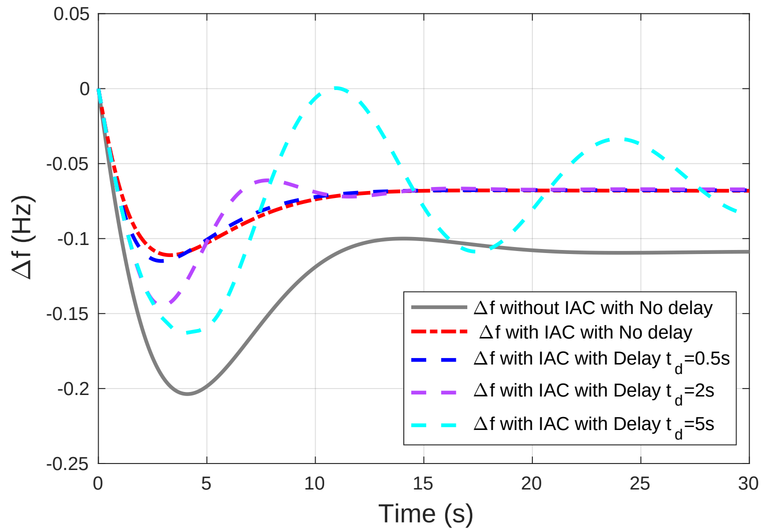

Figure 3.3: The comparisons of inertial response for different time delays.

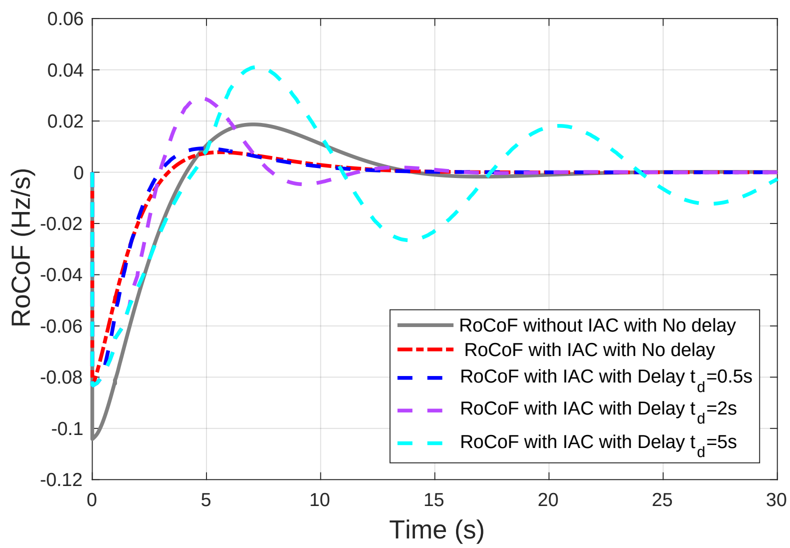

Figure 3.4: The comparisons of ROCOF for different time delays.

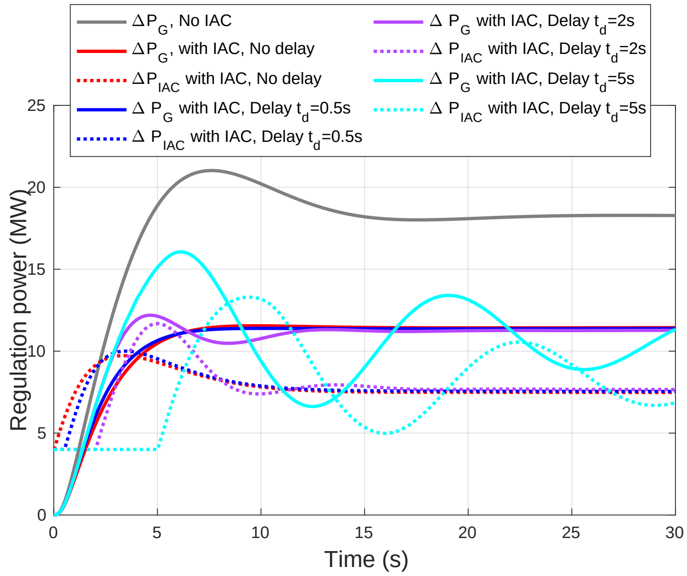

Figure 3.5: The comparisons of regulation power for different time delays.

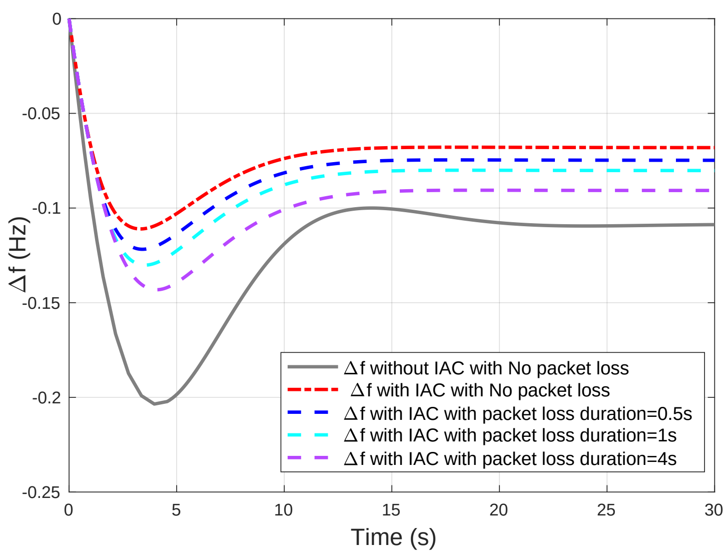

Figure 3.6: The comparison of inertial response for different time durations of packet loss.

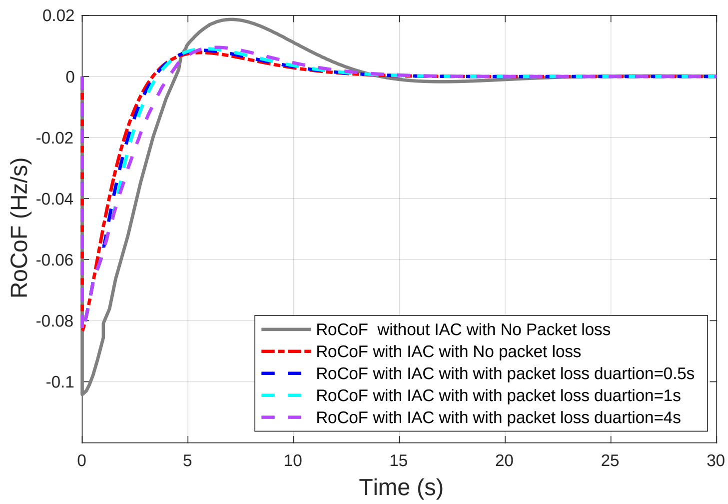

Figure 3.7: The comparison of ROCOF for different time durations of packet loss.

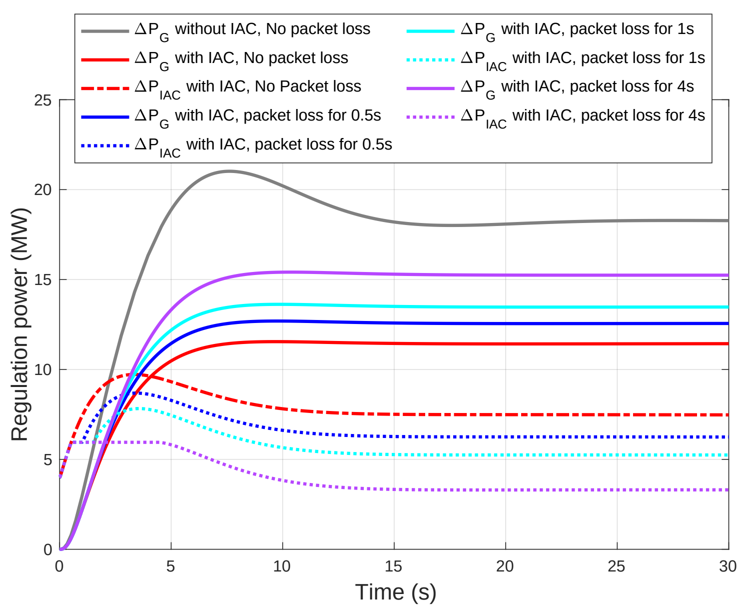

Figure 3.8: The comparison of regulation power for different time durations of packet loss.

excursions. Therefore, adopting a new communication technology, such as 5G, with low latency and packet loss will have a significant impact in improving future smart grids with guaranteed inertia emulation performance.

Chapter 4

Robust Delay Compensation for Primary Frequency Control

In this chapter, a robust delay compensation of demand response for frequency regulation is proposed to arrest system uncertainties as well as delay in data transmission.

This chapter is organized as follows. Section 4.1 introduces the objective for primary frequency control using demand response. Section 4.2 represent the problem formulation for investigating the communication effect on frequency regulation. In 4.3 a robust controller approach is proposed for frequency regulation in the presence of delay and uncertainties following by the numerical results in Section 4.4.

4.1 Objective for Primary Frequency Control

In recent years, there is increasing usage of renewable resources. These renewable resources are mainly connected to the grid with power electronic interfaces and are decoupled electro-mechanically from the grid [82]. Traditional frequency response in the presence of a disturbance is led by synchronous generators that limit the ROCOF by converting kinetic energy into electric power, known as the inertial response. As the rotor speed slows down, the turbine-governor system adjusts the prime mover output to reduce speed deviation. The regulated primary frequency is related to the governor response [99]. Due to the frequency dead-band and response time of the turbine-governor, the inertial response is dominant at the beginning of disturbance occurrence. The swing equation models this process [132]:

$$\Delta f = \frac{1}{2Hs}[\Delta P_m - \Delta P_L] \tag{4.1}$$

where $2Hs\Delta f$ expresses the inertial response. If few synchronous generators are committed due to high penetration of renewable resources, then there is less inertia H in the system and potentially inadequate inertial response. Fast DR control may help the grid frequency regulation by quickly adjusting the demand, such as in adjusting the inverter-interfaced air conditioner (IAC) load.

4.1.1 Application of DR in Primary Frequency Control

Frequency control by adjusting the demand side power regulation has become more viable with the advent of smart metering technology [40]. The traditional approach is for the generation to satisfy the generation-demand mismatch. Adequate response can also be achieved by proper demand control [105], [4]. Recently, the application of DR has been proposed in many studies for frequency excursion control [94], [70]. DR with fast dynamics can operate faster than traditional generators and can improve the frequency response in the presence of disturbances and uncertainties [10]. In this framework, if the frequency deviation of the power system exceeds the defined threshold, the DR control loop is activated, and control signals are sent to appliances to adjust their set points. Supplementary controllers can be designed to limit the ROCOF and frequency nadir when grid support is needed.

The traditional primary frequency control process shown in Fig. 4.1 is governed by the swing equation modified by the active power from the DR [99]:

$$\Delta f = \frac{1}{2Hs}[\Delta P_m - \Delta P_L + \underbrace{G_{\mathrm{DR}}(s)K_{\mathrm{DR}}\Delta f}_{\Delta P_{\mathrm{DR}}}] \tag{4.2}$$

where $G_{DR}(s)$ represents the dynamic response of DR to generate power (ΔP_{DR}) according to the frequency deviation $K_{\mathrm{DR}}\Delta f$.

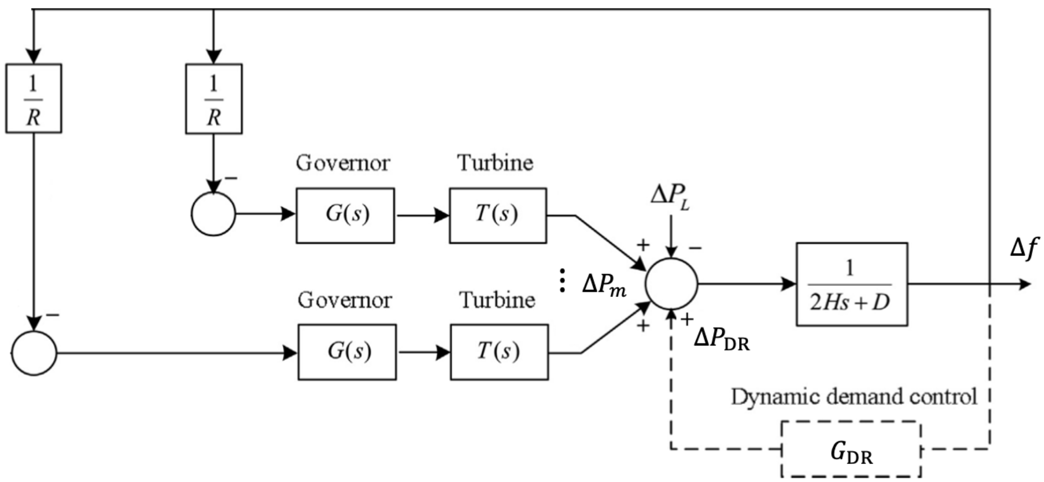

Figure 4.1: Conventional primary frequency control system with DR participation.

As described in [132] and [84], the configuration in Fig. 4.1 can only provide synthetic primary frequency response as the equivalent parameters are time-varying and may be difficult to tune. This poses challenges for dynamic security assessment, stability analysis, and system performance guarantees [99]. Moreover, utilizing DR control to provide grid services requires synchronized wide-area control of a significant number of loads to enable sufficient response. The communication delays in sensors and actuators are also a challenge for primary frequency control with DR [25], [137].

To address the above-mentioned difficulties, the objective of the proposed robust controllers is to provide a primary frequency regulation that achieves near-ideal response in the time scale of primary frequency response in the presence of uncertainties and disturbances. System uncertainties considered here are communication delays, governor dead-band and governor time constant. In other words, we need to compensate the effect induced by $G_{DR}(s)$ in (4.2), which mainly includes the primary mover dynamics and the internal controller response time which is inherent and cannot be compensated by external controllers.

4.2 Primary Frequency Control in Power Systems with IACs

Primary frequency control in power system model with IACs is considered to design robust controllers to compensate the uncertain communication delays and other parametric uncertainties in the system [43]. As (4.2) includes all relevant frequency characteristics, it is sufficient to consider only the parameter uncertainty and the governor dead-band uncertainty. The general structure of the power system with IACs is illustrated in Fig. 4.2, where the DR controller ($DR(s)$) is connected to the IACs to provide the required grid support. In the presence of a disturbance (ΔP_L), the system frequency will deviate from the nominal value and in systems with many renewables, the frequency nadir, and the ROCOF can exceed nominal operational constraints.

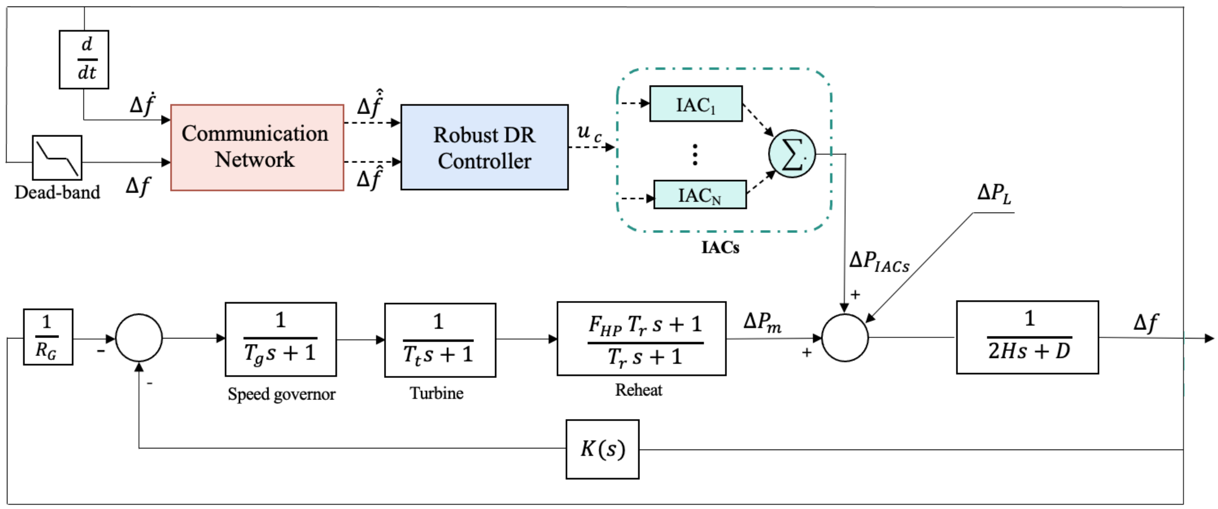

Figure 4.2: Closed-loop system structure of power system with IACs.

A supplementary control to recover the primary frequency response can play a significant role in mitigating disturbances. Traditional generation units can provide appropriate power ΔP_m to recover the system frequency. Still, the DR controller can also reduce the ROCOF ($\Delta\dot{f}$) and the frequency deviation (Δf) by having IACs adjust their power consumption ΔP_{IAC}. The measurement and communication of ROCOF and Δf are subject to delays [124].

Considering IACs as a controllable resource, the frequency regulation capability can be evaluated as [45]:

$$\Delta f_{IACs}(s) = \frac{(1+T_c s)(1+C_i R_i s)DR(s)}{(1+T_c s)(1+C_i R_i s)+k_Q R_i C(s)}\Delta f(s) \tag{4.3}$$

Here, during the short period of the frequency regulation process [45], the outdoor temperature is assumed to be fixed, and there is no change in the set point temperature [43]. The proportional-integral controller $C(s)$ can adjust the compressor's operating frequency [45] to change the load. In this framework, the DR controller providing regulation capacity is designed as a robust controller to compensate for the uncertainties of the model, including uncertain communication delays. The power consumption of the IACs can be described as [45]:

$$P_{IACs} = \frac{K_p}{1+T_c s} f(s) \tag{4.4}$$

The IACs regulation capacity is determined in (4.5), where it interacts with the main model by $\Delta\dot{f}$ and Δf to provide primary frequency control.

$$\Delta P_{IACs} = \frac{K_p(1+C_i R_i s)}{(1+T_c s)(1+C_i R_i s)+k_Q R_i C(s)} DR(s)\Delta d_i(s) \tag{4.5}$$

where $\Delta d_i(s) = [\Delta f(s); \Delta\dot{f}(s)]$, and $C(s) = K_{PC} + K_{IC}/s$. Note that since the regulation capacity provided by a single IAC is small, the aggregated regulation capacity of the numerous IACs is generally considered in modeling and simulation [45], [43].

Based on the presented power system model with IACs in Fig. 4.2, the frequency deviation can be obtained by:

$$(2Hs + D)\Delta f(s) = \Delta P_m - \Delta P_L + \Delta P_{IACs} \tag{4.6}$$

where the regulation power provided by the generator (ΔP_m) is [45]:

$$\Delta P_m = \frac{(F_{HP}T_r s + 1)}{(T_g s + 1)(T_t s + 1)(T_r s + 1)}(-K(s) - \frac{1}{R_G})\Delta f(s) \tag{4.7}$$

Here, $K(s)$ is an integral controller with gain K to increase the regulation capacity provided by generator as the system frequency deviations increase.

In the proposed approach, the system frequency deviation and ROCOF are detected first by the control center. An appropriate control signal will be sent to each IAC controller to adjust consumption. In this send and receive procedure, the communication delay ($e^{-\tau s}$) can occur due to the network bandwidth limits and network congestion. The Padé approximation model can approximate the communication delay process. Here, Δd_i can be affected by the delay and defined as

$$\Delta \hat{d}_i = e^{-\tau s}\Delta d_i \approx \frac{\sum_{j=0}^{m} a_j x^j}{1 + \sum_{k=1}^{n} b_k x^k}\Delta d_i \tag{4.8}$$

where $m \geq 0$, $n \geq 1$, and $\Delta \hat{d}_i$ denotes $[\Delta \hat{f}; \Delta \hat{\dot{f}}]$. Note that in this dissertation, the delay is modeled by a first order Padé approximation in (4.9) with $m = 1$ and $n = 2$. However, all simulation results are presented based on applying the actual delay.

$$e^{-\tau s} \approx \frac{1 - \frac{\tau}{2}s}{1 + \frac{\tau}{2}s} \tag{4.9}$$

4.2.1 Model Uncertainties

There are many uncertain parameters in electric power system models, so appropriate handling of uncertain parameters is essential [27]. The first parametric uncertainty of the physical plant considered is the governor time constant (T_g) expressed by (4.10), which affects the time of maximum frequency deviation and the transient behavior [67]. The second parametric uncertainty considered is the communication delay (τ) modeled as (4.11).

$$T_g = T_{g0} + K_{T_g}\delta_{T_g}, \qquad \delta_{T_g} \in [-1, 1] \tag{4.10}$$

$$\tau = \tau_0 + K_{\tau_s}\delta_{\tau}, \qquad \delta_{\tau} \in [-1, 1] \tag{4.11}$$

That is, $T_g \in [T_{g0} - K_{T_g}, T_{g0} + K_{T_g}]$, $\tau \in [\tau_0 - K_{\tau_s}, \tau_0 + K_{\tau_s}]$.

The significance of modeling governor dead-band is investigated in [59], [100]. The impact of governor dead-band and droop control on the generating unit performance and its impact on primary frequency response are considered as the third uncertainty in the modeling [100]. Governor dead-band is one of the significant factors for settling frequency, as illustrated by this dissertation. Considering the governor's dead-band, frequency deviation must exceed a specific value to trigger the governor action [57]. Generally, the static frequency deviation will be larger given a dead-band [58]. Here, we are modeling the dead-band as an uncertain droop curve ($\frac{-1}{R_G}$) that can vary between the upper and lower bounds of droop to approximate the non-step dead-band as shown in Fig. 4.3.

The droop uncertainty can be represented by:

$$R_G = R_{G0} + K_{R_G}\delta_{R_G}, \qquad \delta_{R_G} \in [-1, 1] \tag{4.12}$$

The interval representing the frequency dead-band can be obtained by an approximate projection on Δf axis in the range of $[-0.6 \times 10^{-3} - \delta_f, 0.6 \times 10^{-3} + \delta_f]$ p.u. based on the intersection of the uncertain droop curve and non-step dead-band [59]. The proposed control structure will manage this uncertain dead-band and communication delays and other parametric uncertainty in the system to provide regulated primary frequency response.

4.3 Robust Control Design

The interconnected systems including uncertainties may be rearranged to fit the general framework for robust control design that is illustrated in Fig. 4.4 where z denotes the

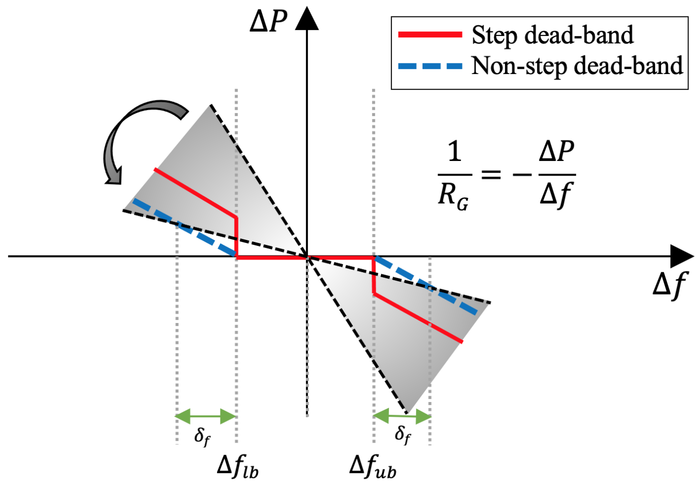

Figure 4.3: Dead-band and droop curve.

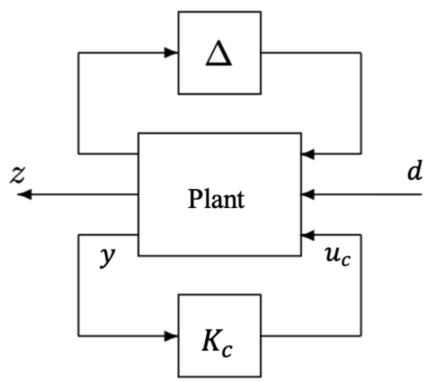

Figure 4.4: General control framework.

controlled signals, d represents the external signals, u_c is the control signal, and y is the measured outputs. In this section, two different robust control methods, a dynamic H_∞ output feedback and a dynamic μ-synthesis output feedback for primary frequency control with DR, are presented. A state-space dynamic model of the proposed model in Fig. 4.2 is also provided for design control procedures. The primary aim of the controllers is communication delay compensation and guaranteed primary frequency response in the presence of uncertainties and disturbances.

4.3.1 State Space Dynamic Model

Let us consider a stable linear time-invariant system as illustrated by the n dimensional state-space model in (4.13).

$$\dot{x}(t) = Ax(t) + Bu(t); \;\; y(t) = Cx(t) + Du(t) \tag{4.13}$$

where A, B, C, and D are the state, control input, output, and control matrices of the plant model. The state-space representation of the augmented physical plant, including the communication delay in (4.9) can be extracted as:

$$\begin{aligned} \dot{x}_p(t) &= A_p x_p(t) + B_p u(t) \\ y_p(t) &= C_p x_p(t) + D_p u(t) \end{aligned} \tag{4.14}$$

where $x_p = [\Delta x_1, \Delta x_2, \Delta x_3, \Delta P_m, \Delta x_5, \Delta P_v, \Delta x_7, \Delta f, \Delta \hat{f}\,]$ represents all state variable of the proposed system. Δx_1, Δx_2, Δx_3 are considered as internal state variables related to ΔP_{IAC} and Δx_5 is defined as state variables related to the reheat system. The measured outputs denoted by y_p are the $\Delta \hat{f}$ and $\Delta \dot{\hat{f}}$, and $u = [u_d, u_c]$ represents the disturbance u_d and the control input u_c. Here, A_p, B_p, C_p, and D_p expressing the state-space model are defined in (4.15). The obtained state-space representation model in (4.14) is used in design control procedure where the uncertain augmented plant is derived based on the closed-loop system diagram with structured uncertainty shown in Fig. 4.5.

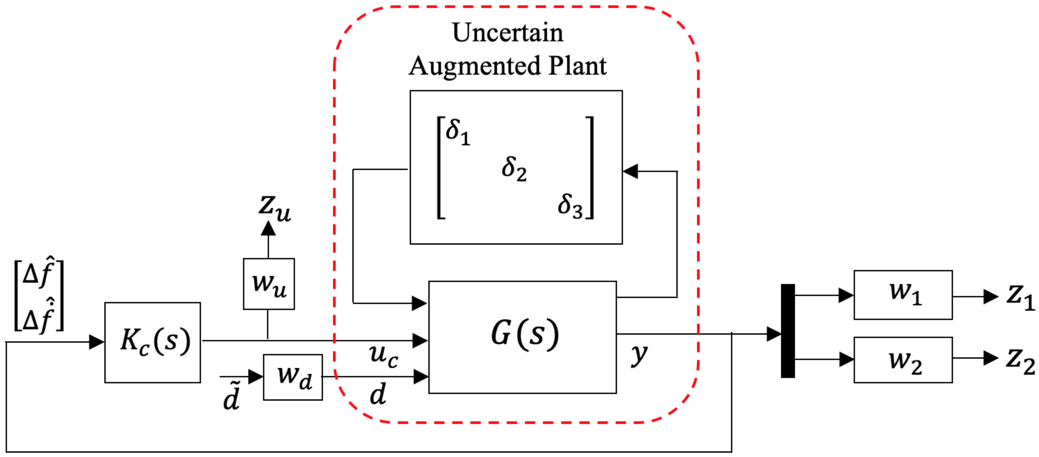

Figure 4.5: Closed-loop system with structured uncertainty.

$$A_p = \begin{bmatrix} 0 & 1 & 0 & 0 & 0 & 0 & 0 & 0 & 0 \\ 0 & 0 & 1 & 0 & 0 & 0 & 0 & 0 & 0 \\ \frac{-K_Q R_i \eta}{T_a T_c} & \frac{-(1+K_Q R_i \zeta)}{T_a T_c} & \frac{-(T_c+T_a)}{T_a T_c} & 0 & 0 & 0 & 0 & 0 & 0 \\ 0 & 0 & 0 & \frac{-1}{T_r} & \frac{1}{T_r} - \frac{F}{T_t} & \frac{F}{T_t} & 0 & 0 & 0 \\ 0 & 0 & 0 & 0 & \frac{-1}{T_t} & \frac{1}{T_t} & 0 & 0 & 0 \\ 0 & 0 & 0 & 0 & 0 & \frac{-1}{T_g} & \frac{1}{T_g} & \frac{-1}{RT_g} & 0 \\ 0 & 0 & 0 & 0 & 0 & 0 & 0 & -K & 0 \\ 0 & \frac{K_p}{2H} & \frac{K_p T_a}{2H} & \frac{1}{2H} & 0 & 0 & 0 & \frac{-D}{2H} & 0 \\ 0 & \frac{K_p}{2HR} & \frac{K_p T_a}{2HR} & \frac{1}{2HR} & 0 & 0 & 0 & \frac{-D}{2HR} + \frac{-2}{\tau R} & \frac{-2}{\tau} \end{bmatrix};$$

$$B_p = \begin{bmatrix} 0 & 0 \\ 0 & 0 \\ \frac{1}{T_c T_a} & 0 \\ 0 & 0 \\ 0 & 0 \\ 0 & 0 \\ 0 & 0 \\ 0 & \frac{1}{2H} \\ 0 & \frac{1}{2HR} \end{bmatrix}; C_p = \begin{bmatrix} 0 & 0 & 0 & 0 & 0 & 0 & 0 & 0 & 1 \\ 0 & \frac{K_p}{2HR} & \frac{K_p T_a}{2HR} & \frac{1}{2HR} & 0 & 0 & 0 & \frac{-D}{2HR} + \frac{-2}{\tau R} & \frac{-2}{\tau} \end{bmatrix};$$

$$D_p = \begin{bmatrix} 0 & 0 \\ 0 & \frac{1}{2HR} \end{bmatrix} \tag{4.15}$$

Here, the structured uncertainty block Δ that is represented by its general form (4.16) can be obtained from the system dynamics. Hence, the augmented system can be illustrated in a standard feedback configuration of lower linear fractional transformation (LFT) [136]. In this work, the defined parametric uncertainties construct a 3×3 parametric diagonal uncertainty as shown in Fig. 4.5.

$$\Delta = \{\delta I_n \quad ; \delta \in \mathbf{C}\} \subset \Delta \subset \mathbf{C}^{n \times n} \tag{4.16}$$

As it can be seen from Fig. 4.5, the weighting functions w_1, w_2, w_d,and w_u are chosen to improve the system performance in the control design procedure where a proper selection is $w_1 = \frac{0.02}{s+0.5}$, $w_2 = \frac{0.001}{s+0.5}$, $w_d = \frac{0.25}{s+0.25}$, $w_u = \frac{0.6s+0.276}{s+1000}$.

The state-space dynamic model, including parametric uncertainties of the system with specified weighting function, is used to design the robust controllers in the following sessions.

4.3.2 H_∞ Control

The theoretical formulation of the H_∞ control problem has been addressed in many books and papers; see [136] for example. This section uses a dynamic output feedback control for delay compensation and disturbance rejection based on the H_∞ control structure for the uncertain system model. The H_∞ control method is an optimization control problem which minimizes the infinity-norm of the lower LFT, $F_L(G, K_c)$, as described in (4.17).

$$\|F_L(G, K_c)\|_\infty < \gamma \tag{4.17}$$

where $F_L(G, K_c) := G_{11} + G_{12}K_c(I - G_{22}K_c)^{-1}G_{21}$ denotes the transfer function matrix of the nominal closed-loop system from the disturbance signal to the controlled output signals [136]. Here, G_{11}, G_{12}, G_{21}, and G_{22} are the partitions of G satisfying

$$\begin{bmatrix} z \\ y \end{bmatrix} = \begin{bmatrix} G_{11} & G_{12} \\ G_{21} & G_{22} \end{bmatrix} \begin{bmatrix} d \\ u_c \end{bmatrix} \tag{4.18}$$

The transfer function matrix of the nominal closed-loop system from the disturbance signal to the controlled output signals can be represented by G_{zd}. Based on the H_∞ control theory, the objective is to find a controller $K_c(s)$ such that the obtained closed-loop system is internally stable and

$$\|G_{zd}\|_\infty \leq \gamma; \quad \text{for some } \gamma > 0 \tag{4.19}$$

However, there is no analytic method to solve the mentioned optimization problem. That is, the solution for this optimization problem is not unique [15], [26]. In this dissertation, the robust control toolbox in MATLAB is used to find the dynamic controller K_c. Note that if the augmented plant is a generalized state-space model with uncertainties or tunable control design blocks, then the algorithm uses the nominal or current value of those elements to find the controller.

4.3.3 μ-Synthesis Method

Although the interconnection structure can become quite complicated for complex systems, many software packages, such as the μ analysis and synthesis toolbox, are available and can be used to generate the interconnection structure from system components [136]. μ-synthesis for the $\alpha = \mu$ case is the general optimization in (4.20) that is not fully solved yet [136].

$$\min_{K_c} \|F_L(G, K_c)\|_\alpha; \quad \text{for } \alpha = 2 \text{ or } \infty \text{ and } \mu \tag{4.20}$$

However, μ may be determined by scaling and applying $\|.\|_\infty$-norm by a reasonable approach called D-K iteration method that is defined as:

$$\min_{K_c} \inf_{D, D^{-1} \in \mathcal{H}_\infty} \|DF_L(G, K_c)D^{-1}\|_\infty \tag{4.21}$$

where, D denotes the minimum phase scaling matrix that is a positive definite symmetric matrix with appropriate dimension that satisfies $D(s)\Delta = \Delta(s)D(s)$ [136]. With either K_c or D fixed, the global optimum in the other variable may be found using the μ and H_∞ solutions [89]. The structured uncertainties to design K_c using the μ-synthesis method may include structured unmodeled dynamics and parametric perturbation. As mentioned in Section 4.2, this dissertation considers parametric uncertainties of the system including uncertain communication delay, governor dead-band and governor time constant that play a significant role in primary frequency control. The D-K iteration process can be defined as follows [12]:

- Using H_∞ synthesis to find a controller that minimizes the closed-loop gain of the nominal system.
- Performing a robustness performance analysis to estimate the robust H_∞ performance of the closed-loop system. This quantity is denoted as a scaled H_∞-norm, including the minimum phase scaling matrix D. (the D step)
- Finding a new controller to minimize the scaled H_∞-norm obtained in the second step. (the K step)
- Returning to the second and the third steps until robust performance stops improving.

Here, μ synthesis MATLAB toolbox is used to do the D-K iteration process and find the optimal dynamic control K_c. In this framework, the upper bound of μ_u of the robust H_∞ performance for the current controller K_c can be obtained in the D step. The D step obtains robust performance for the closed-loop uncertain system $F_L(G, K_c)$.

The proposed robust control method based on μ-synthesis can overcome uncertain communication delays and other specified parametric uncertainty in the system. Thus, the μ-synthesis method can provide an efficient robust controller for primary frequency response in the presence of uncertainties and disturbances. Simulation results to validate the effectiveness of the proposed control method are illustrated in Section 4.4, in comparison with H_∞ control and a conventional PI-based Smith predictor control.

4.4 Numerical Results

4.4.1 System Stability Analysis

The open-loop bode diagram of the proposed system in Fig. 4.6 with all parameters defined in Appendix A.2, is illustrated to show the effect of the delay on the system frequency

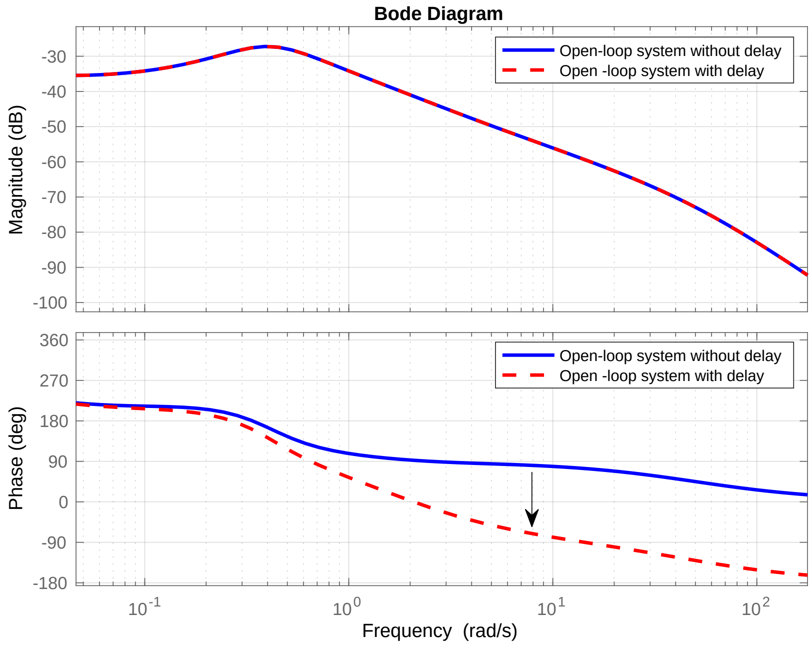

Figure 4.6: Open-loop system bode diagram. (a) Open -loop system without delay (b) Open-loop system considering 1 second delay.

performance. As shown, the delay will affect the system phase margin that may cause instability by reducing the system minimum gain stability margin. The effect of communication delays on the system root locus are also represented in Fig. 4.7. As shown the root loci crosses over from the left-half plane to the right-half plane with 1 s communication delay. Hence, increasing communication delay may result in an unstable system. The result obtained shows that a delay compensator is critical to having a stable system, particularly when the delay is considered as an uncertain parameter and may increase in unforeseen ways.

In general, the H_∞, and μ-synthesis controller obtained using the MATLAB robust control toolbox is a high-order dynamic controller. Hence, the reduced order model of both controllers are provided. The reduced order model of the designed controllers, considering only 5% degradation in performance is used to simplify implementation. The γ value for the H_∞ controller is 3.7×10^{-3}. The γ value for the μ-synthesis controller is 0.9 and the robust performance found by D-K iteration is 0.89. That is, the gain from disturbance to error remains below 0.89 for up to 1/0.89 times the uncertainty specified in the model. Hence, the controller provides robust performance for the full range of defined uncertainties.

The robust performance considering the μ-synthesis controller is evaluated with robust stability margins ($1/\mu$) as shown in Fig. 4.8. The performance level analysis shows the robustness to the modeled uncertainty where the robust performance gain remains below 1 for the full range of the modeled uncertainties. The closed-loop uncertain system bode diagram with μ-synthesis and H_∞ control approach is shown in Fig. 4.9 and Fig. 4.10, respectively. The results show the stability of the system within the defined uncertainty range.

4.4.2 Simulation Results

The proposed controllers are implemented on a power system model using the MATLAB Simulink platform. The closed-loop system performance is tested using the actual delay and dead-band in the simulations. The generation capacity of the system is 800 MW, and the disturbance is a 16 MW load change. The uncertainty bound for K_{T_g}, K_{τ_s}, and K_{R_G} are defined as the intervals $[0.1, 0.3]$, $[0.1, 4]$, and $[0.05, 0.2]$, respectively.

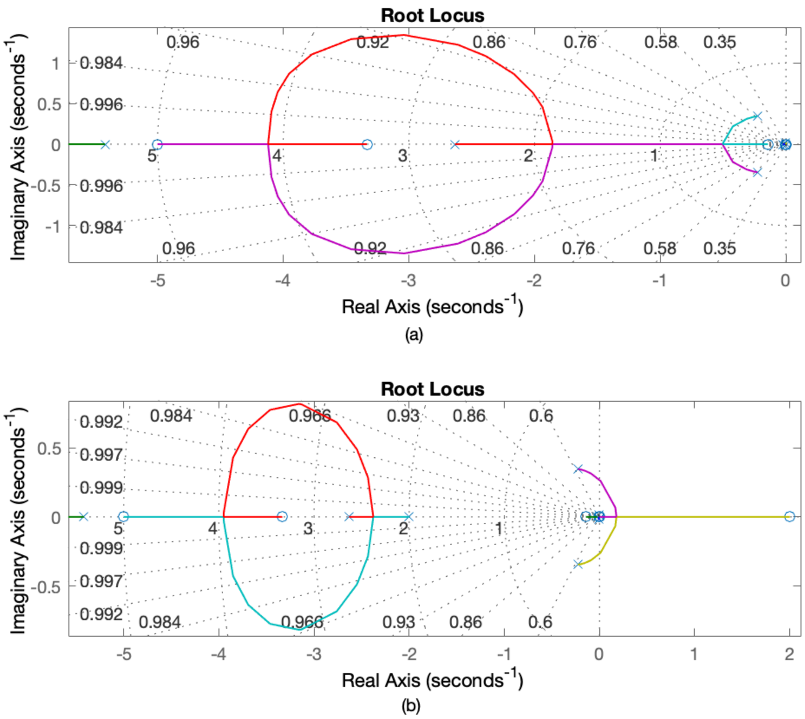

Figure 4.7: Open-loop system root locus. (a) Open-loop system without delay (b) Open-loop system considering 1 second delay.

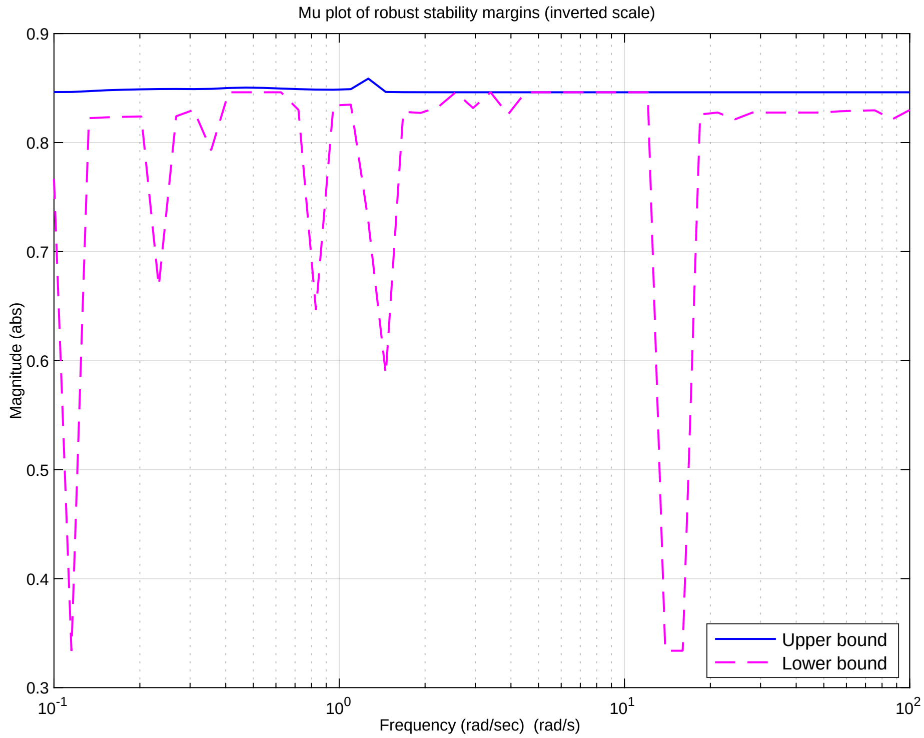

Figure 4.8: Closed-loop system robust stability considering μ-synthesis control.

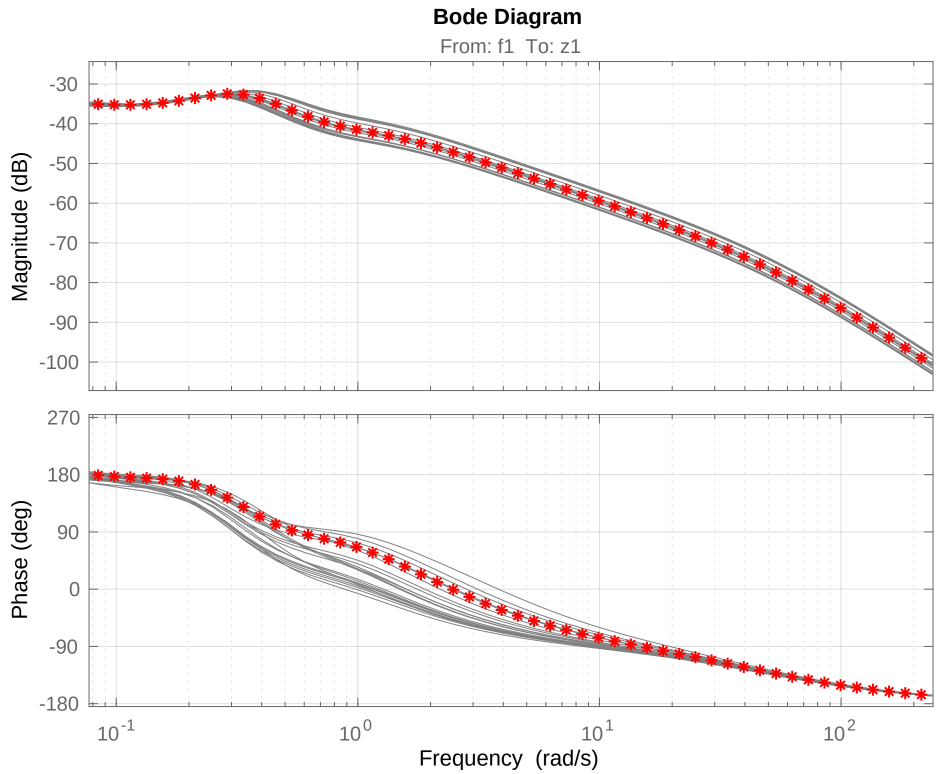

Figure 4.9: Closed-loop uncertain system bode diagram with μ-synthesis control. The red line denotes the closed-loop bode diagram for the nominal system.

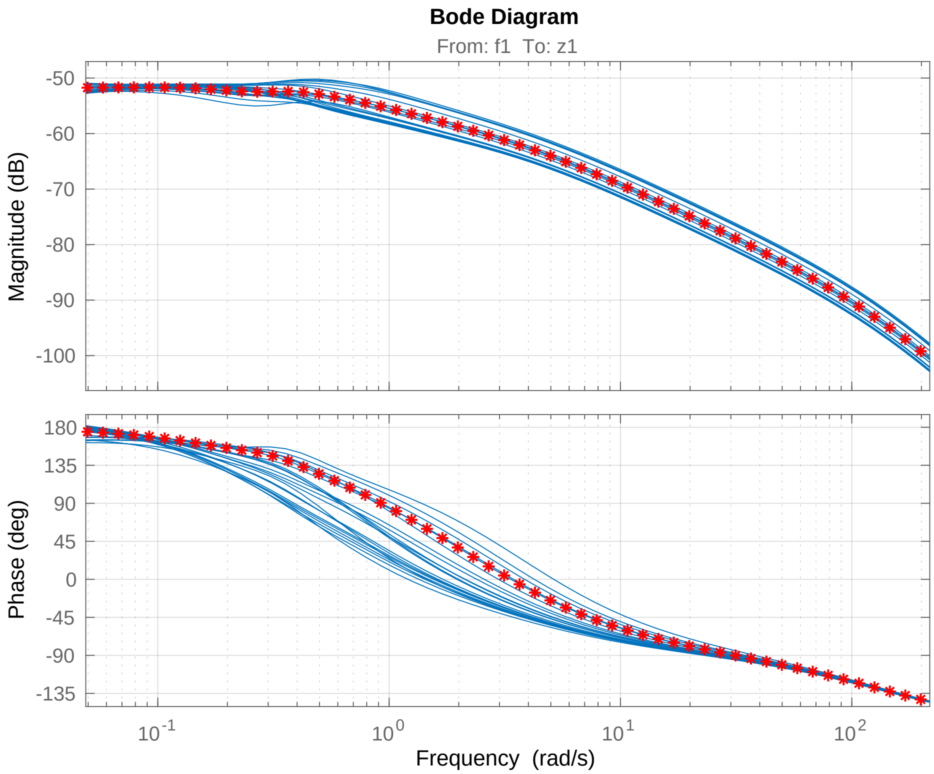

Figure 4.10: Closed-loop uncertain system bode diagram with H_∞ control. The red line denotes the closed-loop bode diagram for the nominal system.

Case I

For the first case, different delays arise from communicating the measurements. There are two scenarios in this case:

- Scenario 1: τ =1s, dead-band=$\pm$ 0.6$\times$10^{-3}, $R_G = 0.07$, $T_g = 0.2$.
- Scenario 2: τ =4s, dead-band=$\pm$ 0.6$\times$10^{-3}, $R_G = 0.07$, $T_g = 0.2$.

The PI-based Smith predictor control method is considered based on the traditional primary frequency control with DR, where its parameters are determined to capture the inertial response. The closed-loop system performance is illustrated in Fig. 4.11 and Fig. 4.12. As shown, the primary frequency response is regulated properly using both H_∞ and μ-synthesis control methods for considered delays. It can be seen that the μ-synthesis control method is more robust than the H_∞ and the conventional PI-based Smith predictor controller in the presence of different communication delays. The result obtained of the μ-synthesis method shows that the maximal robust performance is about 0.89, which means that the gain from disturbance to error remains below 0.89 for up to 1/0.89 times the uncertainty specified in the model. Hence, the controller provides robust performance for the full range of defined uncertainties.

Case II

In the second case, all uncertainties defined in Section 4.2.1 are considered. The closed-loop system performance with different realizations is illustrated in Fig. 4.13 and Fig. 4.14 and compared to the same PI-based Smith predictor control as Case I. There are two scenarios in this case:

- Scenario 1: τ =4 s, dead-band=$\pm$ 0.6$\times$10^{-3}, $R_G = 0.1$, $T_g = 0.1$.
- Scenario 2: τ =0.5 s, dead-band=$\pm$ 0.8$\times$10^{-3}, $R_G = 0.05$, $T_g = 0.3$.

As seen in these figures, system performance under different values of uncertain parameters may change based on the applied robust control methods.

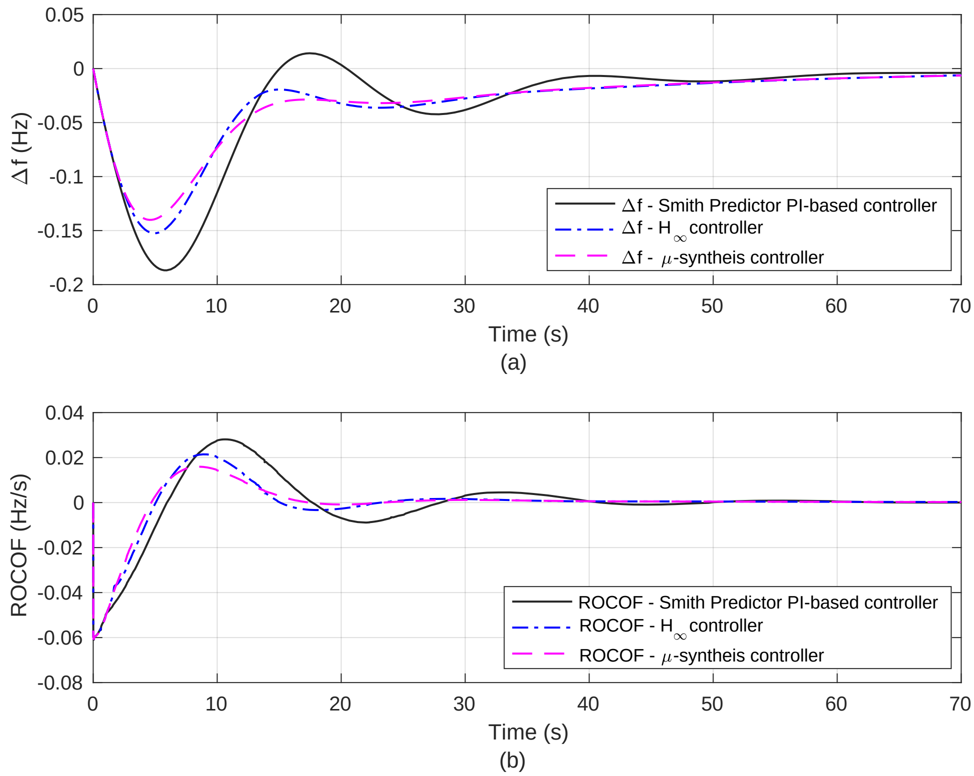

Figure 4.11: Case I: Scenario 1, Closed-loop system response in the presence of uncertain communication delay. (a) Frequency deviation, (b) ROCOF.

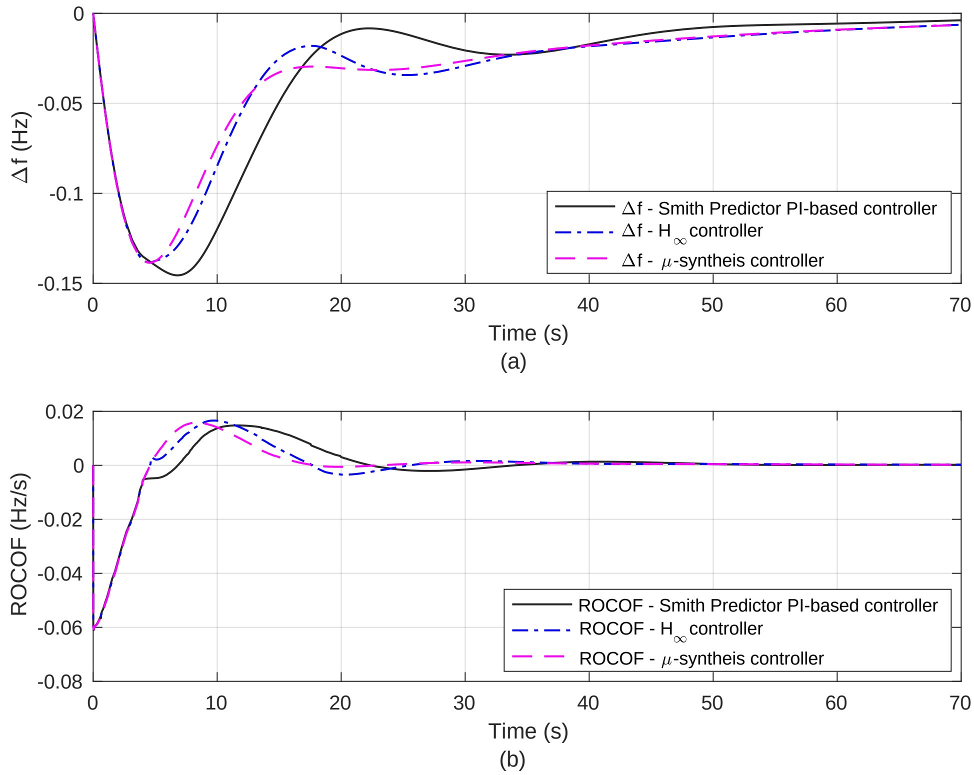

Figure 4.12: Case I: Scenario 2, Closed-loop system response in the presence of uncertain communication delay. (a) Frequency deviation, (b) ROCOF.

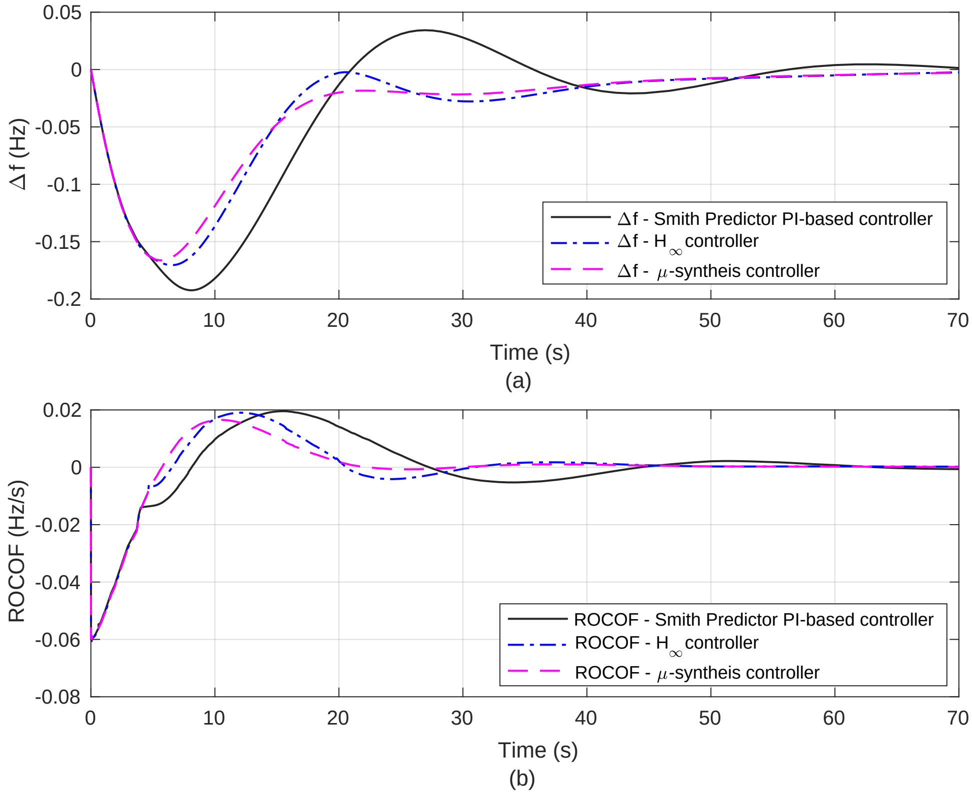

Figure 4.13: Case II: Scenario 1, Closed-loop system response in the presence all uncertainties including communication delays, governor time constant, and uncertain deadband. (a) Frequency deviation, (b) ROCOF.

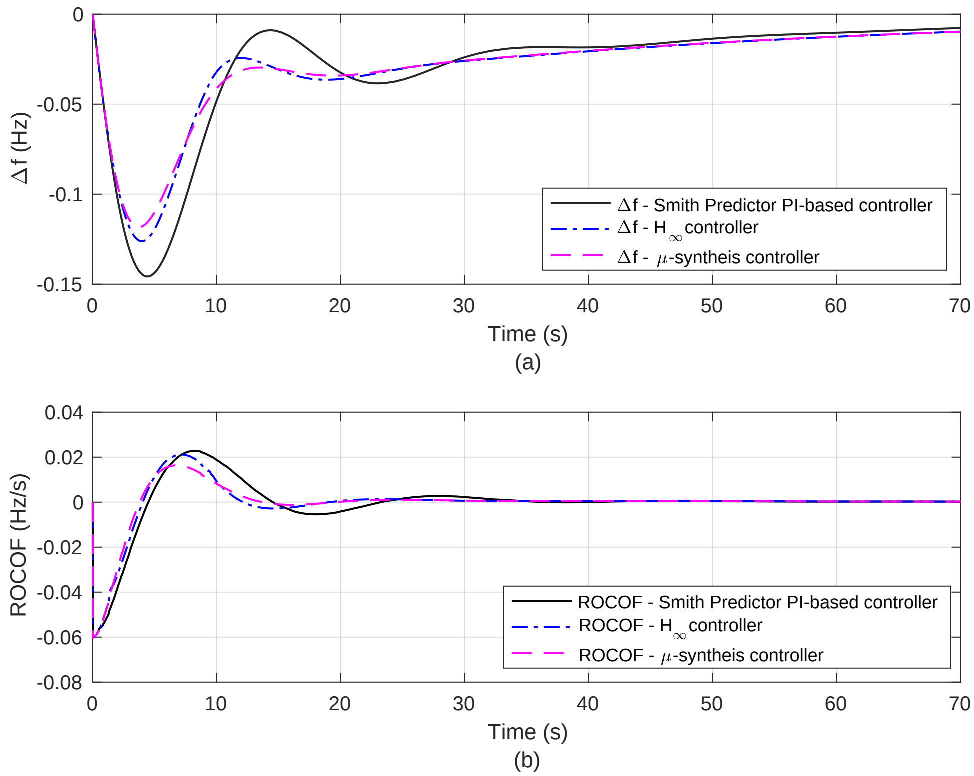

Figure 4.14: Case II: Scenario 2, Closed-loop system response in the presence all uncertainties including communication delays, governor time constant, and uncertain dead-band. (a) Frequency deviation, (b) ROCOF.

The μ-synthesis controller outperforms in all cases by providing a frequency response with smaller oscillations and overshoot compared to the other control methods. In the case of using conventional PI-based Smith predictor controller, system performance is not guaranteed under different uncertainty conditions and larger oscillations can be observed. The frequency nadir is reduced using the designed robust controllers.

4.5 Discussion

Complexity and uncertainty in generation, loads, communication network and nature of DERs are critical challenges and need to be considered to provide reliable power grids. This dissertation investigates the most important uncertainties in the frequency regulation with DR, that are structured and parametric uncertainties. As shown in this chapter, conventional controls may fail to meet the primary frequency control objectives or even in microgrid performance that is studied in [15]. Considering the uncertainties in a realistic power system, this chapter proposes robust control techniques as a powerful technique for inertial and primary frequency control with fast demand response. The contributions of this chapter are not only limited to the applications of the proposed robust control techniques for the primary frequency control with DR. The suggested H_∞ and μ-synthesis controllers could be applied to microgrids with DR and DERs connected to the distribution system. The Microgrid system either in grid forming or grid following operating mode can benefit from the proposed techniques in frequency regulation services.

4.6 Summary

In this chapter, robust H_∞ and μ-synthesis dynamic output feedback control laws for primary frequency regulation with DR are proposed. The suggested robust control techniques aim to overcome parametric uncertainties, including communication delays, governor dead-band, and governor time constants in the power system. The controllers are applied to the full-order model and compare favorably to a conventional PI-based Smith predictor control method.

The performance of the closed-loop system shows improved accuracy with the μ-synthesis controller relative to the H_∞ controller, although they both achieve improved frequency nadir and reduced ROCOF. Therefore, without providing a specified margin for the frequency, adequate primary frequency response with robustness in the presence of disturbances can be achieved by adopting the proposed control approaches. These methods are analyzed for different possible parametric uncertainties scenarios based on an uncertainty range for each parameter, including communication delay.

Chapter 5

Set Theoretic Methods for Safety Verification

In this chapter, safety verification and its application in power systems for guaranteed frequency response are discussed. The barrier certificate approach with an LP relaxation by Handelman's representation as an alternative to the SOS for verifying safety region is proposed.

This chapter is organized as follows. Section 5.1 introduces the general concept of safety verification considering different available approaches. Section 5.2 represent the region of safety definition. Section 5.3 reviews set operation based methods to verify safety region. Section 5.5 proposes barrier function positivty by Handelman's representation technique, including the application of safety verification in power systems.

5.1 Safety Verification

Safety verification is one of the active research areas and its use significantly increased in such modern engineering systems that contain subsystems with safety critical limits, such as chemical processes, biological networks, communication networks and several cooperative control problems [24]. The main challenge would be verifying safety region and safety analysis for large scale systems such as power systems or platooning. Many approaches have been done in this area to provide a scalable solution for these kinds of complex problems. The aim of this chapter is reviewing applicable methods for power systems safety verification. In real world power system operations, to avoid loss of generation and load, maintaining system frequency within operating limits has become more challenging with the advent of renewable generations. Inadequate system frequency response caused by large number of penetrations of renewable in inverter-interfaced sources can occur even in the presence of a small power disturbance [133], leading to unnecessary relay actions. Therefore, it is essential to find the system limits and guidelines for further control design.

In traditional methods for safety verification, the objective is to produce a finite set of trajectories that cover all system behaviors [69]. Some major techniques to achieve this goal are Monte Carlo simulation [37], rapid exploring random trees [17] and robust test case generation [47]. However, these methods are not able to prove that the system is safe if there is no observation for any trajectories crossing the unsafe region, since some trajectories may have been missed due to the uncertain initial states, inputs and parameters [5], see Fig. 5.1. Set theoretic methods including set operation based methods are based on numerical discretization of the continuous systems. These methods try to find the boundaries for all possible trajectories at each time step [20], using either forward reachable sets or backward reachable sets [75]. The proposed solutions are considered as interval mathematics [8],[6], Hamilton-Jacobi partial differential equations (PDEs) [113], [46] and nonlinear optimization [20]. However, computation of the exact reachable set is only possible for special cases [68]. Hence, a possibility to prove the safety of a system is to over approximate the set of reachable states, see Fig. 5.2.(a) and Fig. 5.2.(b) [5].

In passivity based methods, all presented solutions are about finding a barrier that cannot be crossed by system trajectories and separate them from the unsafe region, see Fig. 5.3 [5]. However, the difficulty of this approach is finding a proper barrier certificate for the given problem. Addressing this issue, [24] expresses a novel idea for verifying safety region of a network of interconnected systems that satisfy a dissipativity property. This framework tries to construct an invariant set as the sub-level set of a Lyapunov function comprised of local storage functions for each subsystem [24].

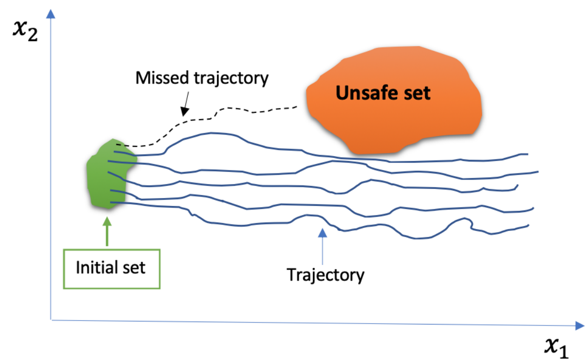

Figure 5.1: Safety verification by simulation.

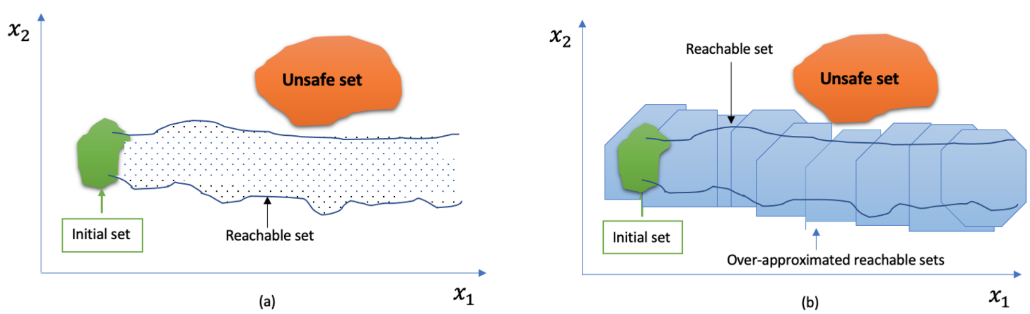

Figure 5.2: Safety verification by (a) reachable sets, (b) over-approximated reachable sets.

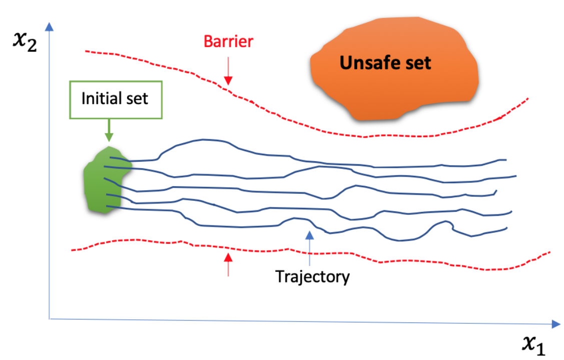

Figure 5.3: Safety verification by barrier function.

Therefore, by only knowledge of local dissipativity features of each subsystem and static interconnection matrix, safety verification can be represented as a SOS feasibility problem.

Constructing a barrier certificate in order to verify safety is another useful tools that can help us design online monitoring functions for multi-mode devices. In this construction, the approach is to show that starting from some initial conditions, system trajectories will not reach the unsafe region [97]. In this case, similar to the Lyapunov approach for proving stability, the main challenge is encoding positivity of the barrier certificate over the domain of interest and finding the function itself. There are various works done in this area that propose different computational methods for verifying a state space constraint of a network of interconnected dynamical systems and finding barrier certificate functions.

To be more classified, if the system dynamics and safety specifications can be represented as polynomials, references [91] and [97] propose a passivity-based approach that formulates safety verification as a SOS optimization problem. As long as the SoS program is feasible, the safety property can be verified, and a polynomial barrier certificate is obtained such that no trajectory of the system starting from the initial set can cross this barrier to reach an unsafe region [134]. In [97], a framework for worst-case and stochastic safety verification using barrier certificate by SoS optimization is proposed. In this case, safety verification can be cast either in the worst-case setting or the stochastic setting. A problem instance in the former setting may consist of a system with an uncertain disturbance input, where a hard bound on the input magnitude is known, and the objective is showing that for all possible disturbance inputs the system cannot yield to the unsafe region [97]. On the other hand, in the latter setting no hard bound is given, but instead a stochastic characterization of the disturbance is available, and we are asked to show that the probability of the system evolving to the unsafe region is sufficiently small [97].

This chapter focuses on safety verification based on worst-case setting to find the proper barrier function. As an application of this method, barrier certificate approach for hybrid system safety verification is considered in [134]. This framework tries to build the condition without specific initial sets. Moreover, despite the mentioned issues, [134] provides useful flexibility between accuracy and computational complexity by choosing an appropriate polynomial order for the barrier function [134]. However, the proposed formulation requires us to define a particular initial set as a SoS polynomial that makes this method conservative for several groups of systems such as power systems. Moreover, the required computations based on the SoS programming would be the primary challenge of this method that makes it inapplicable from a scalability point of view. To solve this problem, a new convex approach to stability analysis of nonlinear systems utilizing Handelman's theorem to discover a new set of affine feasible condition by Linear programming (LP) is introduced in [50],[131].

Although there are various approaches proposed as a solution of safety verification, the reviewed methods are really conservative or not applicable to apply for all dynamical systems, particularly power systems. However, scalability of all presented methods is the most challenging factor that prohibit it from power system application, as realistic power system networks are really high order systems [131].

5.2 Region of Safety

This section represents the concept of ROS, including other required notations and preliminaries.

5.2.1 Notations

The set of real numbers denotes by $\mathbb{R}$ and the Euclidean n-space by $\mathbb{R}^n$. For a function f, column vector gradient with respect to vector variables x is expressed by $\nabla_x f$. The Kronecker product is denoted by $\otimes$ and I_m expresses the $m \times m$ identity matrix.

5.2.2 Definitions

Invariant Set

In the presented methods for safety verification, barrier certificate or Lyapunov function construct an invariant set. A set ν is an invariant set for $\dot{x} = g(x)$ if $x(0) \in \nu \Rightarrow x(t) \in \nu$ for all $t \geq 0$ and ν is said to be robustly invariant for the system $\dot{x} = g(x, w)$ if

$x(0) \in \nu \Rightarrow x(t) \in \nu$ for all $t \geq 0$ and all $w \in W$ [18].

Convex Polyhedra

A convex polyhedron is defined by a conjunction of affine constraints of the form $a_0 + \sum_{j=1}^{n} a_j x_j \geq 0$ where the x_j and a_j are variables and constants in Q, respectively [77].

Region of Safety

System safety is the property that can maintain system trajectories within a given bounded region, meaning that system trajectories starting from a set of possible initial states will remain inside the region of interest [97].

Consider the dynamics of a system governed by a set of ordinary differential equations (ODEs) as:

$$\dot{x}(t) = f(x(t), d(t)); \quad t \in [0, T] \tag{5.1}$$

where $T > 0$ is a terminal time, $x(t)$ is the state vector in $\mathbb{R}^n$ and $d(t)$ denotes disturbances in $\mathbb{R}^m$ that are bounded in a set $\mathbb{D}$. The signal $d(t)$ is assumed to be piecewise continuous and bounded on any finite time interval. The vector field $f : \mathbb{R}^n \times \mathbb{R}^m \to \mathbb{R}^n$ is such that for any d and initial condition x_0, (5.1) has a unique solution defined for all $t \in [0, T]$. Denote the sets of safe, unsafe and computation by X_s, X_u and X, respectively. Also, let X_I be the initial set that belongs to X_s and $\phi(t|x_0, d)$ be the trajectories initialized in $x_0 \in X_I$ under the disturbance d. Then, safety and ROS can be defined as follows [131]:

Definition 5.1 (Safety)**.** *Given (5.1), X, X_I, X_u and $\mathbb{D}$, the system has the safety property if there is no time instant $T \geq 0$ and no piecewise constant bounded disturbance $d : [0, T] \to \mathbb{D}$ such that $\phi(t|x_0, d) \cap X_u \neq 0$ for any $t \in [0, T]$ [134].*

Definition 5.2 (Region of Safety (ROS))**.** *A set that only initializes trajectories with the property specified in the Safety definition is called a ROS [128].*

5.3 Set Operation Based Methods

Verifying safety using set operation based methods can be conducted by forward and backward reachable sets. If we consider analyzing systems of the form (2.14), (or any other differential operator corresponding to the given time domain), there are two ways to approach the problem of reachability analysis, illustrated in Fig. 5.4 [79]. The first one is forward reachability computation method that is verifying reachable set based on the given initial set and follow this set forward in time under the flow of (2.14) to compute what is known as the forward reachable set. The other approach, which is more appreciated, considers the set of terminal states T (Target set) and follows the flow of (2.14) backward in time to compute the backward reachable set [75].

In set operation based method, either forward reachable set or backward reachable set, computation can be considered as Lagrangian and Eulerian (level set) methods. The efficiency of Lagrangian method relies on the acceptable various representation of sets, such as, boxes, ellipsoids, polytops and so on. However, representation of sets as ellipsoids and polytopes (particularly zonotopes) are more common [34].

Lagrangian Methods

Using Lagrangian method, an over-approximation of the reachable set can be obtained by generating the sets under the vector fields of linear systems efficiently [66]. The boundary obtained by Lagrangian method is a barrier of all possible trajectories of a system that is represented by a set of nonlinear differential-algebraic equations in (5.2) under various input and parameter uncertainties [7].

$$\begin{aligned} \dot{x}(t) &= f(x(t), y(t), d(t)) \\ 0 &= g(x(t), y(t), d(t))\ ; \quad t \in [0, T] \end{aligned} \tag{5.2}$$

In this case, proposing an accurate and appropriate model of uncertainties is a critical point. In power grids, a large number of uncertainties and their ranges can be obtained by measurements.

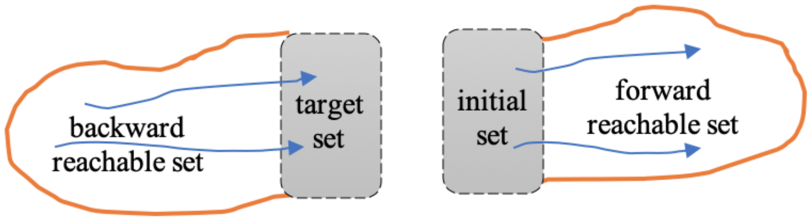

Figure 5.4: Illustration of forward and backward reachable sets.

Measured uncertainties based on their features can be defined as a sub-class of polytops instead of defining them one by one [55]. After obtaining the state space model of the system including uncertainties, the reachable sets at each time step and during time steps can be computed with an over-approximation via the following closed-form solutions [131]:

$$S(t_{j+1}) = e^{An_j} S(t_j) \oplus \phi_0(A, n_j, Z_0) \oplus \varphi_\Delta(Z_{\Delta,n_j}) \tag{5.3}$$

$$\begin{aligned} S(n_j) =& C(S(t_j), e^{An_j} S(t_j) \oplus \phi_0(A, n_j, Z_0)) \oplus \\ & \varphi_\Delta(Z_{\Delta,n_j}) \oplus \psi \end{aligned} \tag{5.4}$$

where $S(t_{j+1})$ is the reachable set at time step t_{j+1}, $S(n_j)$ is the reachable set between t_j and t_{j+1} and $e^{An_j}S(t_j)$ is the impact of the memory of computed reachable sets [131]. $\phi_0(A, n_j, Z_0))$ expresses the gain of reachable set in the presence of uncertainty Z_0 that is a deterministic uncertainty, $\varphi_\Delta(Z_{\Delta,n_j})$ represents the increase of reachable set caused by uncertainty Z_Δ and ψ is the increment of reachable set as a result of trajectories curve in $[t_j, t_{j+1}]$ where $\oplus$ is the Minkowski addition. $C(.)$ represents the convex hall computation function.

The centralized Lagrangian method computes the reachable sets based on (5.3) and (5.4) and can be mentioned as one of the useful methods in control verification [110], [56]. The more advantages of this method are identifications of stability regions [72] and transient stability analysis [29]. Although this method can provide significant advantages in evaluating system dynamics subject to disturbances, it is computationally impractical to apply to a large-scale nonlinear dynamic system due to the high dimensionality and operational flexibility [73]. To solve this problem, a distributed or compositional formal analysis [6], [29] is studied for efficient calculation and verification. In this case, the dynamics of a large-scale system to linear differential inclusions by using the full model can represent and then compositionally computes the set of linearization errors [6], [131].

Eulerian Methods

This method, known as level set method, represents the initial set at time t by the zero sub-level sets of a proper function $\phi(x,t) : \mathbb{R}^n \times \mathbb{R} \to \mathbb{R}$. where the surface of the initial set at t is expressed as $\phi(x,t) = 0$ [131]. Then, by moving (x,t) to another close point $(x+dx, t+dt)$ on the defined surface, the variation in ϕ can be expressed as [131]:

$$\Delta\phi = \phi(x+dx, t+dt) - \phi(x,t) = 0 \tag{5.5}$$

This expression leads to the Hamilton-Jacobi PDE:

$$\sum_i \frac{\partial \phi}{\partial x_i}\frac{dx}{dt} + \frac{\partial \phi}{\partial t} = 0 \tag{5.6}$$

Considering (5.1), we will have

$$\sum_i \frac{\partial \phi}{\partial x_i} f(x,d) + \frac{\partial \phi}{\partial t} = 0 \tag{5.7}$$

The obtained PDE describes the propagation of the reachable set boundary as a function of time under the system vector field [128]. The precise reachable sets can be obtained by solving this PDE. This method is also known as the convergent approximation [113]. This approach is helpful to analyze transient stability [46] and voltage stability [109] in power systems. However, since this method needs to discretize the state space model to obtain numerical solutions, it leads to an exponentially increasing computational complexity and limits its applications to systems with no more than four continuous states [6], [131]. In order to solve this issue, the initial set at time t can be expressed alternatively like the occupation measure in [38]. However, propagating such a measure will lead to other type of PDEs closer to the level set method, Liouville's PDE, that can be mentioned in a different category from the computation perspective. Using this method, safety verification can be analyzed based on the defined desired target that is usually considered as an unsafe set in backward reachable set approximation method. Verifying safety can be obtained by following the forward reachable set and its intersection with the specified unsafe set. Therefore, using the presented set operation methods in this dissertation, the system safety property is guaranteed when (5.8) is satisfied.

$$\text{Reachable set} \cap \text{Unsafe set} = \emptyset \tag{5.8}$$

Set operation based methods carry several advantages such as high accuracy, flexible computation complexity and adjustable shape and representation power. Some disadvantages caused by no closed form description and extremely high computation complexity, particularly in the Eulerian method are still there. The Lagrangian method is not applicable for nonlinear systems and linearization is needed in all cases. These drawbacks motivate us to look for the other techniques to verify safety, such as passivity based methods.

5.4 Passivity-Based Method

Beside the set operation based methods, there are different approaches for safety verification relying on set invariance [18], where invariant sets are established by considering sub-level sets of Lyapunov functions [24].

5.4.1 Dissipativity Approach

One of the contributions of safety verification is to propose a computational method in order to find an invariant set to separate unsafe region of the state space from the safe region by finding a proper Lyapunov function using local dissipativity storage functions and SoS techniques [91]. This work is particularly motivated by networks which induce a unique equilibrium point such as communication systems [52], biological networks [108] and several cooperative control problems [11]. Addressing this motivation, a computational method for verifying a state space safety constraints of a network of interconnected dynamical systems satisfying a dissaptivity property is presented in [24]. In the proposed method an invariant set as the sub-level set of a Lyapunov function consist of local storage functions for all subsystems is constructed and safety verification is posed as a SOS feasibility problem.

Let's consider N dynamical subsystems of the form

$$\dot{x}_i = f_i(x_i, u_i, w), \quad y_i = h_i(x_i) \tag{5.9}$$

where each subsystems has state $x_i \in \mathbb{R}^{ni}$, input $u_i \in \mathbb{R}^m$, output $y_i \in \mathbb{R}^m$ and disturbance $w \in \mathcal{W} \subset \mathbb{R}^m$ that can be assumed as zero [24]. $f_i(x_i, u_i, w)$ is a polynomial function in x_i and u_i and h_i is a polynomial only in x_i. Consider the whole system including interconnected systems via a feedback matrix $K \in \mathbb{R}^{N\times N}$ such that:

$$u = (K \otimes I_m)y \tag{5.10}$$

where $u \triangleq [u_1^T \cdots u_N^T]^T$, $y \triangleq [y_1^T \cdots y_N^T]^T$ and the aggregate state for the interconnected system is $x \triangleq [x_1^T \cdots x_N^T]^T \in \mathbb{R}^n$ where $n = \sum_{i=1}^N n_i$. The considered feedback is static and linear, and its structure is allowed to be arbitrary and Kronecker product with identity serves to accommodate non-scalar subsystems. [24]. Let $\hat{K} \triangleq K \otimes I_m$ such that $u = \hat{K}y$, then we define $h(x) \triangleq [h_1(x_1)^T \cdots h_N(x_N)^T]^T$ followed by $\mu(x) \triangleq \hat{K}h(x)$ where $\mu(x) \in \mathbb{R}^{Nm}$, $h(x) \in \mathbb{R}^{Nm}$ and $\hat{K} \in \mathbb{R}^{Nm\times Nm}$. Therefore $f(x, w)$ can be defined as:

$$f(x, w) \triangleq [f_1(x_1, \mu_1(x), w)^T \cdots f_N(x_N, \mu_N(x), w)^T]^T \tag{5.11}$$

then the closed loop dynamical system including all subsystems defined in (5.7) is expressed by

$$\dot{x} = f(x, w) \tag{5.12}$$

This proposed method is based on dissipativity property considering two primary assumptions. Assumption 4.1 brings unique value for the equilibrium point inputs and outputs of the subsystems (i.e. $u^* \triangleq Ky^*$ and $y^* \triangleq h(x^*)$) as this suggested method is particularly motivated by networks which induce a unique equilibrium.

Assumption 4.1. *When $w = 0$, (5.12) admits a unique equilibrium $x^* \triangleq [x_1^{*^T} \cdots x_N^{*^T}]$ such that $f(x^*, 0) = 0$.*

Since this equilibrium points are from complex interaction subsystems and direct computation may be challenging, theory of equilibrium independent passivity (EIP) is provided in [39] expressed in definition I. EIP allows us to treat unknown equilibrium point as an independent variable in SOS programming.

Definition 5.3. *The system Σ is EIP on u^* if for every $u^* \in U^*$ there exist a once differentiable and positive definite storage function $S_{u^*} : x \to \mathbb{R}$ such that [24]:*

$$S_{u^*}(x)|_{x^*} = 0 \tag{5.13}$$

$$\dot{S}_{u^*} = \nabla_x S_{u^*}(x) f(x,u) \leq (u-u^*)^T (y-y^*) \tag{5.14}$$

where Σ is referring to a general dynamical system described as

$$\begin{aligned} \dot{x} &= f(x,u) \\ y &= h(x,u) \end{aligned} \tag{5.15}$$

The second assumption is the the primary restriction in the proposed method since it makes this methodology applicable for such systems considered in a network context [24].

Assumption 4.2. *For Any subsystems included in the whole system (5.7), there exist nonempty set $\chi_i^* \subset \mathbb{R}^{n_i}$ such that for each $x_i^* \in \chi_i^*$ there exist a unique $u_i^* \in \mathbb{R}^m$ such that*

$$f_i(x_i^*, u_i^*, 0) = 0 \tag{5.16}$$

Now let define $k_{u,i} : \chi_i^* \to \mathbb{R}^m$ such that $f_i(x_i^*, k_{u,i}(x_i^*), 0) = 0$ where $k_{u,i}(.)$ is a map from equilibrium to input for subsystem i. There exist $S_i(.,.) : \mathbb{R}^{ni} \times \mathbb{R}^{ni} \to \mathbb{R} \geq 0$ as a polynomial and $\sigma(.,.) : \mathbb{R}^{ni} \times \mathbb{R}^{ni} \to \mathbb{R}$ such that for all $x_i^* \in \chi_i^*$ each subsystem shows passivity structure by satisfying the following inequality represented in (5.17) [24].

$$\begin{aligned} &\nabla_{x_i} S_i(x_i, x_i^*) f_i(x_i, u_i, w) \leq (u_i - u_i^*)^T (y_i - y_i^*) - \rho_i(y_i - y_i^*) + \sigma_i(x_i, x_i^*) \\ &\forall x_i,\ \forall u_i,\ \forall w \in W \end{aligned} \tag{5.17}$$

where ρ_i is a positive semi-definite function and $y_i* \triangleq h_i(x_i^*)$. In this case, safety condition is to verify that the resulting trajectories of the interconnected systems will not cross the unsafe region, represents by an invariant region as a sub-level set $\{x : V(x) \leq \gamma\}$ where $V(x)$ is a Lyapunov function for $\dot{x} = f(x, 0)$ and $\gamma \in \mathbb{R} \geq 0$. The way of constructing $V(x)$ comprised of the storage function defined in Assumption 4.2. Therefore, using SOS programming technique sub-level set $\nu \triangleq \{x : V(x) \leq 1\}$ satisfies the safety condition, thus verifying safety. Where ν is a robustly invariant set for (5.12) and $V(x)$ is considered as (5.18) for some constant $d_i > 0$. More details are provided in [24] and [23].

$$V(x, x^*) \triangleq \sum_{i=1}^{n} d_i S_i(x_i, x_i^*) \tag{5.18}$$

This method can be helpful for verifying safety of those systems that include interconnected subsystems, but it can be a conservative method since satisfying Assumption 4.2 is a necessary condition to safety verification based on dissipativity approach. Moreover, for other types of systems such as power systems even satisfying Assumption 4.1 is a critical and challenging point, particularly, with a system with extremely large number of states.

5.4.2 Barrier Certificate Approach

As an alternative for automated verification of properties such as safety and reachability for continuous and hybrid systems, the theoretical concept of barrier certificate is proposed in [95], [128]. A barrier certificate is a function of state satisfying some necessary inequalities on both the function itself and its derivative along the flow of the system. The barrier certificate can deliver for both worst-case and stochastic settings [128]. Here the former case is considered. This means that we are looking for a barrier to prevent system trajectories from moving to the unsafe region for all possible disturbance inputs [97]. The existence of a barrier certificate can provide a certificate to guarantee unreachability of the system states from a given initial set to a given unsafe region. The use of barrier certificates for verifying safety is similar to the use of Lyapunov function for proving stability and eliminates the need to propagate sets of states [95]. The key to computing a barrier certificate is to search the functions that are point-wise positive over a set [131]. An illustration of the relation between the safe set and unsafe set using barrier certificate approach is shown in Fig. 5.5.

5.5 Barrier Certificate Positivity

A number of ways could be found to establish the barrier certificate $B(x)$ satisfying the required condition for invariant set-based barrier certificates. The existence of a barrier certificate can be considered by convex conditions for the class of continuous systems and a large class of systems incorporating constraints such as algebraic equations, memory-less uncertainties and integral quadratic constraints as dynamic uncertainties [95].

Since zero sublevel sets of the barrier function can express the region of safety, we only need to find the barrier function as a positive definite polynomial to guarantee stability and verify safety. Let the system in (5.1), X, X_u, X_I and $\mathbb{D}$ be given and assume f is a continuous function where the objective is to find $B(x) : \mathbb{R}^n \to \mathbb{R}$ satisfying the following conditions in (5.19).

$$\begin{aligned}
&B(x) \leq 0 \quad \forall x \in X_I \\
&B(x) > 0 \quad \forall x \in X_u \\
&\frac{\partial B}{\partial x} f(x, d) < 0 \quad \forall (x, d) \in X \times \mathbb{D}
\end{aligned} \tag{5.19}$$

A function $B(x)$ satisfying the above conditions is called a barrier certificate. The zero level set of a barrier certificate provides a barrier between possible system trajectories and the given unsafe region [95].

5.5.1 Handelman's Representation

Representing polynomials by positive linear functions on compact convex polyhedra was first introduced in [35]. Considering K as a compact polyhedron in Euclidean d-space, defined by linear inequalities, $\beta_i \geq 0$, and consider f as a polynomial in d variables that are strictly

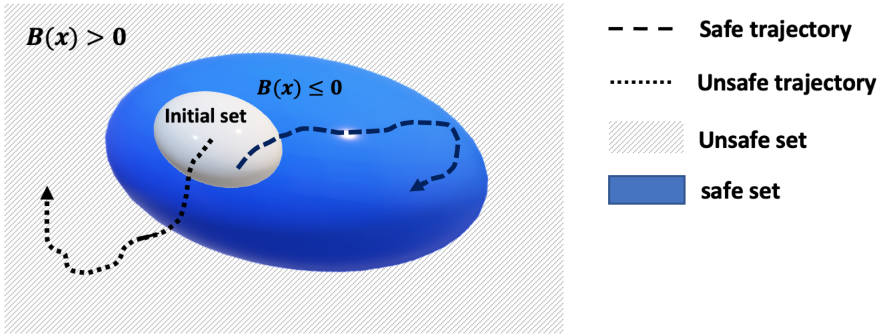

Figure 5.5: The relation between the safe set, unsafe set and region of safety.

positive on K, then f can be represented as a positive linear combination of products of members of $\{\beta_i\}$. To be clear, let K be a compact polyhedra set of the form

$$K := \{x \in \mathbb{R}^d : \beta_i(x, g) \geq 0, \, g \in \mathbb{R}\} \tag{5.20}$$

where $\beta_i \subseteq \mathbb{R}[x]$ are affine functions of x. For each set K defined in (5.20) and n_i for $i = 1, \cdots, m$, the m^{th} Handelman's monomial corresponding to K is defined by

$$P_{n_i}^K(x) = \prod_{i=1}^{m} (\beta_i)^{n_i} \tag{5.21}$$

Then the Handelman's polynomials with degree $\mathfrak{D} \geq 1$ corresponding to K can be expressed by (5.22).

$$P_{\mathfrak{D}}(K) = \sum_{|m| \leq \mathfrak{D}} \lambda_m P_m^K(x), \quad \lambda_m \in \mathbb{R} \geq 0 \tag{5.22}$$

where γ_m are non-negative constants. Hence, to prove the positivity of a polynomial function over the compact polyhedra sets K, the basis can be selected by Handelman's polynomials [35]. The expression of Handelman representation is defined in Theorem 5.4.

Theorem 5.4. *A polynomial $P(x)$ is strictly positive over a compact polyhedron K defined in (5.20) if and only if there exist non-negative coefficients γ_m such that $P(x) : \mathbb{R}^n \to \mathbb{R}$ with a bounded degree $\mathfrak{D}$ can be expressed by [35]*

$$P(x) = \sum_{m} \lambda_m P_m^K(x) \quad \forall \lambda_m \geq 0 \tag{5.23}$$

If $P(x)$ is of degree $\tilde{\mathfrak{D}}$, such that $\tilde{\mathfrak{D}} \geq \mathfrak{D}$, the unknown coefficients (λ_m) can be obtained by solving an equality for each monomials with similar degree. It means that to certify the positivity (non-negativity) of $P(x)$ on K we only need to solve a linear programming feasibility problem. The general procedure for proving positivity of $P(x)$ over K is described as follows [131]:

1. Choose a degree limit $\mathfrak{D}$ and construct the Handelman's polynomial $P_{\mathfrak{D}}(K)$ with unknown multipliers λ_m.

2. Let $P(x) = P_{\mathfrak{D}}(K)$

3. Equate coefficients on both sides (the given polynomial and the Handelman representation) to obtain a set of linear inequality constraints involving λ_m.

4. Use a LP solver to solve these constraints. If feasible, the results yields a proof that $P(x)$ is positive semi-definite over K.

Consider the example in [131] with the polynomial $p(x_1, x_2) = -2x_1^3 + 6x_1^2x_2 + 7x_1^2 - 6x_1x_2^2 - 14x_1x_2 + 2x_2^3 + 7x_2^2 - 9$ and the set $K : (x_1 - x_2 - 3 \geq 0 \wedge x_2 - x_1 - 1 \geq 0)$. Then, the positivity of p over K can be proved by representing p as follows

$$p(x_1, x_2) = \lambda_1 f_1^2 f_2 + 3f_1 f_2 \tag{5.24}$$

where $f_1 = x_1 - x_2 - 3$, $f_2 = x_2 - x_1 - 1 \geq 0$, $\lambda_1 = 2$ and $\lambda_2 = 3$.

5.5.2 An Illustrative Example

Let us consider two interconnected subsystems defined by [24]

$$\dot{x}_1 = -x_1^3 + u_1 + w_1 + C_1, \quad y_1 = x_1^3 \tag{5.25}$$

$$\dot{x}_2 = -x2 + u_2 + w_2 + C_2, \quad y_2 = x_2 \tag{5.26}$$

where C_1, C_2 are given constants and $|w_1(t)| \leq 0.1$ and $|w_2(t)| \leq 1$. The subsystems are connected by $u_1 = y_2$ and $u_2 = -y_1$. The system is in the safe condition when x_1 and x_2 are in the defined safe set $\{x_1 - 4 \leq 0\} \cup \{x_2 - 4 \leq 0\}$. The safety of the system is verified by the proposed method for two different cases with $(C_1, C_2) = (-1, -1)$ and $(C_1, C_2) = (2, -2)$. The obtained safe region is illustrated in Fig. 5.6, which shows that in both cases the safety region could be verified by the zero level-set of the computed barrier function. If we initialize the system trajectories inside the green box (initial set) the will stay inside the safe region and the safety properties are verified.

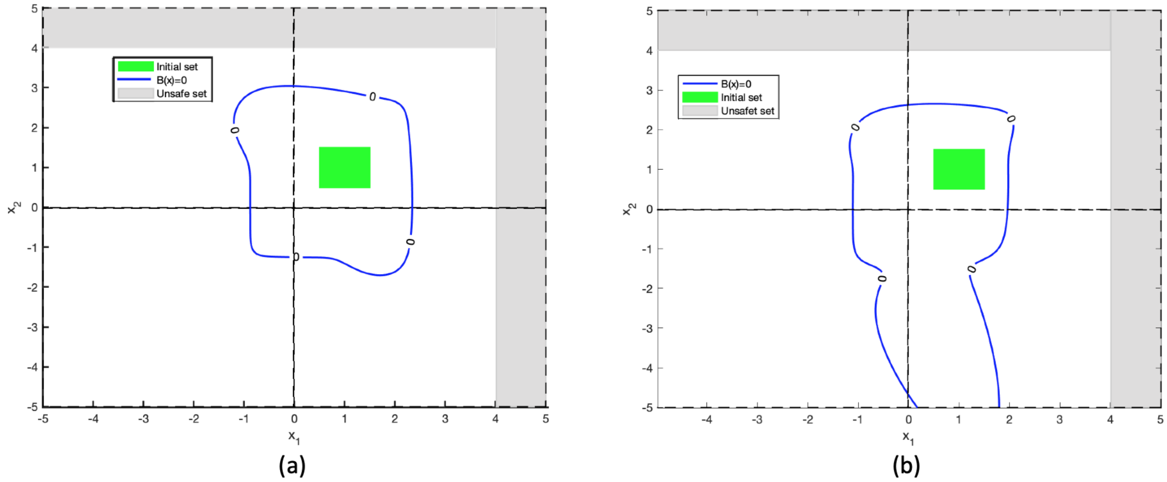

Figure 5.6: Safety verification, (a) $(C_1, C_2) = (-1, -1)$, (b) $(C_1, C_2) = (2, -2)$.

5.5.3 Application of Safety Verification in Power Systems

In general, safety verification of the system carrying critical limits can guide us for further control design. In other words, it can be employed to design the safety supervisory control based on the obtained barrier certificate or safety region to control the system in emergent conditions. Several works have been done based on safety verification for verifying power grid constraints satisfaction in both set operation-based and passivity-based methods. As an example of the set operation-based method, the stability region of a stable equilibrium point with the purpose of power system stability analysis is proposed in [46].

In this case, the backward reachable set is computed based on Hamilton–Jacobi–Isaac (HJI) PDE that yields the stability region of the equilibrium point, and a transient stability design method is presented based on the obtained reachable set. In addition, the stability analysis is performed for a set of operating conditions using reachability analysis [6], which makes it applicable to obtain the bounds for all possible system trajectories.

For the class of passivity-based methods, verifying power grid voltage constraint satisfaction is considered in [92]. This work aims to turn the static power flow equations into a system of differential-algebraic equations and apply a safety verification by the barrier certificate method. Moreover, in some cases, removing timescale separation between voltage and frequency dynamics makes it critical that faster-timescale stabilizing control laws are also guaranteed by constructing the satisfaction of voltage limits during transients[63]. As a solution for this problem, [63] applied a barrier function method to compute distributed active and reactive power set-point control laws that certify satisfaction of voltage limits during transients. As another example, a safety supervisory control for the adequate frequency response in the presence of the worst-case disturbance is designed in [134]. The suggested controller structure has been developed based on the barrier certificate method that could properly separate the ROS from the unsafe region defined for the grid frequency constraint. Similarly, in [131], a hybrid controller is proposed to do the safe recovery procedure based on the largest ROS that is derived based on the barrier certificate methodology. Computational complexity is the primary challenge of all proposed techniques facing large-scale networks such as power systems. However, the advantage of passivity-based methods for safety verification is obtaining the barrier certificate as a function of system states that can be employed in the grid's control structure, such as supervisory control.

5.6 Summary

In this chapter, safety verification methods and their application to power system are presented. The methods are classified into set operation based methods and passivity based methods. Pros and cons of the approaches are discussed. Set operation based methods are analyzed and considered as applicable and efficient for high order systems. Passivity based methods are described based on different approaches such as dissipativity and barrier certificate approach. To encode the positivity of the barrier certificate function, LP relaxation by Handelman's representation is proposed.

Chapter 6

Handelman's based Barrier Certificate Approach for Guaranteed Frequency Performance

Frequency excursions can arise due to a high penetration of DERs and requires a frequency support function to be integrated in future grids. The appropriate design for these support functions with the concept of region of safety to ensure adequate response is critical as stability synthesis of power systems. This chapter reviews a computational method for safety verification with the Handelman's theorem and linear relaxation. The Handelman's representation is used to formulate the problem, leading to a linear program that possesses much lower computational complexity. The proposed approach is validated using power system benchmark case studies with a discussion on further control guidelines.

This chapter is organized as follows. Section 6.1 reviews guaranteed frequency performance with the help of safety verification. Section 6.2 introduces a Handelman's based barrier certificate approach, including the problem formulation and computational method. Section 6.3 validates the proposed framework considering various power system case studies. Section 6.4 provides a discussion on control guidelines, including safety supervisory control implemented on full-scale nonlinear diesel/wind fed microgrid model.

6.1 Guaranteed Frequency Performance

High penetration of DERs as converter-based devices has a significant impact on power system dynamics, particularly the frequency response. Significant power imbalances may lead to severe frequency deviations, stability problems, or even widespread system blackouts [76]. Maintaining frequency variation in a low band requires adjustments in the protection and control set points within the system such as the re-coordination of AGC, time correction, governor response set points, generation and load trip set points, and other frequency controlled protection devices [54]. As shown in Fig. 6.1 [85], any disturbances can cause frequency response crossing the determined safety limit, resulting in unnecessary relay actions. The aim of this dissertation is finding the safe operating region for frequency with further control design guidelines.

Control synthesis towards guaranteed frequency performance is critical as a supplementary control loops for synthetic inertial and primary frequency response. Converter-interfaced sources have received lots of attention as a grid-feeding part of grid-supporting functions where frequency control can be equipped for most converter-interfaced DERs. In this framework, the accuracy of the frequency response can be indexed by a safe performance, where the safe performance means that all trajectories should be maintained in a defined safe region. Constructing a barrier certificate in order to verify safety is a useful tool that can help us design online monitoring functions for multi-mode devices [97]. A barrier certificate is a function of state that divides the state space into safe and unsafe regions. All system trajectories starting from a given initial set inside the barrier function fall into one side while the unsafe region locates on the other. Thus, the problem of safety verification is converted to the problem of barrier certificate generation [123].

6.2 Handelman's based Barrier Certificate Approach

A barrier certificate is a function of state satisfying some necessary inequalities on both the function itself and its derivative along the flow of the system [96]. The barrier certificate can deliver for both worst-case and stochastic settings. Here the former case is considered.

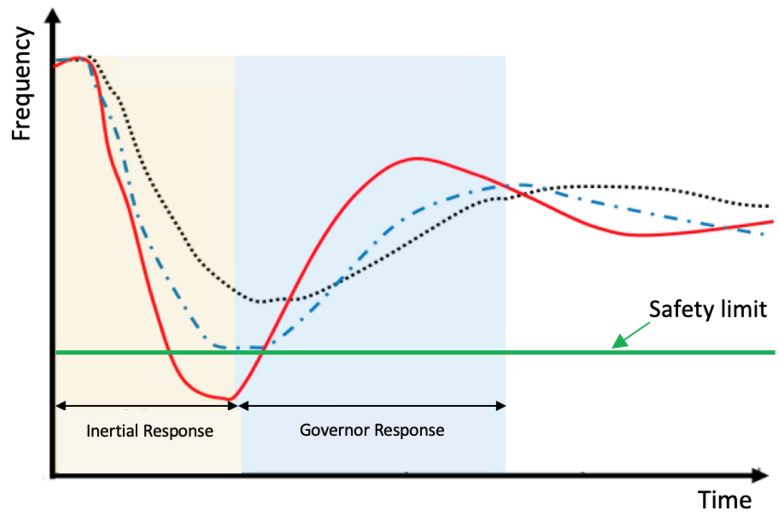

Figure 6.1: Primary frequency response considering safety limit.

This means that we are looking for a barrier to prevent system trajectories from moving to the unsafe region for all possible disturbance inputs [97]. The key to computing a barrier certificate is to search the functions that are point-wise positive over a set [131]. Since zero sublevel sets of the barrier function can express the region of safety, we only need to find the barrier function as a positive definite polynomial to guarantee stability and verify safety as described in Section 5.5.

6.2.1 Network Systems

In this section, a general model for a network of systems is proposed. Consider a network (it might include N dynamical subsystems) of the form:

$$\dot{x} = f(x, u, w); \quad y = h(x, u) \tag{6.1}$$

where x is the systems state vector, u is the input vector, w is the disturbance signal and y represents the output vector of the network. As such (6.1) represents the dynamic of the network, and there is no need to access the individual subsystems dynamic equations. We briefly describe the barrier certificate approach and the Handelman's representation to find the barrier function by solving an LP problem that is based on a convex optimization problem for a network of systems.

6.2.2 Computational Method

Considering preliminaries and definitions in Section 5.5, for a network system (It can be include of interconnected subsystems) constructed by polynomial functions and considering its barrier function as a polynomial, there is a tractable computation method to find a barrier certificate. The Handelman's representation can be used to compute the coefficients of the barrier certificate by solving the corresponding LP. Based on the condition expressed in (5.23), the problem of searching a barrier certificate in (5.2) can be expressed as follows:

$$
\begin{aligned}
&- P_{\mathfrak{D}}(X_I) - B(x) = 0, \quad x \in X_I \\
&- P_{\mathfrak{D}}(X_u) + B(x) = 0, \quad x \in X_u \\
&- P_{\mathfrak{D}}(X \times \mathbb{D}) - \frac{\partial B}{\partial x} f(x, d) = 0, \quad \forall (x, d) \in X \times \mathbb{D}
\end{aligned} \tag{6.2}
$$

where $P_{\mathfrak{D}}(X_I)$, $P_{\mathfrak{D}}(X_u)$, and $P_{\mathfrak{D}}(X \times \mathbb{D})$ are Handelman's polynomials over sets X_I, X_u, and $X \times \mathbb{D}$, respectively. Here, the objective is to prove the positivity of the $B(x)$ as a candidate barrier certificate. Based on the obtained $B(x)$, safety property of the system can be verified [123]. Increasing the degree bound $\mathfrak{D}$ for the representations; and/or subdividing the polyhedra $K_1, \ldots K_p$ such that $K = \bigcup_{j=1}^{p} K_j$ to prove positivity of p over each subdivisions, may help in case of infeasiblity [103]. A comprehensive description to compute the barrier certificate $B(x)$ using Handelman's representation is illustrated in Algorithm 1.

Algorithm 1: Barrier certificate by Handelman's representation

Input: $f(x)$: system vector field, X_I: initial set, X_U: unsafe set, X: computation set, $\mathfrak{D}_0$: degree of barrier certificate, $\mathfrak{D}$: degree bound of Handelman polynomial

Output: $B(x)$: The barrier certificate as ROS

Construct $B(x)$ by polynomial degree $\mathfrak{D}_0$;
Construct $P_{\mathfrak{D}}$ Handelman polynomial degree $\mathfrak{D}$ (5.23);
Set up the linear programming by equating $B(x)$ and $P_{\mathfrak{D}}$ as (6.2);
Solve the LP problem;
if *The LP is feasible* **then**
  Verified ROS by $B(x)$.
else
  "Not found $B(x)$ with the degree bound $\mathfrak{D}$"
end

6.3 Power System Case Studies

As a power system application, this dissertation investigates the region of safety for different power networks, including SMIB benchmark, and a two-area interconnected power system with AGC to verify the scalability for higher order systems in this section.

6.3.1 SMIB Benchmark

In the most power systems, synchronous generators are the critical components such that safety verification or even design a stabilizer starts from modeling of these components [28]. To further demonstrate the proposed approach, a simple example is illustrated as a benchmark. Consider the linearized SMIB system as follows

$$\begin{bmatrix} \Delta\dot{\delta} \\ \Delta\dot{\omega} \end{bmatrix} = \begin{bmatrix} 0 & 6.28 \\ -20.44 & -0.14 \end{bmatrix} \begin{bmatrix} \Delta\delta \\ \Delta\omega \end{bmatrix} \tag{6.3}$$

where the safety specification is defined as $X_u = \{[\Delta\delta, \Delta\omega]^T : -0.5 \leq \Delta\omega \leq 0.5\}$. Define an unsafe set as the gray box shown in Fig. 6.2 and the given computation and initial set an invariant set which is a zero level set of $B(x)$ is obtained as the ROS where the $\mathfrak{D}$ is set to 8. The obtained result shows the region that can maintain the system's trajectories away from the unsafe region. Here the green box is the largest obtained initial set to initialize the trajectory ($\Delta\omega$) to be maintained in the safe region.

6.3.2 Two-Area Power System

Consider a two-area power system, which consists of two interconnected control areas as shown in Fig 6.3 [30]. The two areas are connected by a tie line of reactance X_r. To maintain power balance, the generated active power of the network is the same as power demand, and any disturbance will have an effect on the system frequency regulation. The challenge of this stabilizing procedure is that it may not be able to preserve the frequency in a specified safe boundary.

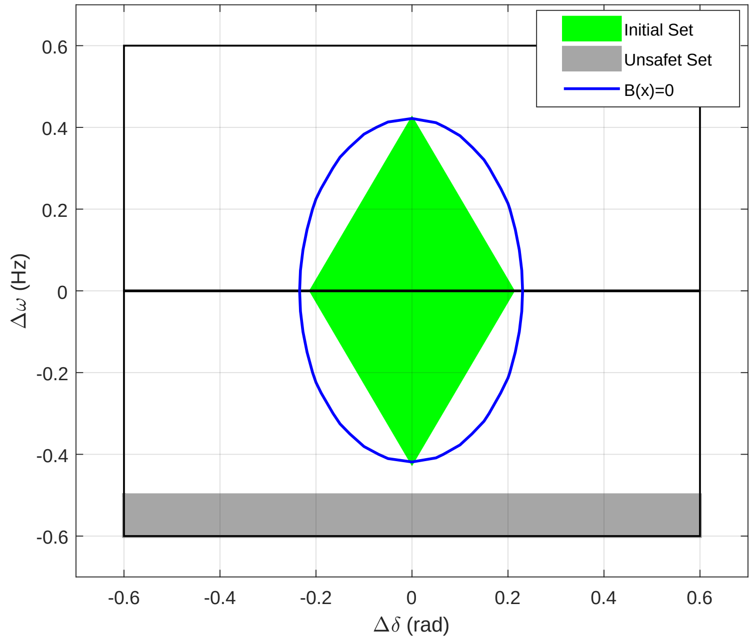

Figure 6.2: Computed ROS for SMIB benchmark.

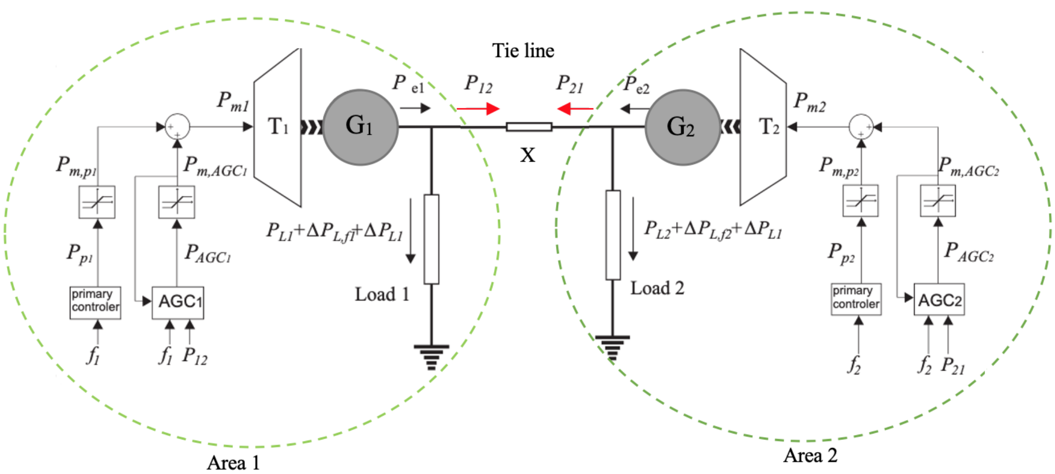

Figure 6.3: Two-area interconnected power system with AGC.

This challenge is the reason for using primary frequency control given by ΔP_{P_1} and ΔP_{P_2} for each area. Also, Each area has to maintain a scheduled power interchange between the areas, which is approximated by a generating unit G_i equipped with primary frequency control [64], [31]. The primary objective of the AGC is regulating the frequency to the desired nominal value and keeping the power exchange between controlled areas to a specified value [30]. Since AGC is one of the control loops without human operator intervention, analyzing its vulnerability by safety verification can be a critical point in such interconnected power systems for further control designs [30].

The model of the two-area power system considered as a case study can be described as [64], [30]

$$\Delta \dot{f}_1 = \frac{f_0}{2H_1 S_{B_1}}(\Delta P_{P_1} + \Delta P_{AGC_1} - \frac{1}{D_{l_1}}\Delta f_1 - P_T sin\Delta\phi) \tag{6.4}$$

$$\Delta \dot{f}_2 = \frac{f_0}{2H_2 S_{B_2}}(\Delta P_{P_2} + \Delta P_{AGC_2} - \frac{1}{D_{l_2}}\Delta f_2 + P_T sin\Delta\phi) \tag{6.5}$$

$$\Delta\dot{\phi} = 2\pi(\Delta f_1 - \Delta f_2) \tag{6.6}$$

$$\begin{aligned}\Delta P_{\dot{AGC_1}} = {} & (\frac{1}{D_{l_1}}\frac{C_{P_1} f_0}{2S_1 H_1 S_{B_1}} - \frac{1}{S_1}\frac{1}{T_{N_1}})\Delta f_1 - \frac{C_{P_1} f_0}{2S_1 H_1 S_{B_1}}\Delta P_{P_1} \\ & - \frac{C_{P_1} f_0}{2S_1 H_1 S_{B_1}}\Delta P_{AGC_1} - (\frac{1}{T_{N_1}} - \frac{C_{P_1} f_0}{2S_1 H_1 S_{B_1}})P_T sin\Delta\phi \\ & - 2\pi C_{P_1} P_T(\Delta f_1 - \Delta f_2)cos\Delta\phi - \frac{K_{a_1}}{T_{N_1}}P_1\end{aligned} \tag{6.7}$$

where $\Delta P_{12} = -\Delta P_{21} = P_T sin\Delta\phi$ is describing the power flow on the tie line (note that the active power losses are neglected on the line). $\Delta P_{1,2} = -\frac{1}{S_{1,2}}\Delta f_{1,2}$ is the primary frequency control law. All required parameters are defined in Appendix A.3 [30].

In this case, the system is considered in a safe condition when the frequency of each area lies in a defined safe set $[-1.5, 1.5]$. Auxiliary variables Z_1 and Z_2 are considered to replace the nonlinear non-polynomial functions $sin\Delta\phi$ and $cos\Delta\phi$ with the polynomials approximation, respectively [90]. Safety verification is analyzed for the worst-case scenario such that both areas are disturbed with a bounded disturbance input $U_d = 350$. The obtained safe region by the proposed method is illustrated in Fig. 6.4.

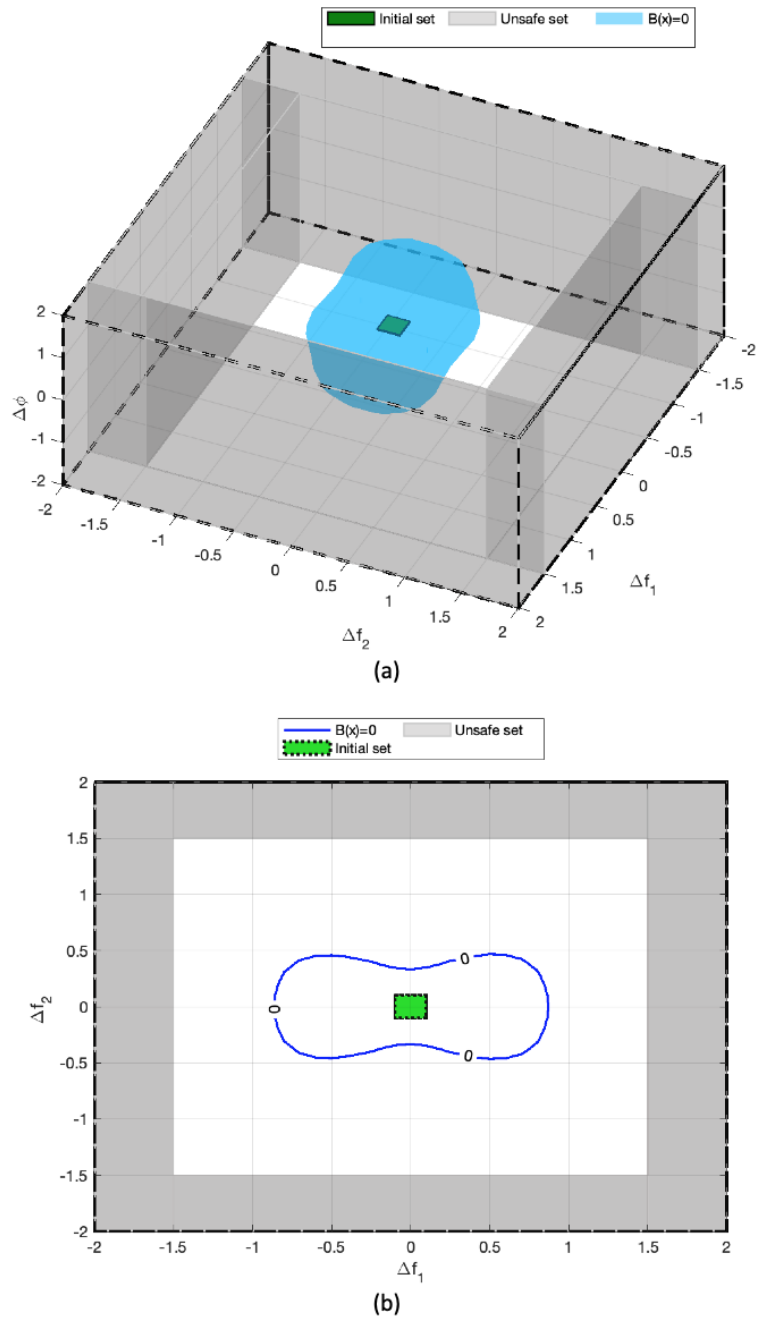

Figure 6.4: Two-area interconnected power system with AGC. (a) $B(x) = 0$ on $\Delta\phi$, Δf_1 and Δf_2 axis, (b) projection of $B(x) = 0$ on Δf_1 and Δf_2 axis.

This set is the zero level set of the computed barrier function that separates the safe and unsafe region to keep the system trajectories inside the desired range.

6.4 Discussion on Further Control Guidelines

Developed control structures for the grid interfacing power electronics converters to provide both grid support and power dispatch functions is highly demanded [74]. Complex switching behaviors have been introduced as converter interfaced power resources (CIPR) can operate in many different modes, including grid-forming and grid-following. As CIPR are capable enough to switch between different modes such as maximum power point tracking (MPPT) and frequency regulation, they can be easily programmed and controlled, particularly in grid-forming. However, providing a precise control to get a reliable contribution from CIPR by stitching between available modes is critical to guaranteed frequency performance.

With the review of the concept ROS, the safe switching synthesis principle is interpreted based on the property of ROS in this section. As a further control guideline, safety supervisory control (SSC) is suggested as the common and applicable approach to synthesize the supportive modes in CIPR such as wind turbine generators (WTGs) to guarantee performance [133]. The SSC control approach is illustrated in Fig. 6.5 where MPPT used as a technique for resources with variable power to maximize energy extraction under all conditions. The proposed switching technique can be applied on photovoltaic (PV) solar systems, and WTGs. The SSC enables the system awareness capability and provides real-time systemic safety margin for renewable sources. A diesel/ wind fed microgrid is considered to show the SSC effectiveness with first verifying its region of safety using the proposed approach in Section 5.5.

6.4.1 Diesel/ Wind Fed Microgrid

A four-bus system as an illustration of a diesel/ wind fed microgrid with a 600 MW thermal plant, including four identical units is considered as shown in Fig. 6.6 [99].

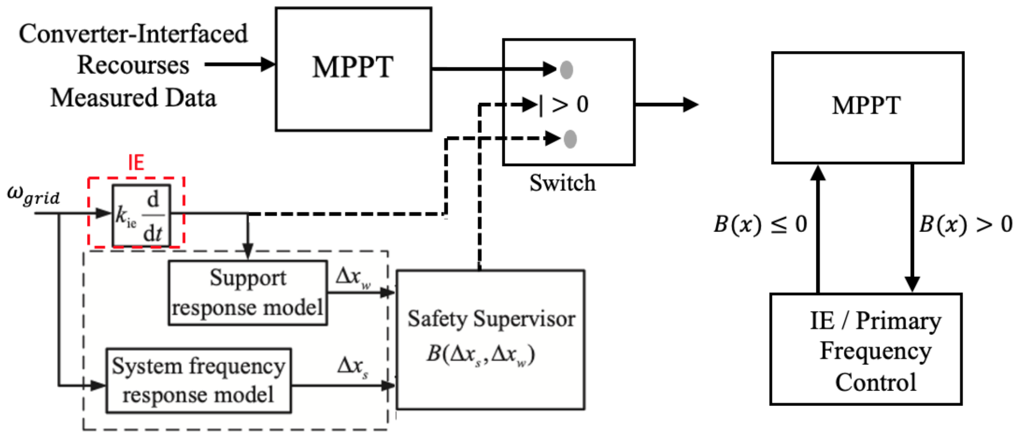

Figure 6.5: SSC integrated in CIPR and its corresponding finite-state machine.

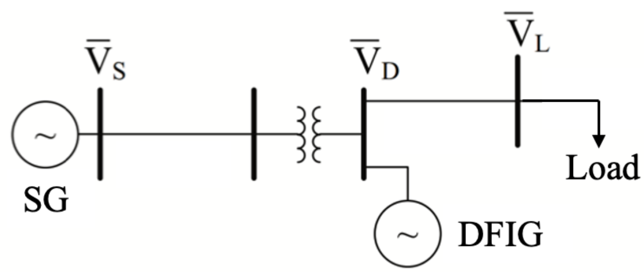

Figure 6.6: Diesel/ wind fed microgrid.

The classic system frequency response model can represent the frequency dynamics of the system as follows:

$$\frac{d\Delta\omega_d}{dt} = \frac{f_b}{2H_D}(\Delta P_m - (\Delta P_d - \Delta P_g) - \frac{D}{f_b}\Delta\omega_d) \tag{6.8}$$

$$\frac{d\Delta P_m}{dt} = \frac{1}{\tau_d}(-\Delta P_m + \Delta P_v) \tag{6.9}$$

$$\frac{d\Delta P_v}{dt} = \frac{1}{\tau_{sm}}(-\Delta P_v - (\frac{\Delta\omega_d}{f_b R_D})) \tag{6.10}$$

where ΔP_d is a large disturbance, such as, generation loss or abrupt load changes, and ΔP_g represents the active power variation due to the frequency control loop form a type-3 WTG connected to a reference bus. Note that the SFR model has the potential to describe system frequency response in a complex power network as shown in many recent studies [78, 106, 33]. The wind farm is assumed to be an aggregation of 200 individual GE 1.5 MW WTGs with rated speed of 450 rad/s (or 72 Hz) and rated output of 300 MW [134]. To model the WTG a reduced-order model can be obtained Based on selected modal analysis (SMA) [99] with $Ard = -0.0723$ and $B_{rd1} = 0.6$, $C_{rd} = 0.0127$ and $D_{rd1} = -0.1$. SMA technique provide a computationally truncable reduced-order model for hybrid system safety verification fully described in [99], [132]. WTG operating condition and other required parameters are given in Appendix A.4.

The disturbance, d is set to 0.24 p.u. at $t = 20$ s as an increment in the load change to verify the ROS. The obtained result in Fig. 6.7 and Fig. 6.8 show the 3D and 2D projection of the ROS. This region is used for the SSC design purpose.

For simulation purposes to verify the SSC effectiveness, the full-order nonlinear model of a synchronous generator (SG) is used but scaled down to microgrid rating. A type-3 wind turbine with an averaged converter model is used as a WTG model. Detailed description of model used in simulation can be found in [134], [133]. The system under the disturbance set about 0.24 p.u. is simulated. The frequency response and the value of safety supervisor are shown in Fig. 6.9. The inertia emulation (IE) to provide guaranteed synthetic inertia is activated when the supervisor's value crosses zero.

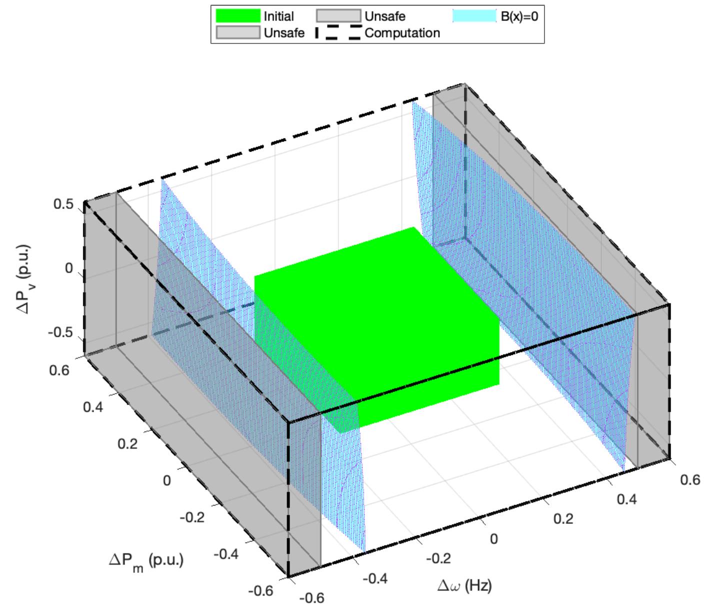

Figure 6.7: Four-bus system region of safety with the disturbance $d = 0.24$.

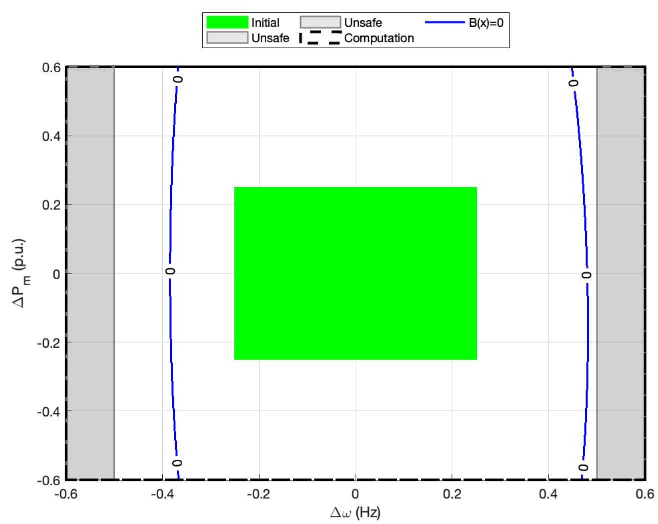

Figure 6.8: Four-bus system region of safety with the disturbance $d = 0.24$.

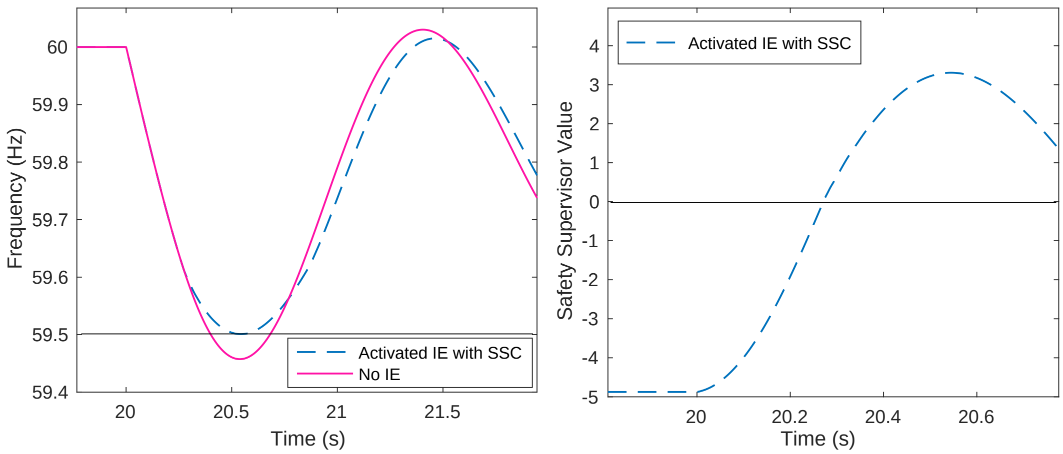

Figure 6.9: Frequency response under no inertia emulation and inertia emulation activated via safety supervisory control (SSC), (a) frequency response, (b) value of safety supervisor.

As seen, the nadir of the frequency response with activated SSC is exactly at the safety limit, indicating the estimated ROS is highly precise.

6.5 Summary

Inadequate frequency response is a critical challenge arising due to the high penetration of DERs in power systems. Large frequency excursion during the transient period, that is, the period of inertial and primary responses can trigger unnecessary relay actions. Frequency regulation supports are needed to overcome the aforementioned challenges. Due to the complex behavior of large-scale systems, including power systems, verifying safety is essential. There are different methods for safety verification with various computational costs and effectiveness. This chapter proposes an LP relaxation with the Handelman's representation to find the barrier certificate for a network systems that can be represented by polynomial functions. The proposed method has potential for applications in practical power grids, including different types of power plants, renewable energy resources, and control actuators since there is no need to represent the network based on its subsystems dynamic equations. Simulation results are provided for three case studies involving interconnected systems. A comprehensive supportive function including inertial emulation, primary response and safety recovery with de-loaded WTGs using the SSC is studied.

Chapter 7

Conclusions and Future Works

7.1 Conclusions

High penetration of renewable sources can reduce the operating cost by partially replacing the more expensive generators. Renewable energy sources such as wind are connected to the grid using power electronic interfaces. The variable nature of renewable power poses challenges for frequency control in mixed diesel-renewable microgrids. To address the frequency stability challenges, renewable energy sources need to be equipped with innovative frequency control approaches that contribute to frequency regulation operations. These controls can be employed either in grid connected mode or in islanded mode. A greater demand for regulation capacity to maintain the system balance between power generation and consumption is required to decrease the adverse effect on system frequency in the presence of disturbances and fluctuations caused by the renewable resources. Traditional frequency regulation implemented by large generation units may not satisfy the need in systems with high levels of renewable energy resources. Recent developments in communication infrastructure provide an opportunity for using DR to regulate the power imbalance and control frequency excursions.

In chapter 2, new output feedback LQR and H_∞ control laws for inertia emulation using balanced truncation and the Luenberger observer are proposed. The controllers are applied to a full order nonlinear model and compared favorably to a PI controller and a conventional inertia emulation using a washout filter. The diesel generator speed follows the reference model in the time scale of inertial response, and accurate emulated inertia is guaranteed by generating additional active power from the WTG. The performance of the closed loop system shows improved accuracy with the H_∞ controller relative to the LQR controller, although they both achieve the desired frequency response. Therefore, without providing a specified margin for the frequency, adequate frequency response with robustness in the presence of disturbances can be achieved by setting the desired inertia based on the network operating point. The proposed technique is analyzed for different SCR scenarios where a lower bound to guarantee the performance is obtained.

Chapter 3 investigates the effect of communication delays and packet losses on inertia emulation using a power system model considering services provided by IACs. The results show that time delays and packet losses in the transmission of the ROCOF signal to the DR aggregator through the communication network can cause instability and/or severe frequency excursions. Therefore, adopting a new communication technology, such as 5G, with low latency and packet loss will have a significant impact in improving future smart grids with guaranteed inertia emulation performance.

A robust H_∞ and μ-synthesis dynamic output feedback control laws for primary frequency regulation with DR are proposed in chapter 4. The suggested robust control techniques aim to overcome parametric uncertainties, including communication delays, governor dead-band and governor time constants in a power system. The controllers are applied to the full-order model and compared favorably to a conventional PI-based Smith predictor control method. The performance of the closed-loop system shows improved accuracy with the μ-synthesis controller relative to the H_∞ controller, although they both achieve improved frequency nadir and reduced ROCOF. Therefore, without providing a specified margin for the frequency, adequate primary frequency response with robustness is obtained by adopting the proposed robust delay compensation control.

In chapter 5 safety verification methods and their application to power system are presented. The methods are classified into set operation based methods and passivity based methods. Pros and cons of the approaches are discussed. First, set operation based methods are analyzed and considered as applicable and efficient for high order systems. Then, passivity based methods are described based on different approaches such as dissipativity and barrier certificate approach. To encode the positivity of the barrier certificate function, LP relaxation by Handelman's representation is proposed.

The Handelman's based barrier certificate approach for guaranteed frequency performance is proposed in chapter 6. This chapter proposes an LP relaxation thanks to the Handelman's representation to find the barrier certificate for a network of systems that can be represented by polynomial functions. The proposed method has the potential for applications in practical power grids, including different types of power plants, renewable energy resources, and control actuators. Simulation results are provided for three case studies involving interconnected systems. A comprehensive supportive function including inertial emulation, primary response and safety recovery with de-loaded WTGs using the SSC is studied.

7.2 Future Works

Based on the works to date, continuing research in the following direction is needed.

- Considering the fast regulating time and programmability of power electronic converters, the proposed safety-supervisory controller will be designed for converter-interfaced sources/loads to limit the frequency response nadir as a support of power grids.
- Robust unknown-input observer-based control may be considered for grids integrated with DERs for delay compensation and false data rejection.
- Novel demand response control technologies for frequency regulation services with high integration of renewable recourses should be studied. Analysis of 5G potential applications with hardware in the loop test bench in future power grids is needed.
- Motivated by the computational issues to implement barrier certificate approach on large scale systems, the Handelman's based barrier certificate approach can be utilized

and validated on large scale power systems with experimental implementation. To scale the safety verification technique for guaranteed frequency performance to higher dimensional systems, data based methods and data driven control should be studied.

Bibliography

[1] Abad, G., Lopez, J., Rodríguez, M., Marroyo, L., and Iwanski, G. (2011). *Doubly fed induction machine: modeling and control for wind energy generation*. John Wiley & Sons, Hoboken, New Jersey. 20, 21

[2] Agiwal, M., Roy, A., and Saxena, N. (2016). Next generation 5G wireless networks: A comprehensive survey. *IEEE Communications Surveys Tutorials*, 18(3):1617–1655. 47

[3] Ahnlund, J. (2014). Short-circuit contributions from fully-rated converter wind turbines: Modeling and simulation of steady-state short-circuit contributions from FRC wind turbines in offshore wind power plants. Master's thesis, KTH Royal Institute of Technology. 42

[4] Albadi, M. H. and El-Saadany, E. F. (2008). A summary of demand response in electricity markets. *Electric Power Systems Research*, 78(11):1989–1996. 59

[5] Althoff, M. (2010). *Reachability analysis and its application to the safety assessment of autonomous cars*. PhD thesis, Technische Universität München. 9, 87

[6] Althoff, M. (2014). Formal and compositional analysis of power systems using reachable sets. *IEEE Transactions on Power Systems*, 29(5):2270–2280. 87, 94, 95, 105

[7] Althoff, M. (2019). Reachability analysis of large linear systems with uncertain inputs in the krylov subspace. *IEEE Transactions on Automatic Control*. 92

[8] Althoff, M., Stursberg, O., and Buss, M. (2007). Reachability analysis of linear systems with uncertain parameters and inputs. In *2007 46th IEEE Conference on Decision and Control*, pages 726–732. IEEE. 87

[9] Antoulas, A. C., Sorensen, D. C., and Gugercin, S. (2001). A survey of model reduction methods for large-scale systems. *Contemporary Mathematics*, 280:193–219. 9, 25, 29, 35

[10] Babahajiani, P., Shafiee, Q., and Bevrani, H. (2016). Intelligent demand response contribution in frequency control of multi-area power systems. *IEEE Transactions on Smart Grid*, 9(2):1282–1291. 59

[11] Bai, H., Arcak, M., and Wen, J. (2011). *Cooperative control design: a systematic, passivity-based approach*. Springer Science & Business Media. 96

[12] Balas, G. J., Doyle, J. C., Glover, K., Packard, A., and Smith, R. (1993). μ-analysis and synthesis toolbox. *MUSYN Inc. and The MathWorks, Natick MA*. 72

[13] Baran, M. E. and Wu, F. F. (1989). Network reconfiguration in distribution systems for loss reduction and load balancing. *IEEE Power Engineering Review*, 9(4):101–102. 33

[14] Bevrani, H. (2014). *Robust power system frequency control*, volume 4. Springer. 2

[15] Bevrani, H., Feizi, M. R., and Ataee, S. (2015). Robust frequency control in an islanded microgrid: $\{\infty\}$ and μ-synthesis approaches. *IEEE transactions on smart grid*, 7(2):706–717. 71, 84

[16] Bhana, R. and Overbye, T. J. (2016). The commitment of interruptible load to ensure adequate system primary frequency response. *IEEE Transactions on Power Systems*, 31(3):2055–2063. 9

[17] Bhatia, A. and Frazzoli, E. (2004). Incremental search methods for reachability analysis of continuous and hybrid systems. In *International Workshop on Hybrid Systems: Computation and Control*, pages 142–156. Springer. 87

[18] Blanchini, F. (1999). Set invariance in control. *Automatica*, 35(11):1747–1767. 91, 96

[19] Camphouse, R. C., Djouadi, S. M., and Myatt, J. H. (2006). Feedback control for aerodynamics (preprint). 27

[20] Choi, H., Seiler, P. J., and Dhople, S. V. (2016). Propagating uncertainty in power-system dae models with semidefinite programming. *IEEE Transactions on Power Systems*, 32(4):3146–3156. 87

[21] Chávez, H. and Hezamsadeh, M. R. (2013). The need for market-based provision of inertia and frequency response to integrate wind power in nordel. Technical report, Royal Institute of Technology, Stockholm, Sweden. 6

[22] Conroy, J. F. and Watson, R. (2008). Frequency response capability of full converter wind turbine generators in comparison to conventional generation. *IEEE Transactions on Power Systems*, 23(2):649–656. 6

[23] Coogan, S. and Arcak, M. (2013). Verifying safety of interconnected passive systems using sos programming. In *52nd IEEE Conference on Decision and Control*, pages 5951–5956. 99

[24] Coogan, S. and Arcak, M. (2015). A dissipativity approach to safety verification for interconnected systems. *IEEE Transactions on Automatic Control*, 60(6):1722–1727. 86, 87, 96, 97, 98, 99, 103

[25] Debbarma, S., Hazarika, C., and Singh, K. M. (2018). Virtual inertia emulation from hvdc transmission links to support frequency regulation in presence of fast acting reserve. In *2018 2nd International Conference on Power, Energy and Environment: Towards Smart Technology (ICEPE)*, pages 1–6. IEEE. 3, 7, 61

[26] Djouadi, S. M. and Morovati, S. (2020). Distributed spatially invariant systems: An input-output approach. In *2020 59th IEEE Conference on Decision and Control (CDC)*, pages 2178–2183. 71

[27] Dreidy, M., Mokhlis, H., and Mekhilef, S. (2017). Inertia response and frequency control techniques for renewable energy sources: A review. *Renewable and Sustainable Energy Reviews*, 69:144–155. 2, 64

[28] Dulau, M. and Bica, D. (2015). Design of Robust Control for Single Machine Infinite Bus System. *Procedia Technology*, 19:657–664. 112

[29] El-Guindy, A., Chen, Y. C., and Althoff, M. (2017). Compositional transient stability analysis of power systems via the computation of reachable sets. In *2017 American Control Conference (ACC)*, pages 2536–2543. IEEE. 94

[30] Esfahani, P. M., Vrakopoulou, M., Margellos, K., Lygeros, J., and Andersson, G. (2010a). Cyber attack in a two-area power system: Impact identification using reachability. In *Proceedings of the 2010 American control conference*, pages 962–967. IEEE. 112, 114

[31] Esfahani, P. M., Vrakopoulou, M., Margellos, K., Lygeros, J., and Andersson, G. (2010b). A robust policy for automatic generation control cyber attack in two area power network. In *49th IEEE conference on decision and control (CDC)*, pages 5973–5978. IEEE. 114

[32] Feltes, J. W. and Fernandes, B. (2012). Wind turbine generator dynamic performance with weak transmission grids. In *2012 IEEE Power and Energy Society General Meeting*, pages 1–7. IEEE. 42

[33] Gevorgian, V., Zhang, Y., and Ela, E. (2014). Investigating the impacts of wind generation participation in interconnection frequency response. *IEEE transactions on Sustainable Energy*, 6(3):1004–1012. 118

[34] Girard, A. (2005). Reachability of uncertain linear systems using zonotopes. In *International Workshop on Hybrid Systems: Computation and Control*, pages 291–305. Springer. 92

[35] Handelman, D. (1988). Representing polynomials by positive linear functions on compact convex polyhedra. *Pacific Journal of Mathematics*, 132(1):35–62. 100, 102

[36] He, W., Yuan, X., and Hu, J. (2017). Inertia provision and estimation of PLL-based dfig wind turbines. *IEEE Transactions on Power Systems*, 32(1):510–521. 6

[37] Hegazy, Y., Salama, M., and Chikhani, A. (2003). Adequacy assessment of distributed generation systems using monte carlo simulation. *IEEE Transactions on Power Systems*, 18(1):48–52. 87

[38] Henrion, D. and Korda, M. (2013). Convex computation of the region of attraction of polynomial control systems. *IEEE Transactions on Automatic Control*, 59(2):297–312. 95

[39] Hines, G. H., Arcak, M., and Packard, A. K. (2011). Equilibrium-independent passivity: A new definition and numerical certification. *Automatica*, 47(9):1949–1956. 98

[40] Hosseini, S. A., Toulabi, M., Dobakhshari, A. S., Ashouri-Zadeh, A., and Ranjbar, A. M. (2019). Delay compensation of demand response and adaptive disturbance rejection applied to power system frequency control. *IEEE Transactions on Power Systems*, 35(3):2037–2046. 59

[41] Hu, J., Wang, S., Tang, W., and Xiong, X. (2016). Full-capacity wind turbine with inertial support by adjusting phase-locked loop response. *IET Renewable Power Generation*, 11(1):44–53. 7

[42] Hu, R., Qian, Y., and Wang, J. (2012). Recent advances in wireless technologies for smart grid [guest editorial]. *IEEE Wireless Communications*, 19(3):12–13. 11, 47

[43] Hui, H., Ding, Y., Chen, T., Rahman, S., and Song, Y. (2020a). Dynamic and stability analysis of the power system with the control loop of inverter air conditioners. *IEEE Transactions on Industrial Electronics*, 68(3):2725–2736. 49, 51, 52, 53, 61, 63

[44] Hui, H., Ding, Y., Shi, Q., Li, F., Song, Y., and Yan, J. (2020b). 5G network-based internet of things for demand response in smart grid: A survey on application potential. *Applied Energy*, 257:113972. 47, 49

[45] Hui, H., Ding, Y., and Zheng, M. (2018). Equivalent modeling of inverter air conditioners for providing frequency regulation service. *IEEE Transactions on Industrial Electronics*, 66(2):1413–1423. 51, 52, 63, 64

[46] Jin, L., Kumar, R., and Elia, N. (2010). Reachability analysis based transient stability design in power systems. *International Journal of Electrical Power & Energy Systems*, 32(7):782–787. 87, 95, 105

[47] Julius, A. A., Fainekos, G. E., Anand, M., Lee, I., and Pappas, G. J. (2007). Robust test generation and coverage for hybrid systems. In *International Workshop on Hybrid Systems: Computation and Control*, pages 329–342. Springer. 87

[48] Junyent-Ferré, A., Pipelzadeh, Y., and Green, T. C. (2015). Blending HVDC-Link Energy Storage and Offshore Wind Turbine Inertia for Fast Frequency Response. *IEEE Transactions on Sustainable Energy*, 6(3):1059–1066. 7

[49] Kaloi, G. S., Wang, J., and Baloch, M. H. (2016). Active and reactive power control of the doubly fed induction generator based on wind energy conversion system. *Energy Reports*, 2:194–200. 22

[50] Kamyar, R., Murti, C., and Peet, M. M. (2014). Constructing piecewise-polynomial lyapunov functions for local stability of nonlinear systems using handelman's theorem. In *53rd IEEE Conference on Decision and Control*, pages 5481–5487. 90

[51] Kayikçi, M. and Milanovic, J. V. (2009). Dynamic contribution of DFIG-based wind plants to system frequency disturbances. *IEEE Transactions on Power Systems*, 24(2):859–867. 6, 7

[52] Kelly, F. P., Maulloo, A. K., and Tan, D. K. (1998). Rate control for communication networks: shadow prices, proportional fairness and stability. *Journal of the Operational Research society*, 49(3):237–252. 96

[53] Kirby, B. J. (2005). Frequency regulation basics and trends. Technical report, Oak Ridge National Laboratory. 3

[54] Kirby, B. J., Dyer, J., Martinez, C., Shoureshi, R. A., Guttromson, R., Dagle, J., et al. (2003). *Frequency control concerns in the North American electric power system*. United States. Department of Energy. 108

[55] Kochdumper, N. and Althoff, M. (2020). Sparse polynomial zonotopes: A novel set representation for reachability analysis. *IEEE Transactions on Automatic Control*, 66(9):4043–4058. 94

[56] Koschi, M., Pek, C., Maierhofer, S., and Althoff, M. (2019). Computationally efficient safety falsification of adaptive cruise control systems. In *2019 IEEE Intelligent Transportation Systems Conference (ITSC)*, pages 2879–2886. IEEE. 94

[57] Kothari, D. P. and Nagrath, I. (2003). *Modern power system analysis*. Tata McGraw-Hill Education. 65

[58] Kou, G., Hadley, S., and Liu, Y. (2014). Dynamic model validation with governor deadband on the eastern interconnection. *Oak Ridge National Laboratory (ORNL), Oak Ridge, TN, USA*. 65

[59] Kou, G., Markham, P., Hadley, S., King, T., and Liu, Y. (2016). Impact of governor deadband on frequency response of the u.s. eastern interconnection. *IEEE Transactions on Smart Grid*, 7(3):1368–1377. 65

[60] Krpan, M. and Kuzle, I. (2018). Introducing low-order system frequency response modelling of a future power system with high penetration of wind power plants with frequency support capabilities. *IET Renewable Power Generation*, 12(13):1453–1461. 15, 25

[61] Krpan, M. and Kuzle, I. (2019). Coordinated control of an ultracapacitor bank and a variable-speed wind turbine generator for inertial response provision during low and above rated wind speeds. In *2019 IEEE Sustainable Power and Energy Conference (iSPEC)*, pages 1693–1698. 2

[62] Krpan, M. and Kuzle, I. (2020). Dynamic characteristics of virtual inertial response provision by DFIG-based wind turbines. *Electric Power Systems Research*, 178:106005. 2

[63] Kundu, S., Nandanoori, S. P., Kalsi, K., Geng, S., and Hiskens, I. A. (2019). Distributed barrier certificates for safe operation of inverter-based microgrids. In *2019 American Control Conference (ACC)*, pages 1042–1047. IEEE. 105

[64] Kundur, P., Balu, N. J., and Lauby, M. G. (1994). *Power system stability and control*, volume 7. McGraw-hill New York. 114

[65] Kurtz, J. and Hovsapian, R. (2021). Aries advanced research on integrated energy systems research plan. Technical report, National Renewable Energy Lab.(NREL), Golden, CO (United States). 3

[66] Kurzhanskiy, A. A. and Varaiya, P. (2007). Ellipsoidal techniques for reachability analysis of discrete-time linear systems. *IEEE Transactions on Automatic Control*, 52(1):26–38. 92

[67] Kuzle, I., Tomisa, T., and Tesnjak, S. (2004). A mathematical model for studying power system frequency changes. In *2004 IEEE Africon. 7th Africon Conference in Africa (IEEE Cat. No. 04CH37590)*, volume 2, pages 761–764. 65

[68] Lafferriere, G., Pappas, G. J., and Yovine, S. (2001). Symbolic reachability computation for families of linear vector fields. *Journal of Symbolic Computation*, 32(3):231–253. 87

[69] Le Guernic, C. (2009). *Reachability analysis of hybrid systems with linear continuous dynamics*. PhD thesis, Université Joseph-Fourier-Grenoble I. 87

[70] Ledva, G. S., Vrettos, E., Mastellone, S., Andersson, G., and Mathieu, J. L. (2017). Managing communication delays and model error in demand response for frequency regulation. *IEEE Transactions on Power Systems*, 33(2):1299–1308. 59

[71] Li, Y., Xu, Z., and Wong, K. P. (2017a). Advanced control strategies of PMSG-based wind turbines for system inertia support. *IEEE Transactions on Power Systems*, 32(4):3027–3037. 6, 7

[72] Li, Y., Zhang, P., and Luh, P. B. (2017b). Formal analysis of networked microgrids dynamics. *IEEE Transactions on Power Systems*, 33(3):3418–3427. 94

[73] Li, Y., Zhang, P., and Yue, M. (2018). Networked microgrid stability through distributed formal analysis. *Applied energy*, 228:279–288. 94

[74] Ma, Y., Cao, W., Yang, L., Wang, F., and Tolbert, L. M. (2017). Virtual synchronous generator control of full converter wind turbines with short-term energy storage. *IEEE Transactions on Industrial Electronics*, 64(11):8821–8831. 116

[75] Maidens, J. N., Kaynama, S., Mitchell, I. M., Oishi, M. M., and Dumont, G. A. (2013). Lagrangian methods for approximating the viability kernel in high-dimensional systems. *Automatica*, 49(7):2017–2029. 87, 92

[76] Makarov, Y. V., Etingov, P. V., Zhou, N., Ma, J., Samaan, N. A., Diao, R., Malhara, S. V., Guttromson, R. T., Du, P., and Sastry, C. (2010). Analysis methodology for balancing authority cooperation in high penetration of variable generation. Technical report, Pacific Northwest National Lab.(PNNL), Richland, WA (United States). 2, 108

[77] Maréchal, A., Fouilhé, A., King, T., Monniaux, D., and Périn, M. (2016). Polyhedral approximation of multivariate polynomials using handelman's theorem. In *International Conference on Verification, Model Checking, and Abstract Interpretation*, pages 166–184. Springer. 91

[78] Miller, N. W., Shao, M., and Venkataraman, S. (2011). California iso (caiso) frequency response study. *GE Energy*, 9. 118

[79] Mitchell, I. M. (2002). *Application of level set methods to control and reachability problems in continuous and hybrid systems*. stanford university. 92

[80] Moore, B. (1981). Principal component analysis in linear systems: Controllability, observability, and model reduction. *IEEE Trans. on Automatic Control*, 26(1):17–32. 26

[81] Morovati, S., Djouadi, S. M., Olama, M., Dong, J., Tomsovic, K., Fathy, A., and Kuruganti, T. (2021a). Inertia emulation control using demand response via 5G communications. In *2021 IEEE 12th International Symposium on Power Electronics for Distributed Generation Systems (PEDG)*, pages 1–5. 1, 7, 9, 46, 47, 49

[82] Morovati, S. and Pulgar-Painemal, H. (2021). Control coordination between DFIG-based wind turbines and synchronous generators for optimal primary frequency response. In *2020 52nd North American Power Symposium (NAPS)*, pages 1–6. 2, 51, 58

[83] Morovati, S., Zhang, Y., Djouadi, S. M., Tomsovic, K., Wintenberg, A., and Olama, M. (2021b). Robust output feedback control design for inertia emulation by wind turbine generators. *IEEE Transactions on Power Systems*, 36(6):5056–5067. 2, 3, 5, 6, 7, 9, 15, 18, 23, 26, 33, 35, 42, 51

[84] Morren, J., De Haan, S. W., Kling, W. L., and Ferreira, J. (2006). Wind turbines emulating inertia and supporting primary frequency control. *IEEE Transactions on power systems*, 21(1):433–434. 6, 16, 61

[85] Mujcinagic, A., Kusljugic, M., and Nukic, E. (2020). Wind inertial response based on the center of inertia frequency of a control area. *Energies*, 13(23):6177. 108

[86] NERC (2016). Balancing and frequency control. Technical report, North American Electric Reliability Council, Princeton, NJ, USA. 6

[87] Nimpitiwan, N., Heydt, G. T., Ayyanar, R., and Suryanarayanan, S. (2007). Fault current contribution from synchronous machine and inverter based distributed generators. *IEEE Transactions on Power Delivery*, 22(1):634–641. 33

[88] Osseiran, A., Boccardi, F., Braun, V., Kusume, K., Marsch, P., Maternia, M., Queseth, O., Schellmann, M., Schotten, H., Taoka, H., Tullberg, H., Uusitalo, M. A., Timus, B., and Fallgren, M. (2014). Scenarios for 5G mobile and wireless communications: The vision of the metis project. *IEEE Communications Magazine*, 52(5):26–35. 49

[89] Packard, A. and Doyle, J. (1993). The complex structured singular value. *Automatica*, 29(1):71–109. 71

[90] Papachristodoulou, A. and Prajna, S. (2005). Analysis of non-polynomial systems using the sum of squares decomposition. In *Positive polynomials in control*, pages 23–43. Springer. 114

[91] Parrilo, P. A. (2000). *Structured semidefinite programs and semialgebraic geometry methods in robustness and optimization*. PhD thesis, California Institute of Technology. 89, 96

[92] Pedersen, R., Sloth, C., and Wisniewski, R. (2016). Verification of power grid voltage constraint satisfaction—a barrier certificate approach. In *2016 European Control Conference (ECC)*, pages 447–452. IEEE. 105

[93] Pourmousavi, S. A. and Nehrir, M. H. (2012). Real-time central demand response for primary frequency regulation in microgrids. *IEEE Transactions on Smart Grid*, 3(4):1988–1996. 49

[94] Pourmousavi, S. A. and Nehrir, M. H. (2014). Introducing dynamic demand response in the LFC model. *IEEE Transactions on Power Systems*, 29(4):1562–1572. 49, 59

[95] Prajna, S. (2005). *Optimization-based methods for nonlinear and hybrid systems verification*. PhD thesis, California Institute of Technology. 99, 100

[96] Prajna, S. and Jadbabaie, A. (2005). Methods for safety verification of time-delay systems. In *Proceedings of the 44th IEEE Conference on Decision and Control*, pages 4348–4353. 108

[97] Prajna, S., Jadbabaie, A., and Pappas, G. J. (2007). A framework for worst-case and stochastic safety verification using barrier certificates. *IEEE Transactions on Automatic Control*, 52(8):1415–1428. 89, 91, 99, 108, 110

[98] Pulendran, S. and Tate, J. E. (2017). Energy storage system control for prevention of transient under-frequency load shedding. *IEEE Transactions on Smart Grid*, 8(2):927–936. 9

[99] Pulgar-Painemal, H. A. (2010). *Wind Farm Model for Power System Stability Analysis*. PhD thesis, Univ. of Illinois at Urbana-Champaign, Champaign, IL. 15, 21, 23, 33, 58, 59, 61, 116, 118

[100] Quint, R. and Ramasubramanian, D. (2017). Impacts of droop and deadband on generator performance and frequency control. In *2017 IEEE Power & Energy Society General Meeting*, pages 1–5. IEEE. 65

[101] Rumeng, T., Ying, S., Tong, W., and Wentao, Z. (2020). Electromagnetic field safety compliance assessments for 5g wireless networks. In *2020 IEEE International Symposium on Electromagnetic Compatibility & Signal/Power Integrity (EMCSI)*, pages 659–662. IEEE. 47

[102] Sahyoun, S., Dong, J., and Djouadi, S. M. (2013). Reduced order modeling for fluid flows based on nonlinear balanced truncation. In *2013 American Control Conference*, pages 1284–1289. 9, 25

[103] Sankaranarayanan, S., Chen, X., et al. (2013). Lyapunov function synthesis using handelman representations. *IFAC Proceedings Volumes*, 46(23):576–581. 111

[104] Sauer, P. W. and Pai, M. (1997). *Power system dynamics and stability*. Prentice Hall, New Jersey, USA. 33

[105] Shi, Q., Li, F., Hu, Q., and Wang, Z. (2018). Dynamic demand control for system frequency regulation: Concept review, algorithm comparison, and future vision. *Electric Power Systems Research*, 154:75–87. 59

[106] Singhvi, V., Pourbeik, P., Bhatt, N., Brooks, D., Zhang, Y., Gevorgian, V., Ela, E., and Clark, K. (2013). Impact of wind active power control strategies on frequency response of an interconnection. In *2013 IEEE Power & Energy Society General Meeting*, pages 1–5. IEEE. 118

[107] Slootweg, J., De Haan, S., Polinder, H., and Kling, W. (2003). General model for representing variable speed wind turbines in power system dynamics simulations. *IEEE Transactions on power systems*, 18(1):144–151. 18

[108] Sontag, E. D. (2002). Asymptotic amplitudes and cauchy gains: A small-gain principle and an application to inhibitory biological feedback. *Systems & Control Letters*, 47(2):167–179. 96

[109] Susuki, Y. and Hikihara, T. (2007). Predicting voltage instability of power system via hybrid system reachability analysis. In *2007 American Control Conference*, pages 4166–4171. IEEE. 95

[110] Susuki, Y., Sakiyama, T., Ochi, T., Uemura, T., and Hikihara, T. (2008). Verifying fault release control of power system via hybrid system reachability. In *2008 40th North American Power Symposium*, pages 1–6. IEEE. 94

[111] Tande, J. O., Di Marzio, G., and Uhlen, K. (2007). System requirements for wind power plants. *SINTEF energy res.* 42

[112] Tessaro, H. J. and de Oliveira, R. V. (2020). Operating point optimization of wind turbine generators for provision of inertial response and frequency control. *International Transactions on Electrical Energy Systems*, 30(6):e12382. 2

[113] Tomlin, C. J., Mitchell, I. M., Bayen, A. M., and Oishi, M. K. (2005). Computational techniques for the verification and control of hybrid systems. In *Multidisciplinary*

Methods for Analysis Optimization and Control of Complex Systems, pages 151–175. Springer. 87, 95

[114] Ulbig, A., Borsche, T. S., and Andersson, G. (2014). Impact of low rotational inertia on power system stability and operation. *IFAC Proceedings Volumes*, 47(3):7290–7297. 9

[115] Ullah, N. R., Thiringer, T., and Karlsson, D. (2008). Temporary primary frequency control support by variable speed wind turbines— potential and applications. *IEEE Transactions on power systems*, 23(2):601–612. 23

[116] Uriarte, F. M., Smith, C., VanBroekhoven, S., and Hebner, R. E. (2015). Microgrid ramp rates and the inertial stability margin. *IEEE Transactions on Power Systems*, 30(6):3209–3216. 11

[117] Wang, B., Zhang, Y., Sun, K., and Tomsovic, K. (2018a). Quantifying the synthetic inertia and load-damping effect of a converter-interfaced power source. In *2018 IEEE International Energy Conference (ENERGYCON)*, pages 1–6. 7

[118] Wang, B., Zhang, Y., Sun, K., and Tomsovic, K. (2018b). Quantifying the synthetic inertia and load-damping effect of a converter-interfaced power source. In *2018 IEEE International Energy Conference (ENERGYCON)*, pages 1–6. 16

[119] Wang, C., Li, J., and Hu, Y. (2019). Frequency control of isolated wind-diesel microgrid power system by double equivalent-input-disturbance controllers. *IEEE Access*, 7:105617–105626. 2

[120] Wang, S. (2018). *A Comprehensive Frequency Control Framework for High Penetration of Wind*. PhD thesis, The University of Tennessee, Knoxville. 2, 5

[121] Wang, S. and Tomsovic, K. (2018). A novel active power control framework for wind turbine generators to improve frequency response. *IEEE Transactions on Power Systems*, 33(6):6579–6589. 2

[122] Willcox, K. and Peraire, J. (2002). Balanced Model Reduction via the Proper Orthogonal Decomposition. *AIAA Journal*, 40(11):2323–2330. 26, 27, 28

[123] Yang, Z., Huang, C., Chen, X., Lin, W., and Liu, Z. (2016). A linear programming relaxation based approach for generating barrier certificates of hybrid systems. In *International Symposium on Formal Methods*, pages 721–738. Springer. 108, 111

[124] Zhang, F., Sun, Y., Cheng, L., Li, X., Chow, J. H., and Zhao, W. (2014). Measurement and modeling of delays in wide-area closed-loop control systems. *IEEE Transactions on Power Systems*, 30(5):2426–2433. 51, 63

[125] Zhang, L., Harnefors, L., and Nee, H. P. (2011). Power-synchronization control of grid-connected voltage-source converters. *IEEE Transactions on Power Systems*, 25(2):809–820. 6

[126] Zhang, W., Cantarellas, A. M., Rocabert, J., Luna, A., and Rodriguez, P. (2016). Synchronous power controller with flexible droop characteristics for renewable power generation systems. *IEEE Transactions on Sustainable Energy*, 7(4):1572–1582. 6

[127] Zhang, X., Han, Q., Ge, X., Ding, D., Ding, L., Yue, D., and Peng, C. (2020). Networked control systems: A survey of trends and techniques. *IEEE/CAA Journal of Automatica Sinica*, 7(1):1–17. 11, 46, 47

[128] Zhang, Y. (2018). *Utilizing converter-interfaced sources for frequency control with guaranteed performance in power systems*. PhD thesis, The University of Tennessee, Knoxville. 3, 5, 6, 7, 11, 20, 21, 91, 95, 99

[129] Zhang, Y., Huang, S. F., Schmall, J., Conto, J., Billo, J., and Rehman, E. (2014). Evaluating system strength for large-scale wind plant integration. In *2014 IEEE PES General Meeting — Conference Exposition*, pages 1–5. 42

[130] Zhang, Y., Li, J., Zheng, D., Li, P., and Tian, Y. (2018a). Privacy-preserving communication and power injection over vehicle networks and 5G smart grid slice. *Journal of Network and Computer Applications*, 122:50–60. 47

[131] Zhang, Y., Li, Y., Tomsovic, K., Djouadi, S., and Yue, M. (2020). Review on set-theoretic methods for safety verification and control of power system. *IET Energy Syst. Integr.* early access. 11, 90, 91, 94, 95, 100, 102, 103, 105, 110

[132] Zhang, Y., Melin, A. M., Djouadi, S. M., Olama, M. M., and Tomsovic, K. (2018b). Provision for guaranteed inertial response in diesel-wind systems via model reference control. *IEEE Transactions on Power Systems*, 33(6):6557–6568. 2, 9, 16, 22, 23, 25, 26, 28, 29, 32, 33, 59, 61, 118

[133] Zhang, Y., Raoufat, M. E., Tomsovic, K., and Djouadi, S. M. (2019). Set theory-based safety supervisory control for wind turbines to ensure adequate frequency response. *IEEE Transactions on Power Systems*, 34(1):680–692. 87, 116, 118

[134] Zhang, Y., Tomsovic, K., Djouadi, S. M., and Pulgar-Painemal, H. (2017). Hybrid controller for wind turbine generators to ensure adequate frequency response in power networks. *IEEE Journal on Emerging and Selected Topics in Circuits and Systems*, 7(3):359–370. 7, 9, 11, 25, 89, 90, 91, 105, 118

[135] Zhao, Z., Yang, P., Guerrero, J. M., Xu, Z., and Green, T. C. (2016). Multiple-time-scales hierarchical frequency stability control strategy of medium-voltage isolated microgrid. *IEEE Trans. on Power Electronics*, 31(8):5974–5991. 2

[136] Zhou, K. and Doyle, J. C. (1998). *Essentials of robust control*, volume 104. Prentice hall Upper Saddle River, NJ. 27, 28, 31, 32, 70, 71

[137] Zhu, J., Guerrero, J. M., Hung, W., Booth, C. D., and Adam, G. P. (2014). Generic inertia emulation controller for multi-terminal voltage-source-converter high voltage direct current systems. *IET Renewable Power Generation*, 8(7):740–748. 3, 7, 61

Appendix

A Summary of Parameters

A.1 Modified 33-Bus Microgrid Parameters

Variables are in per unit unless specified otherwise.

$S_{base} = 1.1$ MVA, $V_{base} = 575$ V, $\bar{f} = 377$ (rad/s).

Operating condition: Wind speed: 11 m/s, $P_g = 0.8$, $Q_g = 0$, $V_{ds} = 0$, $V_{qs} = 1$.

Equilibrium point for the linearization: (for the dynamic equations) $\lambda_{ds} = 1.015$, $\lambda_{qs} = 0.002$, $\lambda_{dr} = 1.041$, $\lambda_{qr} = 0.223$, $\omega_r = 1.19$, $x_1 = -0.641$, $x_2 = 0.261$, $x_3 = 0.011$, $x_4 = 0.005$. (For the algebraic equations) $i_{ds} = 0.084$, $i_{qs} = -0.631$, $i_{dr} = 0.261$, $i_{qr} = 0.671$, $V_{qr} = -0.196$, $V_{dr} = 0.048$.

Diesel generator: rated power = 1 MW, $H_D = 1$ (s), $\tau_{sm} = 0.1$ (s), $\tau_d = 0.2$ (s).

Wind turbine generator:

rated power = 1 MW, $H_w = 2$ (s), $\tau_{sm} = 0.1$ (s), $\tau_d = 0.2$ (s), $K_{I_\tau} = 0.1$, $K_{P_c} = 0.6$, $K_{I_c} = 8$, $K_{I_Q} = 5$, $K_{P_Q} = 1$.

A.2 Power System Model with IACs Parameters

Variables are in per unit unless specified otherwise. $S_{base} = 800$ MVA, $f_{base} = 60$ Hz.

IACs operating condition: $T_c = 0.02$, $C_i = 60.55$, $R_i = 3.191$, $k_Q = 0.034$, $k_p = 0.016$, $K = 0.5$, $K_{PC} = 0.52$, $K_{IC} = 0.032$, $\tau_0 = 1$s.

Diesel generator: $H = 10$ (s), $T_{g_0} = 0.2$ (s), $T_t = 0.3$ (s), $T_r = 7$ (s), $F_r = 0.3$ (s), $R_{G_0} = 0.05$, $D = 1$.

A.3 Two-Area Power System with AGC Parameters

$S_{B_{1,2}} = 10$, $f_0 = 50$ (Hz), $H_{1,2} = 50$, $S_{1,2} = 0.002$ (Hz/MW), $C_{P_1} = 0.1$, $T_{N_1} = 30$, $P_T = 1000$ (MW), $K_a = 100$, $D_{l_{1,2}} = 1/200$ (MW/Hz).

A.4 Diesel/ Wind Fed Microgrid Parameters

$\omega_s = 60$ (Hz), $D = 1$, $H_D = 4$(s), $\tau_d = 0.3$ (s),$\tau_{sm} = 0.1$(s), $R_D = 0.05$.

Vita

Samaneh Morovati received the B.S. degree in Electrical Engineering with a concentration in control systems from Imam Khomeini International University, Iran, in 2011 and the M.S. degree in Electrical Engineering with a concentration in control and signalling from Iran University of Science and Technology, Iran, in 2017. She has also received the M.S. degree in Electrical Engineering with concentration in control systems form the University of Tennessee, Knoxville, TN, USA, in 2021. She is currently pursuing the Ph.D. degree in Electrical Engineering at the University of Tennessee, Knoxville, TN, USA.

Her main research interests include control system theory, power system dynamics and control, renewable energy and smart grids.